University of New Mexico
UNM Digital Repository

Spring 5-8-2018

Birth and Evolution of the Virgin River: ~1 km of post-5 Ma uplift of the western Colorado Plateau

Cory J. Walk

Follow this and additional works at: https://digitalrepository.unm.edu/eps_etds

Part of the Geology Commons

Cory J. Walk
_____

Candidate

Earth and Planetary Sciences
_____

Department

This thesis is approved, and it is acceptable in quality and form for publication:

Approved by the Thesis Committee:

Karl E. Karlstrom, Chairperson
_____

Ryan S. Crow
_____

Laura J. Crossey
_____

Louis Scuderi
_____

BIRTH AND EVOLUTION OF THE VIRGIN RIVER:
~1 KM OF POST-5 MA UPLIFT OF THE
WESTERN COLORADO PLATEAU

by

CORY J. WALK

B.S. GEOLOGY
BRIGHAM YOUNG UNIVERSITY–IDAHO
2015

THESIS

Submitted in Partial Fulfillment of the
Requirements for the Degree of

Master of Science
Earth and Planetary Sciences

The University of New Mexico
Albuquerque, New Mexico

July 2018

ACKNOWLEDGEMENTS

BIRTH AND EVOLUTION OF THE VIRGIN RIVER FLUVIAL SYSTEM: ~1

KM OF POST-5 MA UPLIFT OF THE WESTERN COLORADO PLATEAU

By

Cory Walk

B.S., Geology, Brigham Young University – Idaho, 2015

M.S., Earth and Planetary Sciences, University of New Mexico, 2018

ABSTRACT

The uplift history of the Colorado Plateau has been debated for over a century with still no unified hypotheses for the cause, timing, and rate of uplift. $^{40}Ar/^{39}Ar$ dating of semi-continuous basaltic volcanism over the past ~6 Ma within the Virgin River drainage system, southwest Utah and southern Nevada, provides a way to calibrate differential river incision and compare patterns of basaltic migration, mantle velocity structure, channel steepness, lithology, incision history and the birth and evolution of the Virgin River.

New detrital sanidine ages constrain the arrival of the Virgin River across the Virgin Mountains to a maximum depositional age of 5.9 Ma. Incision magnitudes and rates of the Virgin River show a stair-step increase in bedrock incision as the river crosses multiple N-S trending normal faults. Average calculated rates are 23 m/Ma in the Lake Mead block, 85 m/Ma in the combined St. George and Hurricane blocks, and 338 m/Ma in the Zion block. Block-to-block differential incision adds cumulatively such that the Zion block has been deeply incised ~1 km (~315 m/Ma) over 3.6 Ma relative to the Colorado River confluence. We test two hypotheses: 1) observed differential incision magnitudes and rates along the Virgin River system are a measure of mantle-driven

differential uplift of the Colorado Plateau relative to sea level over the past ~5 Ma. 2) Observed differential river incision relates to river integration across previously uplifted topography and differential rock types with no post 5 Ma uplift.

Strong correlations exist between high channel steepness (k_{sn}) and low mantle velocities throughout the Virgin River drainage while weaker correlations exist between high k_{sn} and resistant lithologies. Basaltic volcanism, which has migrated at a rate of ~18 km/Ma parallel to the Virgin River between ~13 and 0.5 Ma suggests a possible mantle-driven mechanism for the combined observations of differential uplift across faults and additional young Colorado Plateau epeirogenic uplift tracked by headward river propagation. Thus, we interpret the Virgin River to be a < 4.5 Ma disequilibrium river system responding to ongoing upper mantle modification and related basalt extraction, which is driving ~ 1 km of young uplift of the western Colorado Plateau.

TABLE OF CONTENTS

List of Figures

List of Tables

PREFACE

This thesis will be submitted for publication as a multi-authored manuscript to the CRevolution 2 issue of the journal *Geosphere*. The author of this thesis, Cory Walk, was the lead author of the paper and performed over 75% of the overall research, writing, figures and data analysis. Co-author and M.S. advisor to the M.S. candidate, Karl Karlstrom, contributed in a variety of ways including reviews to the paper, fieldwork, sample collection, funding for fieldwork and detrital sanidine analyses, and many informal yet influential discussions on the primary concepts and data interpretations found within the paper. Co-author Matt Heizler helped a great deal in the dating of detrital sanidine grains at New Mexico Geochronology Research Laboratory. Co-author Ryan Crow's initial Ph.D. work in 2012 was the starting point of this paper while he also helped in reviews and constructive criticism.

INTRODUCTION

The timing and processes of the Colorado Plateau (CP) uplift from sea level at
70 Ma to its present 2 km average elevation, has been debated for over a century. CP
uplift likely occurred in 3 stages: Laramide, mid-Tertiary, and post-10 Ma (Karlstrom et
al., 2012), but the relative magnitudes of each uplift episode is debated. Neotectonic
uplift (post-10 Ma) of the CP has been hypothesized based on differential incision
studies of the Colorado River (CR) through Grand Canyon (Karlstrom et al., 2007;
Karlstrom et al., 2008; Crow et al., 2014); although, the cause of this uplift is still in
debate. Some hypothesize the influence of dynamic topography, or small-scale upper
mantle convection due to lithospheric thinning and delamination as driving forces for
uplift (Karlstrom et al., 2007; Karlstrom et al., 2008; Moucha et al., 2009; van Wijk et
al., 2010; Crow et al., 2011; Levander et al., 2011; Karlstrom et al., 2012). Other young
uplift mechanisms include isostatic rebound due to differential denudation in the past
~10 Ma but this is likely a contributor rather than a primary driver for differential uplift
(Lazear et al., 2013). Normal faults on the western boundary of CP are now envisioned
to be upper crustal adjustments embedded in broader epeirogenic mantle-driven uplift
(Crow et al., 2014) rather than being the direct mechanism for uplift (Karlstrom et al.,
2007; Karlstrom et al., 2008). Here we use the Virgin River fluvial system to test this
hypothesis that the CP has been uplifted relative to sea level in the past 5 Ma.

The Virgin River (VR) drainage system (Fig. 1) is an excellent laboratory to test
the relationship between uplift and erosion, as its headwaters on the CP are at ~2.5 km
elevation, about 2,275 m higher than its pre-dam (Hoover Dam) confluence with the CR
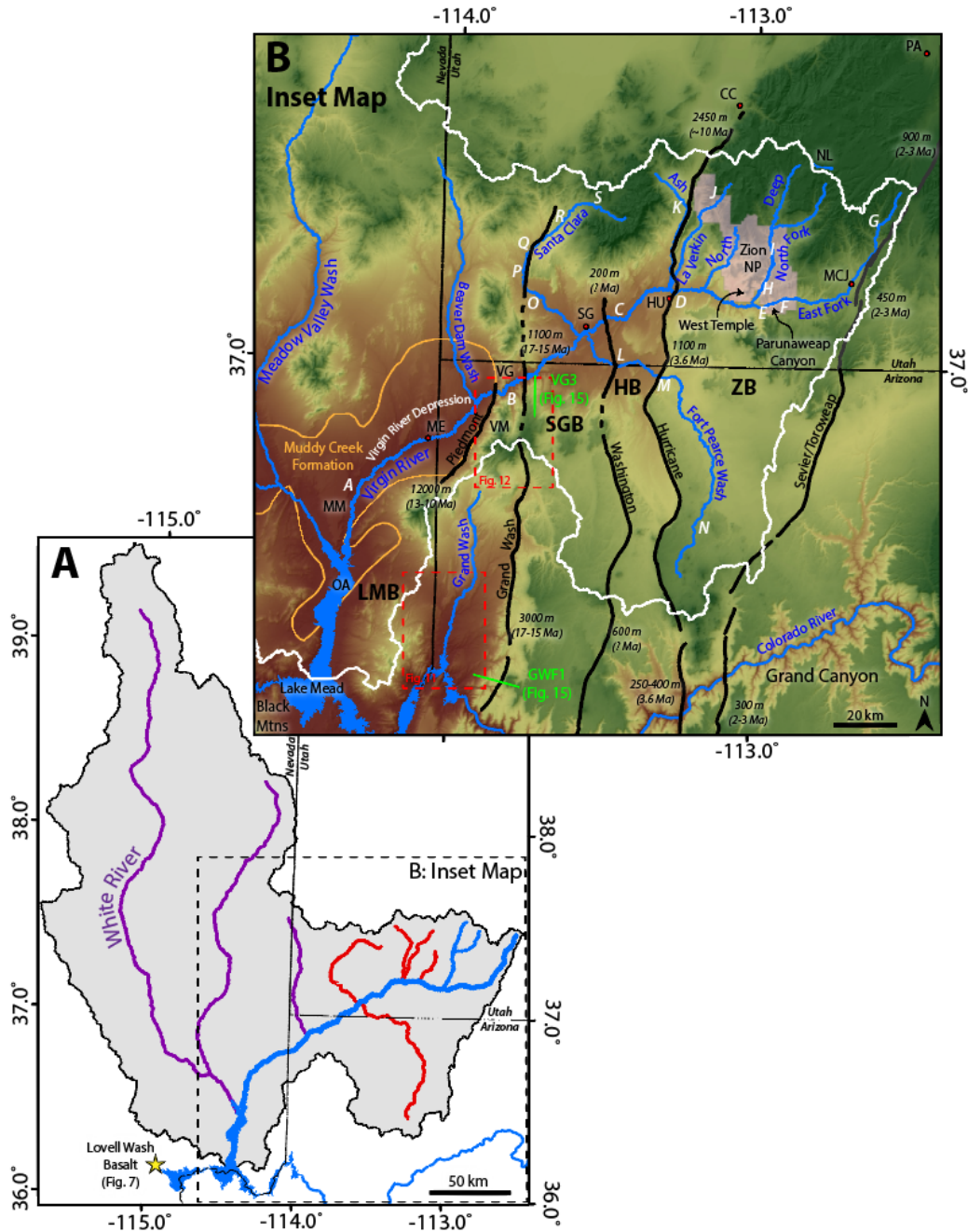
Figure 1. A) The Virgin River (VR) watershed including 11 major tributaries. Tributaries are colored in accordance with river profile groupings: Main stem Virgin River and its 2 forks (blue), CP-TZ Tributaries (red), and Basin and Range tributaries (purple). B) Inset map of the primary area of interest. Major N-S trending normal faults (Piedmont, Grand Wash, Washington, Hurricane, Sevier/Toroweap) separate the western margin of the Colorado Plateau into 4 major structural blocks: LMB – Lake Mead Block, SGB – St. George Block, HB – Hurricane Block, ZB – Zion Block. Other reference locations: ME – Mesquite, NV; SG – St. George, UT; HU – Hurricane, UT; CC – Cedar City, UT; PA – Panguitch, UT; MCJ – Mount Carmel Junction, UT; MM – Mormon Mesa; OA – Overton Arm; VG – Virgin Gorge; VM – Virgin Mountains; NL – Navajo Lake. White letters (A-S) show locations of major knickpoints (see Table 1). Values show displacement along faults with the timing in parentheses. Orange outline indicates the extent of the Muddy Creek Formation.

near Lake Mead in the Basin and Range (BR) province at 225 m. The common base level at the confluence of the CR and the VR since ~ 4 Ma that we document here, allows comparisons between Grand Canyon and Zion Plateau incision along two different major rivers that have carved impressive young canyons across the CP – BR boundary zone. Located in the desert landscape of southwestern Utah, the VR headwaters form at the confluence of two distinct tributaries, the North and East forks. North Fork VR begins north of Zion National Park, as water exits from a spring in cliffs of the Claron Formation, below Navajo Lake (Fig. 1). The North Fork flows south, forming the spectacular 'Narrows' of Zion National Park. The East Fork VR starts northeast of Zion National Park and flows south until turning west near Mt. Carmel Junction, UT. Deep, narrow, incised canyons form in the lower Navajo Sandstone about 15 km east of the confluence of the East and North Forks. The VR crosses Hurricane and Washington faults, enters the ~600 m deep Virgin River Gorge cut into Paleozoic carbonates about 20 km southwest of St. George, UT, and joins the CR in what is now the Overton Arm of Lake Mead, with a pre-dam confluence elevation of 225 m (Birdseye, 1924).

The primary purpose of this study is to reconstruct the birth and evolution of the Virgin River fluvial system. This includes the watershed evolution and its interaction with faulting, magmatism, and climate for the past 5 Ma. Within this overarching purpose, we test two end member hypotheses that may explain the differential incision rates observed by many studies along the western margin of the CP (Hamblin et al., 1981; Willis and Biek, 2001; Crow, 2012; Crow et al., 2014). The first hypothesis considers post-5 Ma regional mantle-driven uplift as the primary cause for spatially variable incision rates. The alternate hypothesis posits no post-5 Ma regional uplift but instead

suggests geomorphic conditions such as cyclic climate changes (Small and Anderson,

1998; Molnar, 2004; Chapin, 2008) and/or variable strength rock type (Pederson and

Tressler, 2012; Bursztyn et al., 2015) are the primary factors needed to explain the

observed differential incision and/or variable channel gradients. This secondary end

member hypothesis infers that the high relief canyons may be the product of lake spill-

over (Meek and Douglass, 2001) across a previously uplifted CP (Pederson et al., 2002).

This would have allowed CP drainage to respond to the lowered base level of the Gulf of

California by driving canyon incision at the edge of the CP (Pelletier, 2010; Pederson et

al., 2013), perhaps creating transient knickpoints (Cook et al., 2009). Therefore, this

study seeks to evaluate primary versus contributing drivers of differential incision along

the western CP margin.

   This study also consists of 3 primary goals that contribute to the VR story. The

first goal of this paper is to identify the birth of the VR. The birth of the through-going

VR (integration of a major river draining from the CP to near its present base level) has

been interpreted to be ~6 to 4 Ma based on studies of the VR depression filled with the

fluvial upper Muddy Creek Formation (Williams, 1996; Dickinson et al., 2014). These

interpreted ages are tested in this paper using detrital sanidine dating to search for young

grains representing a maximum depositional age of the first-arriving far-traveled gravels

in the upper Muddy Creek Formation. Lower Muddy Creek Formation sediments are

fine-grained and are interpreted to record low energy internal drainage in the Mesquite

and Mormon (Virgin River Depression; Fig. 1) basins before major rivers entered from

the CP (Pederson, 2008; Muntean, 2012). The upper Muddy Creek Formation contains

gravel clasts interpreted to represent the arrival of the paleo Virgin River across the

topographic divide formed by the basement-cored Virgin Mountains (Fig. 1; Williams, 1996; Swenberg, 2012). A paleo Grand Wash tributary flowing south into the CR, perhaps from the St. George, UT area (Fig. 1), is also examined in terms of its rounded far-traveled clasts from relatively high energy streams observed beneath the 4.71 Ma basalts of the Grand Wash trough (Beard et al., 2007; Howard et al., 2010; this study).

A second goal of this paper is to reconstruct the evolution of deep canyons and incision history of the VR drainage system. This area is ideal to test and quantify the hypothesized neotectonic uplift of the CP because of the nearly continuous record of late Cenozoic basaltic volcanism ranging from 14.19 to 0.12 Ma (Fig. 2) that allows for accurate dating of paleoriver deposits and ancient landscapes. Our goal is to evaluate when the CP's ~2 km modern elevation, and its high relief river gorges formed. This study builds on and extends similar studies by Hamblin et al. (1981), Willis and Biek (2001) and Crow (2012). We also build on recent work supporting the "young" canyon hypothesis (c.f. Wernicke 2010) as proposed by Karlstrom et al. (2014), Darling and Whipple (2015), and Winn et al. (2017).

The concept that differential incision of major river systems can be used to better quantify magnitude, duration, history, and mechanisms of tectonic uplift has been used in many orogens (Tibetan Plateau – Clark et al., 2005; Schoenbohm et al., 2006; Seong et al., 2008; Ouimet et al., 2010; Andean Plateau – Schildgen et al., 2007; Pyrenees – Calvet et al., 2015). This concept relies on studies of major rivers that show that concave-up equilibrium profiles are achieved rapidly after river integration (Pazzaglia et al., 1998), km-scale relief generation implies young base level fall/ headwater uplift (Donahue et al., 2013; Schmidt et al, 2015), and incision patterns and

river profiles are sensitive gauges of river evolution (Kirby and Whipple, 2001) and

Figure 2. An age distribution plot of all dated basalt flows within the eastern lobe of the Virgin River drainage system and the Lake Mead area (Appendix A). Errors are plotted to 2σ. Note the large amount of flows with ages <1.5 Ma and fewer flows >1.5 Ma. Dot colors represent dating method for each basalt: red (•) – K/Ar, blue (•) – $^{40}Ar/^{39}Ar$, and black (•) – ^{14}C of wood burned by Santa Clara lava flow.

geomorphic processes (Darling and Whipple, 2015). We make the implicit assumption that differential incision is equal to differential uplift due to several qualifying characteristics of the Virgin River fluvial system. First, Howard et al. (2015) show that the Colorado River profile (Virgin River baselevel) was graded to a Pliocene sea level since 4.5 Ma. They suggest downstream subsidence or baselevel drop could not be a major driver of the observed incision. Second, basalt flows entering paleodrainages allow for incision rates to be calculated back to ~6 Ma. This timescale causes any potential effect of climate cycles to be averaged out and ultimately viewed as an overprinting as opposed to a major driver of observed incision. Third, our measured incision rates are quasi-steady with no indication of transient knickpoints allowing for the assumption that differential incision is driven by differential uplift.

A third goal is to understand temporal and spatial relationships between incision and the locus of basaltic volcanism to help evaluate mechanisms of uplift. Some papers have hypothesized young and ongoing mantle-driven CP uplift, but proposed mechanisms have differed from: edge-driven upper mantle convection driving uplift (van Wijk et al., 2010), asthenospheric upwelling and buoyancy change driving uplift (Karlstrom et al., 2008; Crow et al., 2014), delamination of lithosphere and asthenospheric return flow around the Escalante anomaly (Levander et al., 2011), and whole mantle flow driving dynamic topography (Moucha et al., 2009). The observed west-to-east sweep of basaltic magmatism may be an indication of timing and nature of mantle convection below this region (Best et al., 1980; Wenrich et al., 1995; Nelson and Tingey, 1997; Roy et al., 2009; Crow et al., 2011).

The mainstem CR and its major tributary, the VR, are comparable in the sense

that they both have been documented to generate km scale relief in the past ~5 Ma (Winn et al., 2017; this study) and they both flow across the CP-BR transition zone. Therefore, empirical data measured within both drainage systems can be compared to determine whether CP uplift accompanied or pre-dated carving of adjacent high relief canyons (Grand Canyon and VR Gorge). We test the two end member hypotheses, both spatially and temporally, by comparing acquired datasets such as normalized channel steepness (k_{sn}), variable rock strengths (Bursztyn et al. 2015), and mantle velocities at 80 km depth (Schmandt and Humphreys, 2010). Potential evidence or observations that would support (or weaken) the mantle-driven uplift hypothesis are as follows. Temporally steady but spatially variable bedrock incision rates would suggest persistent external uplift forcings rather than, for example temporally unsteady incision rates that might result from transient knickpoints along the entire profile that record climate change, geomorphic events, or downstream baselevel fall/subsidence. A spatial correlation between low mantle velocities and increased channel steepness (k_{sn}) would suggest that increased channel steepness might be the result of mantle-driven uplift. In contrast, spatial correlation between hard rock type and greater channel steepness would suggest bedrock controls on differential incision. The area is large enough that variable climate conditions represented by different precipitation amounts also needs to be examined as a possible factor influencing differential incision.

We present and evaluate several datasets. 1) Nested river profiles of the VR and its major tributaries and knickpoints provide information about relationships between topography, faults, rock type, and other features that may help explain profile geometry (Table 1, Fig. 3). 2) The near continuum of $^{40}Ar/^{39}Ar$ and K/Ar dated basaltic volcanism

Table 1: Virgin River Drainage Knickpoints

ID (fig. 1)	Tributary	Proposed Reason	Location	Largest Scale Identified	Knickzone Max k_{sn} (m$^{0.9}$)	Knickzone Avg. k_{sn} (m$^{0.9}$)	Latitude	Longitude	Notes
A	VR	DEM error? Lithology?	Overton Arm	20	486	163	36.6467	-114.3151	influx of sediment? Error in ksn analysis assumptions (drainage area = discharge)
B	VR	Fault	Virgin Gorge	20	467	182	36.9190	-113.8685	Crossing Grand Wash and Piedmont faults
C	VR	Lithology	Virgin Anticline	10	295	111	37.1177	-113.4429	Inner anticline, harder limestones
D	VR	Fault	Hurricane Fault	20	381	245	37.1969	-113.2519	
E	EF	Lithology?	Upstream of NF conf.	4	210	146	37.1577	-112.9794	landslide, talus, influx of sediment?
F	EF	Lithology	Parunuweap Canyon	20	744	272	37.1802	-112.8716	Navajo to Kayenta
G	EF	Lithology	Spencer Bench basalt	4	167	95	37.3946	-112.5585	
H	NF	Landslide	Sentinel Rockfall	10	224	137	37.2343	-112.9623	
I	NF	DEM error? Lithology? Transient?	Zion NP Narrows	4	317	157	37.3190	-112.9538	Influx of gravels from Orderville Canyon?
J	LC	Fault? Lithology? Transient?	Headwaters	4	247	131	37.4298	-113.1304	small fault, knickpoint lies within a graben, Navajo formation, small landslide present
K	AC	Dam	Ash creek resevoir	10	250	131	37.4110	-113.2366	
L	FPW	Fault	Washington Fault	4	290	172	36.9982	-113.4553	
M	FPW	Fault	Hurricane Fault	20	1238	513	36.9698	-113.3029	
N	FPW	Lithology	Seven knolls basalt	10	202	105	36.6354	-113.1583	
O	SC	Fault	Gunlock Fault	4	191	106	37.1924	-113.7742	downstream crossing of gunlock fault
P	SC	Dam	Gunlock Resevoir	4	165	75	37.2514	-113.7772	
Q	SC	Fault	Gunlock Fault	10	251	161	37.3191	-113.7256	upstream crossing of gunlock fault
R	SC	Dam	Baker Resevoir	4	181	122	37.3759	-113.6416	
S	SC	Lithology	NW Pine Valley Mts	10	255	159	37.4052	-113.5276	Basalts in the channel
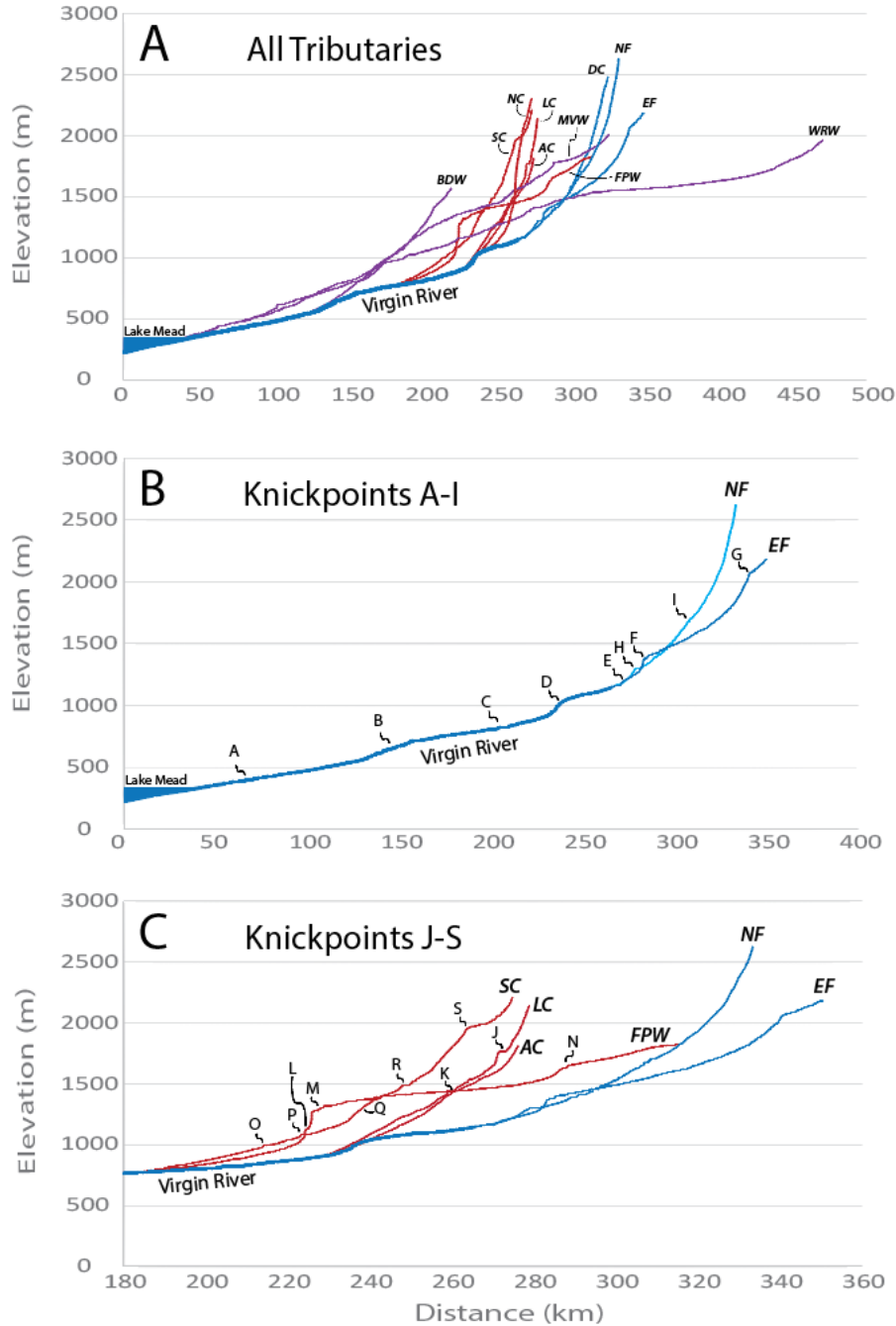
Figure 3. A) Longitudinal river profiles of the Virgin River and 11 major tributaries: WRW – White River Wash, MVW – Meadow Valley Wash, BDW – Beaver Dam Wash, SC – Santa Clara River, FPW – Fort Pearce Wash, AC – Ash Creek, LC – La Verkin Creek, NC – North Creek, DC – Deep Creek, NF – North Fork Virgin River, and EF – East Fork Virgin River. B) main-stem Virgin River profiles and knickpoints (A-I; Table 1). Locations of knickpoints can be seen in map view in figure 1. C) Virgin River tributary profiles that contain identified knickpoints (J-S; Table 1). Profile data was extracted from 10m resolution USGS digital elevation models using ArcGIS. Distances are calculated from the historic (pre-dam) confluence of the Virgin and Colorado Rivers (Birdseye, 1924).

From ca. 15 Ma to present (Fig. 2) provides timing constraints to evaluate differential river incision (e.g. in areas where basalts overlie river gravels) and to test a potential sweep of ages that may indicate relationships between mantle melting, locus of volcanism, and surface responses (Appendix A). 3) ~100 new calculated incision rates are presented in the context of a synthesis of published incision rates (Hamblin et al., 1981; Willis and Biek, 2001; Hayden and Sable, 2008; Crow, 2012) to provide a complete differential incisional history of the VR and its tributaries (Appendix B). 4) Correlations among normalized river steepness (k_{sn}; Kirby and Whipple, 2012), incision rate and magnitude data, upper mantle tomographic data (Schmandt and Humphreys, 2010), rock type, and precipitation are used to attempt to discriminate possible deep and shallow (rock type) controls on river evolution. 5) A sediment provenance analysis using detrital zircons and detrital sanidines of ancestral Virgin River gravels is used to help date the birth of the VR system and examine its provenance (Appendix C).

GEOLOGIC BACKGROUND

Compressional forces of the Sevier and Laramide orogenies followed by BR extension established the present physiographic framework of the VR region by ~ 17 Ma. Best et al. (1980) and Wenrich et al. (1995) observed an eastward propagating sweep of basaltic volcanism in which basalts get younger and also become more asthenospheric in Nd composition to the east (Crow et al., 2011). The combined data have been interpreted to mean that the CP lithosphere is being thinned and replaced by asthenosphere as North America moves SW (absolute velocity) over warm mantle. This has been envisioned as the East Pacific Rise mantle domain by Moucha et al. (2009), edge-driven convection around the CP margin (Karlstrom et al., 2008; van Wijk et al.,

2010; Crow et al., 2011), or lithospheric delamination tectonism and its surface response (Levander et al., 2011).

Similar to magmatism, normal faulting is propagating eastward from the BR into the CP (Pearthree, 1998; Karlstrom et al., 2007). Similarly, the Wasatch fault system that forms the western CP boundary to the north transitions southward into several faults that represent a southward continuation of the intermountain seismic zone (Smith and Arabasz, 1991), termed the Utah Transition Zone (Wannamaker et al., 2001). The Sevier/Toroweap and Hurricane faults act as the western neotectonic boundary of the CP with older (~ 17 Ma; Faulds et al., 2001) normal faults of the Grand Wash fault zone forming the physiographic western boundary of the CP (Brumbaugh, 1987). The ~90 km distance between the Grand Wash and Sevier/Toroweap faults represents a transition zone between the BR and CP provinces (Fig. 1). The Sevier fault zone within the Virgin River drainage system links to Toroweap and Aubrey faults to the south to form the easternmost edge of BR extension. This fault system extends ~250 km from south of Grand Canyon northward to Panguitch, UT. Displacement along the fault increases northward and ranges from ~300 m in northern Arizona near Grand Canyon (Pearthree, 1998) to 450 m near Mt. Carmel Junction, UT where the East Fork Virgin River turns west, and 900 m at its northernmost segment (Anderson and Christenson, 1989). The initiation of faulting is poorly dated but early estimates are 15-12 Ma (Davis, 1999) in the northernmost section of the fault trace. Using this age and the average displacements, calculated slip rates range from 20 to 75 m/Ma. This would be much lower than other large Basin and Range style normal faults in this region (Lund et al., 2008) and therefore this assigned age is probably an overestimate. Also, the southern

segments of the Sevier/Toroweap fault appears to be among the most active and youngest (3-2 Ma) of the west dipping, western CP bounding, normal faults (Jackson, 1990; summarized in Karlstrom et al., 2008).

The Hurricane fault zone spans 250 km, similar to the Sevier fault zone, and extends from Grand Canyon in the south (Karlstrom et al., 2007) to Cedar City, UT in the north (Fig. 1). Although segmented into complex seismogenic zones, total stratigraphic separation generally increases to the north. The southernmost segment is displaced 250-400 m at the Colorado River in Grand Canyon (Karlstrom et al., 2007) and up to 2450 m at the northern segment near Cedar City, UT (Biek et al., 2010). Initiation of northern segments of Hurricane fault began ~10 Ma based on the age of basalts near Cedar City, UT (Rowley et al., 2006). Importantly for this study, initiation of southern segments of the Hurricane fault began no earlier than 3.6 Ma based on equivalent displacement of the 3.6 Ma Bundyville basalt flow with total throw of underlying Mesozoic strata in northern Arizona (Billingsley and Workman, 2000). The segmented nature of the Hurricane fault allows for differential slip rates along its 250 km length. Quaternary slip rates calculated from displaced basalt flows across the fault trace decrease to the south ranging from 530 m/Ma in the last 0.63 Ma near Cedar City, Utah (Lund et al., 2001) to 70-80 m/Ma in the last ~0.2 Ma near Grand Canyon (Fenton et al., 2001; Karlstrom et al., 2007). Lund et al. (2001) calculated an average slip rate of 210 m/Ma where the Virgin River crosses the Hurricane fault. The slip rates calculated by Lund et al. (2001) are similar to Quaternary incision rates calculated in this paper. Average incision rates of the 5 northernmost incision data points along Black Ridge (south of Cedar City) is 533 m/Ma while slip rates are estimated between 530 and 570 m/Ma at that location (Lund et al., 2001). Average

incision rates calculated in this paper near the southern segments of the Hurricane fault is 50 m/Ma along Fort Pearce Wash while slip rates are estimated at 80 m/Ma (Fenton et al., 2001).

Washington fault, located ~20 km west of Hurricane fault, spans ~120 km from St. George, Utah down into northern Arizona (Fig. 1). Displacement along the Washington fault decreases northward, as slip on the Hurricane fault increases northward, and ranges from 600 meters in northern Arizona to only 200 meters in its northernmost extent (Biek et al., 2010). Displacement shows activity as young as 0.18 Ma along the Washington fault near St. George, UT (Fig. 1; Biek et al., 2010).

The Grand Wash fault system, located ~30 km west of Washington fault, forms the easternmost physiographic boundary of the BR province (Fig. 1). Displacement decreases to the north ranging from 3000 meters at Grand Canyon (Lucchitta, 1979) to 1,100 meters at the Virgin Gorge near the northern Arizona border (Billingsley and Workman, 2000). Activity on Grand Wash fault near Grand Canyon occurred from 17 to 11 Ma (Lucchitta, 1979; Bohannon et al., 1993; Faulds et al., 2001; Beard et al., 2007) with the majority of slip at 17-15 Ma (Fitzgerald et al., 1991; Reiners et al., 2000; Fitzgerald et al., 2009; Quigley et al., 2010). The Piedmont fault lies just west of the Grand Wash fault and acts as the eastern boundary of the Virgin River Depression (Fig. 1). Bohannon (1993) uses seismic reflection data to record ~12 km of down-dip displacement along the fault making the adjacent Mesquite basin the deepest basin in the region. The Piedmont fault was active from 13-10 Ma but is also suggested to have been active during deposition of the Muddy Creek formation (11-4 Ma) and into the Quaternary (Moore, 1972; Bohannon, 1993). Using a 13 Ma age of initiation and 12 km

of displacement gives an approximate slip rate of 900 m/Ma, which resulted in significant isostatic footwall uplift of the Virgin Mountains (Wernicke and Axen, 1988).

Hamblin et al. (1981) first proposed calculating differential incision across the Hurricane fault as a measure of CP tectonic uplift; he calculated a differential uplift of 364 m/Ma across the Grand Wash and Hurricane faults using 4 incision points. Willis and Biek (2001) had a more constricted study area but added new ^{40}Ar/^{39}Ar ages of basalts and 12 new incision points along the Virgin River and found 307 m/Ma of differential uplift across the Hurricane and Washington faults. Others have performed similar analyses in the Grand Canyon (Pederson et al., 2002; Karlstrom et al., 2007; 2008; Crow et al., 2014) to quantify differential neotectonic uplift. Howard et al. (2015) made the case that the CR was graded to near sea level by 4.5 Ma, with major aggradation of Bullhead gravels from 4.5-3.5 Ma (Howard et al., 2015; Crow et al., 2016). This reinforces the concept that differential incision along the CR system and major tributaries like the VR can be used to infer uplift of the CP (Lucchitta, 1979; Karlstrom et al., 2007; Karlstrom et al., 2008).

The birth of the VR drainage system is defined here as the age of arrival of the first coarse-grained, far traveled gravels to appear in the Mesquite Basin (eastern basin adjacent to the Piedmont Fault within the Virgin River Depression, Fig. 1). These well-rounded river gravels are identified as the upper Muddy Creek Formation. The VR arrival was pre-dated by deposition of the lower Muddy Creek Formation, located west of the Grand Wash fault, which generally consists of locally derived, fine-grained, basin-fill deposits ranging in age from 11-4 Ma. The location and age of this formation makes it a primary target for a provenance analysis that can shed light on the birth of the

Virgin River. Williams (1996) mapped a sharp contact of well-rounded gravels and cobbles above fine-grained sands of the Muddy Creek Formation. He interpreted this to represent a rapid arrival of an ancestral VR across the Virgin Mountains, which he considered to have been a previous drainage divide. Swenburg (2012) found a similar outcrop of well-rounded, far-traveled gravels sharply above angular, locally derived gravels near the northernmost extent of Lake Mead. Pederson (2008), in agreement with Longwell (1928), performed petrographic analyses of fine-grained sand of lower Muddy Creek Formation and concluded that none of these sediments represented material derived from the CP and hence were not paleo-CR deposits. Instead, Pederson (2008) inferred that the source of the observed sediments were closely related to modern Virgin River sources. Muntean (2012) and Dickinson et al. (2014) performed provenance analyses and dated zircons found within 6-4 Ma Muddy Creek Formation deposits. The age constraints on this Muddy Creek stratigraphy come from two separate basalts that intrude (?) or are interbedded with interpreted first arriving Virgin River gravels (6.02 Ma, Feuerbach et al., 1991; 4.1 Ma, Williams, 1996). The distribution of dated zircons were interpreted to provide evidence for the arrival of an ancestral river draining the CP across the Virgin Mountains at 6-4 Ma.

METHODS

Profile Analysis

Longitudinal profiles of the VR and 10 of its major tributaries were extracted from 10m resolution digital elevation models (DEMs) using ArcGIS. Distances of river profiles were calculated starting at the historic (pre-dam) confluence of the VR and CR

as mapped by Birdseye (1924). Observation of knickpoints (oversteepened segments of the river profile) and varying stream gradients were quantified using Topotoolbox in MatLab to calculate normalized channel steepness values (k_{sn}) from a USGS 30 meter digital elevation model (DEM) of the entire drainage basin. 10 meter DEMs were not used to calculate k_{sn} values due to our limitations in computing power required. However, k_{sn} values extracted from 30 m DEMs are deemed sufficient (Kirby and Whipple, 2012; Rosenberg et al., 2014) to compare relative steepness values from one tributary to another and to quantify reaches such as knickpoints that are oversteepened relative to their position along the river profile.

k_{sn} values give the gradient of the streambed normalized by the upstream area at each location along the channel:

$$k_{sn} = \frac{S}{A^{-\theta_{ref}}},\qquad(1)$$

where S is the gradient, A is the upstream drainage basin area, and Θ_{ref} is the reference concavity index. This method uses upstream contributing area as a proxy for discharge so shallow gradients of large channels with high discharges can be compared to steeper gradients of headwater channels with lower discharges. Concavity is the measure of how gradient changes with respect to a changing drainage area. Reference concavities, average concavities within a region, are commonly used and range from 0.35-0.65 (Wobus et al., 2006). We use a reference concavity index value of 0.45 (Θ_{ref}), as opposed to a concavity value calculated from the regression of raw slope-area data of the Virgin landscape, to allow for comparison of our k_{sn} values to other basins with varying drainage areas (Kirby et al., 2003; Wobus et al., 2006; Kirby and Whipple,

2012; Rosenberg et al., 2014). The choice of this parameter does not strongly affect the comparisons we wish to make. To smooth out inconsistencies in stream segment elevations from cell-to-cell we use an average moving window of 1 km.

Knickpoints were quantitatively identified by calculating the difference between average k_{sn} values of upper and lower halves within 4, 10 and 20 km segments moving along the profile. We use different segment lengths to identify knickpoints at different scales. A knickpoint is identified if the difference between averaged upper and lower segments exceed 80 $m^{0.9}$. This cutoff value was chosen because it identifies and best represents the observed knickpoints on the longitudinal river profiles but also identifies knickpoints that are not visibly apparent (Fig. 3). We use k_{sn} values, instead of gradient, to take into consideration the concavity that is present in all river profiles as contributing drainage area, and discharge, increase downstream. Using gradient, instead of k_{sn}, identifies false knickpoints at the headwaters of all tributaries due to the natural upstream increase in slope.

To perform correlations among different datasets, data (k_{sn}, gradient, mantle velocity, rock type, and annual precipitation) were collected at 1 km intervals along the entire drainage system. This study performs an analysis of the correlation between upper mantle velocity and k_{sn} values along the Virgin River and its tributaries using 30-meter DEM instead of previously used 90-meter DEM (Crow, 2012). Low mantle velocities are suggestive of the presence of partial melt in buoyant and rheologically weaker and hotter mantle, which acts as a potential cause for uplift (Sine et al., 2008; Karlstrom et al., 2008; Schmandt and Humphreys, 2010). Rock type was also taken into consideration by classifying the rock type underlying each data point into slope and cliff forming

lithologies. The slope and cliff formers were identified based upon the unit descriptions found in geologic maps throughout the region (Billingsley and Workman, 2000; Billingsley and Wellmeyer, 2003; Sable and Herefore, 2004; Beard et al., 2007; Ludington et al., 2007; Biek et al., 2010). This study also compares average tensile strength measurements taken from the CR drainage (Bursztyn et al., 2015) and channel steepness within the VR drainage (this study). Bursztyn et al. (2015) provided average tensile strengths for seven formations (Navajo, Kayenta, Shinarump, Moenkopi, Kaibab, Esplanade, Redwall) found in common between the two drainages. Formation average tensile strengths measured along the CR were then compared to calculated formation average k_{sn} data along the VR. This analysis assumes tensile rock strength of a particular formation is consistent across the region in adjacent drainages. The underlying mantle velocities at the same data point locations that overlie the 7 formations were also used to search for a correlation between mantle velocity and channel steepness.

Magmatic Sweep

Previously published $^{40}Ar/^{39}Ar$ and K/Ar basalt ages throughout the eastern VR drainage system were compiled into Appendix A. $^{40}Ar/^{39}Ar$ ages were recalibrated using a modern Fish Canyon Tuff standard age of 28.201 Ma (Kuiper et al., 2008) and a decay constant of 5.543e-10/a (Min et al., 2000). An age distribution plot (Fig. 2) produced from the compiled basalt ages shows frequent magmatism over the past 15 Ma. An abundance of young (<1.5 Ma) low volume basalt flows in many places in southwestern Utah might obscure any trends in first arriving volcanism. Hence, we plot the age of initiation of basaltic magmatism in given sub-regions (similar to Crow et al., 2011). We use the oldest vent located within a 0.5 x 0.5 degree grid for analysis of

migration direction and rates. Magmatic migration rates were calculated by measuring distances between volcanic sources (e.g. cinder cones, vents) and dividing these distances by the difference in age between flows. The Lovell Wash member basalt flow (13.3 Ma) is the oldest flow in the study area with a known vent location and is located in the southwestern corner of the study area (Fig. 1). This basalt flow is used as the location and age from which all distances to other vents are measured and elapsed time to other flows are calculated. Some basalt flows in this region are known to have flowed for many miles. Using a location that is miles away from the basalt source may skew the data; therefore, some basalt flows are not taken into consideration in this analysis if the source location is unknown. The average magmatic migration rate is calculated as the slope of the age-distance regression line fit to the data.

Differential Incision

Our incision measurements are designed to understand bedrock incision in the erosional landscape of the CP. Thus, in relation to Pederson et al. (2002) and Karlstrom et al. (2007) we calculate heights of bedrock straths above the modern river (as opposed to bedrock strath below the modern river) and use best age constraints (primarily basalt flow ages) on overlying river deposits to give average bedrock incision rates (in m/Ma). The differential incision hypothesis posits that differential incision can be explained in terms of uplift of the faster incising reach relative to the more slowly incising reach (Karlstrom et al., 2007; Karlstrom et al., 2008). Assumptions within this hypothesis and alternative explanations for differential incision are explored carefully and include: 1) steady incision versus knickpoint transience, 2) headwater uplift vs downstream subsidence 3) rock type controls, and 4) climatic variability.

Steady incision versus transient knickpoint migration is tested in reaches that have multiple ages and heights of paleochannels or terraces. Headwater uplift rather than baselevel fall is tested using the VR-CR confluence as the datum. Howard et al. (2015) suggest the Colorado River has been graded to sea level since 4.5 Ma such that we infer there has been no major downstream alteration of baselevel in the last 4.5 Ma and that headwater uplift has been a major driver of differential incision. To analyze rock type controls, we assume all unit descriptions that include "cliff forming" rock types represent resistant lithologies while "slope forming" rock types represent less resistant lithologies. Climate can influence incision both spatially and temporally. We assume that by observing bedrock incision at the million-year time scale we are able to average out 100 ka glacial-interglacial cycles of incision and aggradation over the past 2.6 Ma. We use modern mean annual precipitation as a proxy for spatial variations in climate. We understand climate has changed through time and space; however, this is the best available dataset that can represent spatial variations at the scale of the Virgin River drainage.

We use recalibrated K/Ar and ^{40}Ar/^{39}Ar ages of basalts that cap perched gravels of the ancestral VR to quantify 'preferred' incision rates (Appendix B). Other basalt flows have elongated and sinuous outcrop geometries indicating they flowed down paleo-drainages even if river gravels have not been mapped directly beneath the flow. We use bases of flows as data points to calculate 'approximate' incision rates. Each basalt flow tells a different story and all flows were analyzed independently when calculating incision rates. The majority of heights used in incision rate calculations for the VR and its tributaries were estimated from 1:24,000 scale quadrangle maps and

Google Earth while others were measured in the field using a laser range finder. Following the methods of Crow et al. (2014), heights measured from quadrangle maps and a laser range finder are given uncertainties of ±10 m and ±2 m, respectively. Heights at 'preferred' locations were measured from the top of the bedrock strath beneath the ancestral river gravels to the current river/tributary elevation to quantify bedrock incision. 'Approximate' rates from flows were measured from the contact between the basalt flow and the underlying bedrock to the current river/tributary elevation as used by Willis and Biek (2001; Grant Willis, personal communication, 2016).

Averages of incision rates within structural blocks were calculated using the slope of a best-fit linear trendline among the incision points that lie ≥5 km away from major faults. Crow et al. (2014) estimated a distance of 10 km to be sufficient to eliminate differential incision observed along the Colorado River due to localized flexural influences (e.g. hanging wall anticline, footwall uplift) and more closely record regional block uplift amounts. Along the Virgin River, we observe a stabilization of incision rates ~5 km away from major faults. In the Zion block, decreased incision rates near the headwaters of VR tributaries were excluded from regional uplift calculations because these points represent geomorphic controls, as headwater reaches do not have sufficient stream power to fully incise and represent block uplift. A decrease in incision rates near headwaters is expected in all tributaries and is observed in Appendix D. One outlying data point along Fort Pearce Wash with an abnormally low incision rate (incision point 1, Appendix B) in comparison to other rates on the Zion Block was also excluded from the average block calculations. This point can potentially be explained by a lack of discharge/precipitation, lack of uplift, or some combination of the two

controlling factors. The St. George and Hurricane blocks were combined when calculating averages due to the lack of basalt flows that exist in the Hurricane block > 5 km from any major fault. Only one flow exists in the Hurricane block that complies with these criteria and therefore a trendline could not be drawn to calculate the slope.

Provenance Analysis

Understanding the source of ancestral VR gravels throughout its history as a major river system is key for understanding the evolution of the drainage system. Field observations of gravel clasts in Grand Wash Trough greatly influenced our understanding of a proposed model of the Virgin River evolution. We collected 3 samples of first arriving ancestral VR gravels in the upper Muddy Creek Formation. Two of these samples are from locations that had previously been analyzed for detrital zircons (Forrester, 2009; Muntean, 2012; Dickinson et al., 2014) and by clast counts (Forrester, 2009; Muntean, 2012). $^{40}Ar/^{39}Ar$ dating of sanidine grains instead of zircons allows for much more precise ages and can help understand the exact source of ancestral river deposits. From these samples, sanidine grains were concentrated using heavy liquid mineral separation techniques and approximately 150 sanidine grains were handpicked from each density separate using index of refraction. Sanidine grains were distinguished from plutonic K-feldspar by their optical clarity and lack of twinning when viewed in spearmint oil. $^{40}Ar/^{39}Ar$ dating of individual sanidine grains was performed by single crystal laser fusion with a CO_2 laser and was measured on an ARGUS VI noble gas mass spectrometer at the New Mexico Geochronology Research Center. Additional details can be found in Appendix C.

RESULTS

Profile Analysis

The nested longitudinal profile of the VR and its major tributaries are shown in Figure 3 and are divided into 3 unique groups of rivers: 1) main-stem VR (including Deep Creek and North and East Forks), 2) Colorado Plateau –Transition Zone tributaries, and 3) Basin and Range tributaries (Appendix E). These groups are described here and will be interpreted in terms of age and history, later in this paper.

Nineteen knickpoints were identified throughout the VR drainage system (Figs. 1 & 3). Once oversteepened reaches (knickpoints) are identified (Table 1), interpretation of their significance can be guided by correlations between knickpoint locations and possible controlling factors such as rock type, differential incision patterns and possible tectonic forcings such as faults (Ouimet et al., 2009). Crow (2012) noted a difference in average k_{sn} values between Deep Creek (~130 $m^{0.9}$) and East Fork (~90 $m^{0.9}$) tributaries of the upper VR. We analyzed these and two additional tributaries, La Verkin Creek and Fort Pearce Wash, for possible spatial associations with climatic, rock type and tectonic parameters. Figure 4 shows the profiles color-coded for mean annual precipitation (Fig. 4A). La Verkin Creek, Deep Creek and East Fork Virgin River are all south flowing tributaries sourced in higher elevation, wetter regions near Zion National Park and show similar precipitation amounts; Fort Pearce Wash drains the lower and dryer Hualapai Plateau on the south side of the mainstem VR. There is no observed correlation of higher normalized channel steepness with annual precipitation. Figure 4B shows changing lithology along the profiles in terms of rock erodibility as manifested by cliff forming versus slope forming rock types. More resistant cliff forming lithologies seem to be

24
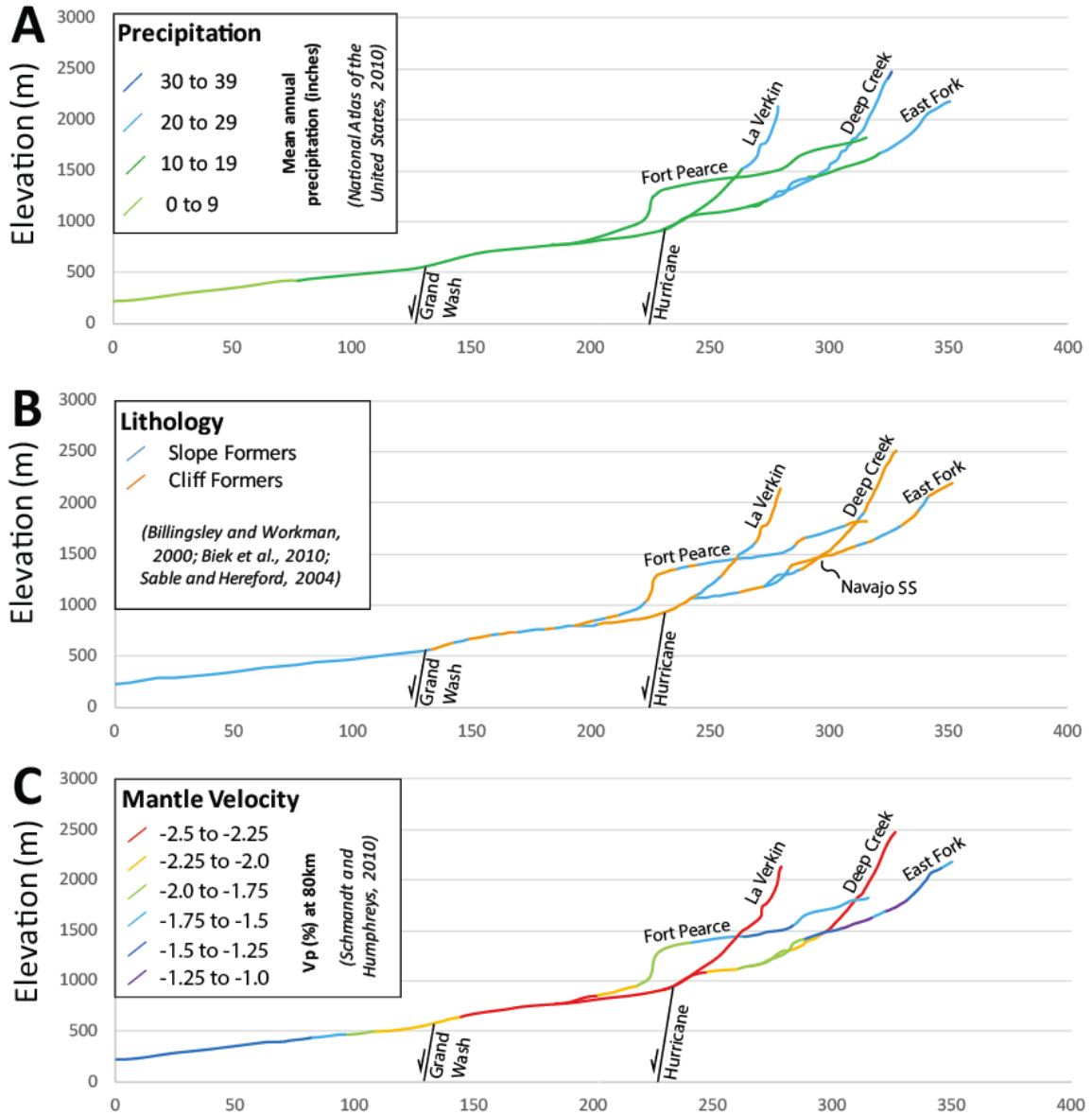
Figure 4. Longitudinal river profiles of the Virgin River and 4 of its tributaries (after Crow, 2012) located on the Zion block with respect to A) mean annual precipitation, B) lithology, and C) underlying p-wave upper mantle velocities at a depth of 80 km. Note the lower gradient streams are underlain by higher velocities and steeper streams are underlain by lower velocities.

associated with knickpoints and steeper tributaries to some extent, but the difference in gradient between Deep Creek and East Fork is not readily explained by rock type as the same mixture of units occurs in both tributaries. Figure 4C shows possible tectonic forcings. Mantle velocity differs greatly below the steeper gradients of La Verkin Creek and Deep Creek, which are underlain by low velocity mantle, and the shallower gradients of Fort Pearce Wash and East Fork Virgin River, which are underlain by high velocity mantle.

A regional "wedge" plot of Vp vs k_{sn} along the main-stem Virgin River and the CP-TZ tributaries is shown in Figure 5A. Three separate trends can be regressed depending on how much credence is put on highest k_{sn}, versus background, data. All three regressions show an increase in max k_{sn} as mantle velocity decreases, similar to that shown by Crow et al. (2012). Highest k_{sn} points reflect steepest portions of knickpoints as the VR and its tributaries cross major faults or lithologic contacts. The intermediate regression reflects steep reaches between knickpoints, and the background data show modest increase in channel steepness in areas above low velocity mantle. Figure 5B considers lithologic erodibility and shows that, rather than high k_{sn} values being associated with cliff forming bedrock, there is a wide range of k_{sn} values in both slope and cliff forming rock types. Figure 5C also shows a lack of strong correlation between normalized channel steepness and annual precipitation amounts. A summary table of k_{sn} values on the main-stem VR and the Colorado Plateau – Transition Zone tributaries (Fig. 5D) shows that the average k_{sn} in tributaries underlain by low velocity mantle (delta Vp < -1.9) is about 70% greater ($100.85 \ m^{0.9}$) than the average k_{sn} in areas underlain by high velocity mantle (delta Vp > -1.89) where k_{sn} averages $59.07 \ m^{0.9}$. k_{sn} is also higher in

A

Ksn (m^0.9) vs Vp (%) at 80 km depth

B Lithology — Cliff, Slope

Ksn (m^0.9) vs Vp (%) at 80 km depth

C Precipitation — 0-10 in/yr, 15-30 in/yr

Ksn (m^0.9) vs Vp (%) at 80 km depth

D
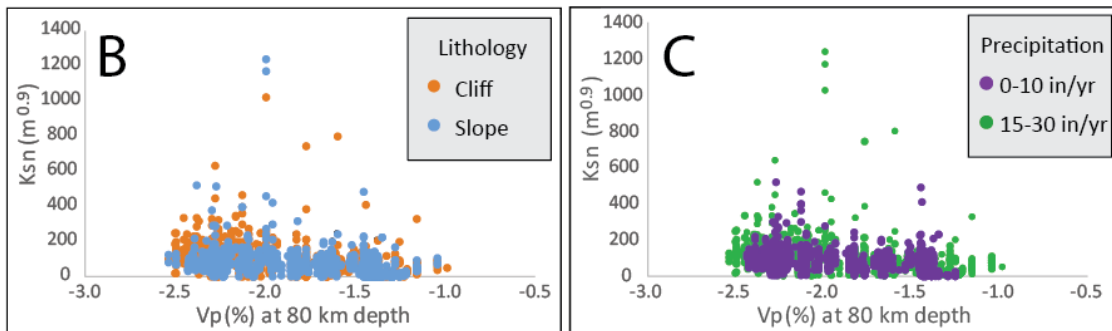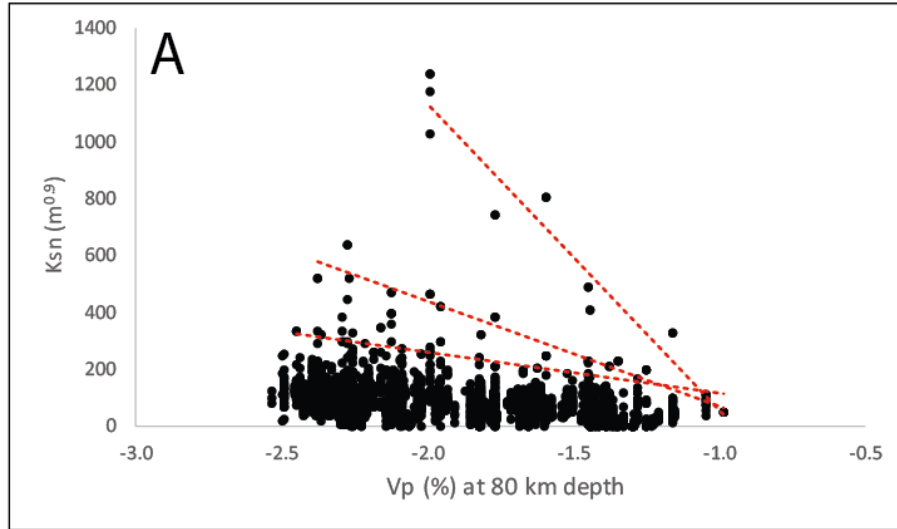
Summary of Ksn Controls						
	Mantle Velocity		Lithology		Precipitation	
	< -1.90 (n = 1222)	> -1.89 (n = 1221)	Slope (n = 1277)	Cliff (n = 1166)	0-10 in. (n = 1122)	15-30 in. (n = 1321)
Average ksn ($m^{0.9}$)	100.85	59.07	70.15	90.72	77.37	82.18
Median ksn ($m^{0.9}$)	86.73	50.56	58.37	79.92	73.10	67.54
% Increase in Average Ksn ($m^{0.9}$)	70.7%		29.3%		4.80%	
% Increase in Median Ksn ($m^{0.9}$)	71.5%		36.9%		-5.56%	

Figure 5. A) Scatter plot showing correlations between calculated k_{sn} values and p-wave upper mantle velocities at 80 km depth (after Crow, 2012). Data was collected from points every 1 km along the Virgin River and its tributaries within the eastern lobe of the watershed. B) Figure 5A with data points grouped by basic lithologic properties shows a wide range of k_{sn} values exist within both cliff and slope forming rock types. C) Figure 5A with data points grouped by mean annual precipitation shows a wide range of k_{sn} values exist within both high and low precipitation averages. D) A summary table showing average and median k_{sn} values for each subset of data points along with the percent increase between upper and lower calculated values.

27

cliff forming (90.72 $m^{0.9}$) versus slope forming (70.15 $m^{0.9}$); however, this is only a

~30% increase. Differences among areas of high precipitation (15-30 in/yr) and low

precipitation (0-10 in/yr) show only a 5% increase from average k_{sn} values of 82.18 $m^{0.9}$

and 77.37 $m^{0.9}$, respectively. Therefore, correlations exist among all potential k_{sn} controls

within this analysis (e.g. mantle velocity, lithology, and precipitation); however, we see

the largest correlation with mantle velocity. Figure 6A plots rock tensile strength from

Bursztyn et al. (2015) against average k_{sn} values for seven Paleozoic and Mesozoic units

within the VR drainage and shows no correlation ($R^2 = 0.004$). In contrast, Figure 6B

shows a strong correlation ($R^2 = 0.98$) between mantle velocity and k_{sn} regionally when

Vp is plotted against binned average k_{sn} for different mantle velocities.
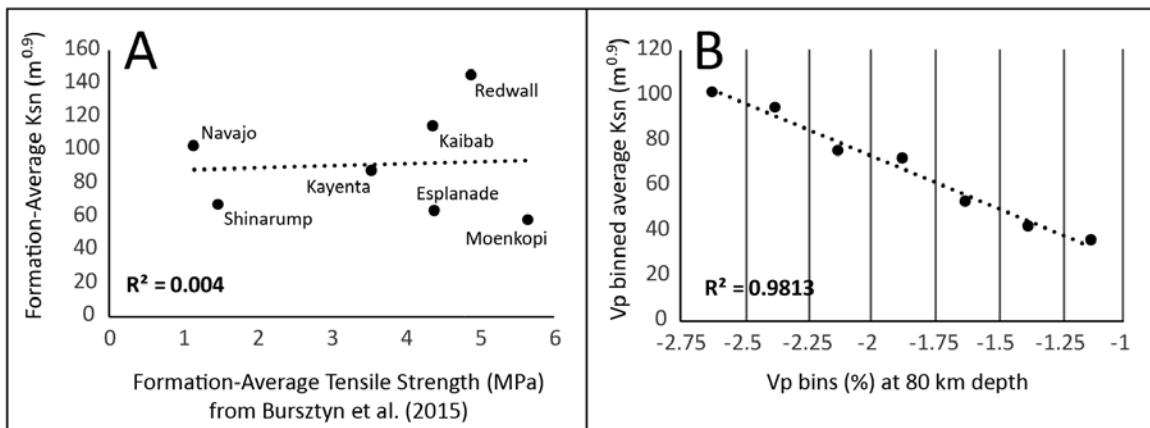
Figure 6. A comparison of bedrock lithology and upper mantle velocities as a control on k_{sn}. Data was used from the 7 formations found in common between study areas of Bursztyn et al. (2015) and this research. A) Formation average k_{sn} of this research with respect to formation average tensile strengths of Bursztyn et al. (2015) give an R^2 value of 0.004. B) Average k_{sn} of 0.25% binned upper mantle p-wave velocities give an R^2 value of 0.981. This analysis assumes that average rock strength of a particular rock formation along the Colorado River is similar to average rock strength of the same formation along the Virgin River.

Magmatic Sweep

An analysis of ages and locations of basalt flows in northwestern Arizona, southern Nevada, and southwestern Utah shows a northeast-trending migration of Cenozoic volcanism (Fig. 7). Many flows have long run-outs along paleodrainages such that we plotted only vent locations. Contouring the oldest vent ages within each 0.5 x 0.5 degree grid shows a strong northeastward younging trend (yellow stars) which is also seen when all known vent ages are plotted (red dots) (Appendix F). Best et al. (1980) and Wenrich et al. (1995) calculated a NE-migration rate of 12 km/Ma in western Grand Canyon. This study includes basalt flows throughout the Lake Mead area and the eastern lobe of the Virgin River drainage (SW Utah) to acquire newly calculated migration rates. Our migration rates calculated from all vent locations and oldest vent locations (first arriving flows) in each sub-region are higher and range from 15.8 to 17.8 km/Ma with R^2 values of 0.738 and 0.965, respectively.

Differential Incision

Incision rates vary spatially along the VR and its major tributaries at both local and regional scales (Appendix G). Small transient knickpoints may have swept through the drainage system throughout the last 5 Ma, however, our calculated incision rates show quasi-steady incision through time within each structural block. Figure 8 shows incision vectors along the profile scaled to rate (in m/Ma) for two time periods, 0.9-0.2 Ma and 4-1 Ma. Even the short-term rates are averaged over 200 ka and hence span more than one glacial-interglacial oscillation such that we interpret them to reflect realistic estimates of bedrock incision (c.f. Karlstrom et al., 2013; Pederson et al., 2013). Variations in bedrock incision (differential incision) occurs dramatically at local scale, immediately across
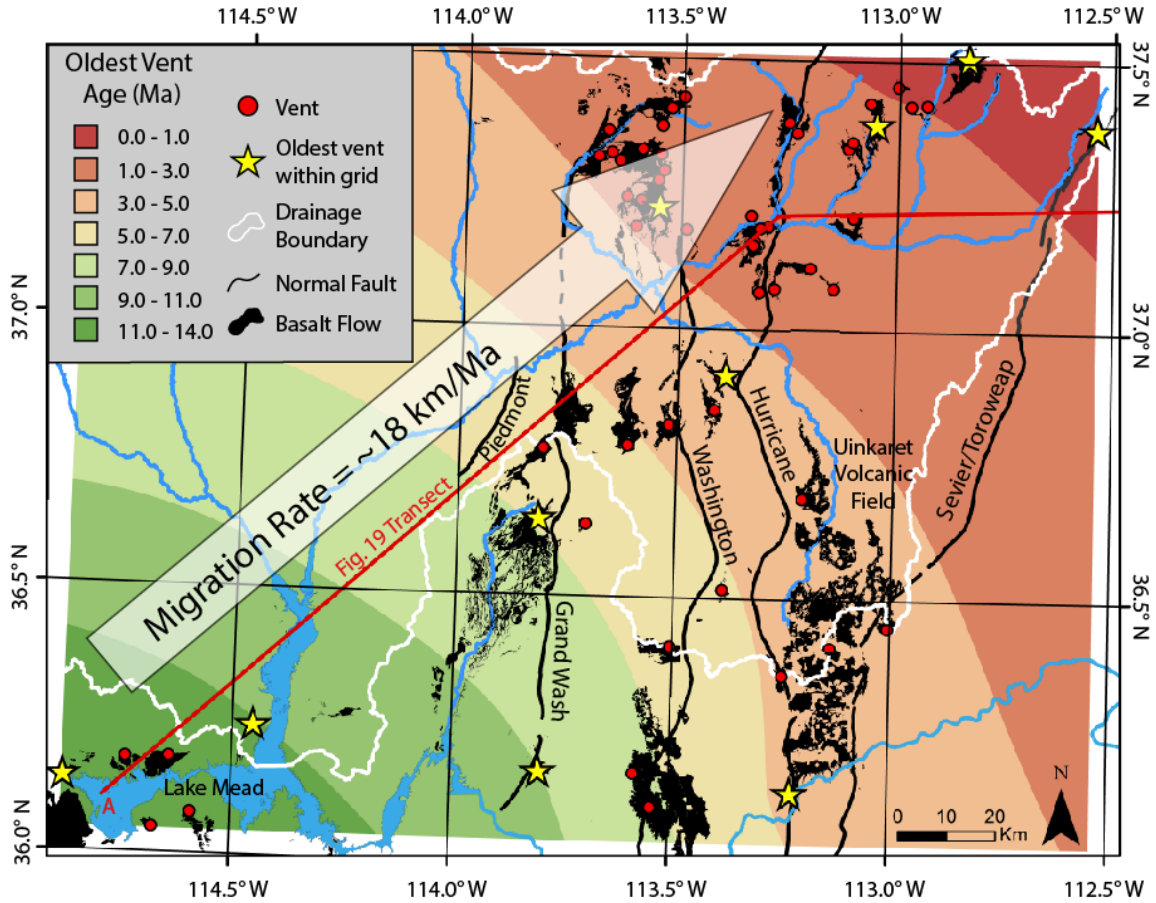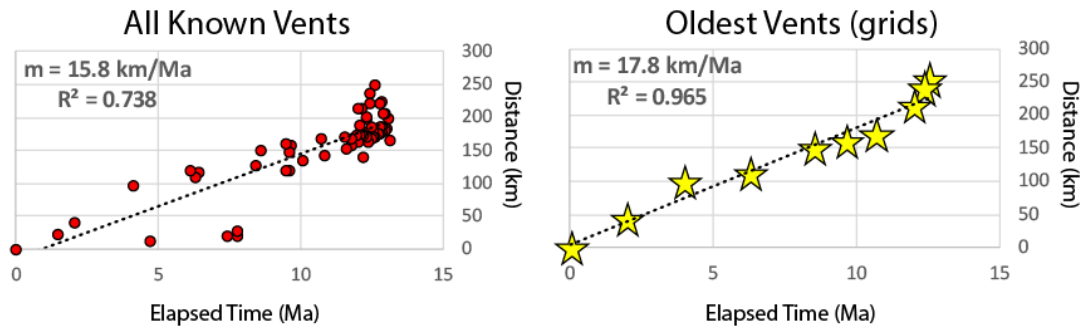
Figure 7. A contour map of the oldest vent ages throughout the southeastern Virgin River drainage system showing the migration path of the onset of basaltic volcanism. The contours were generated using the 'Topo to Raster' interpolation method in ArcGIS. Red points represent locations of known basaltic vents while yellow stars represent the location of the oldest dated vent within each 0.5 x 0.5 degree grid. The white arrow shows the general migration path of the basalts based on the contours. Two plots used to calculate migration rates of all known sources and the oldest sources within each grid. The oldest sources within each grid are used to observe the onset of magmatism through time. Strong trends appear in all plots showing a strong general northeastward march of magmatism at ~18 km/Ma.
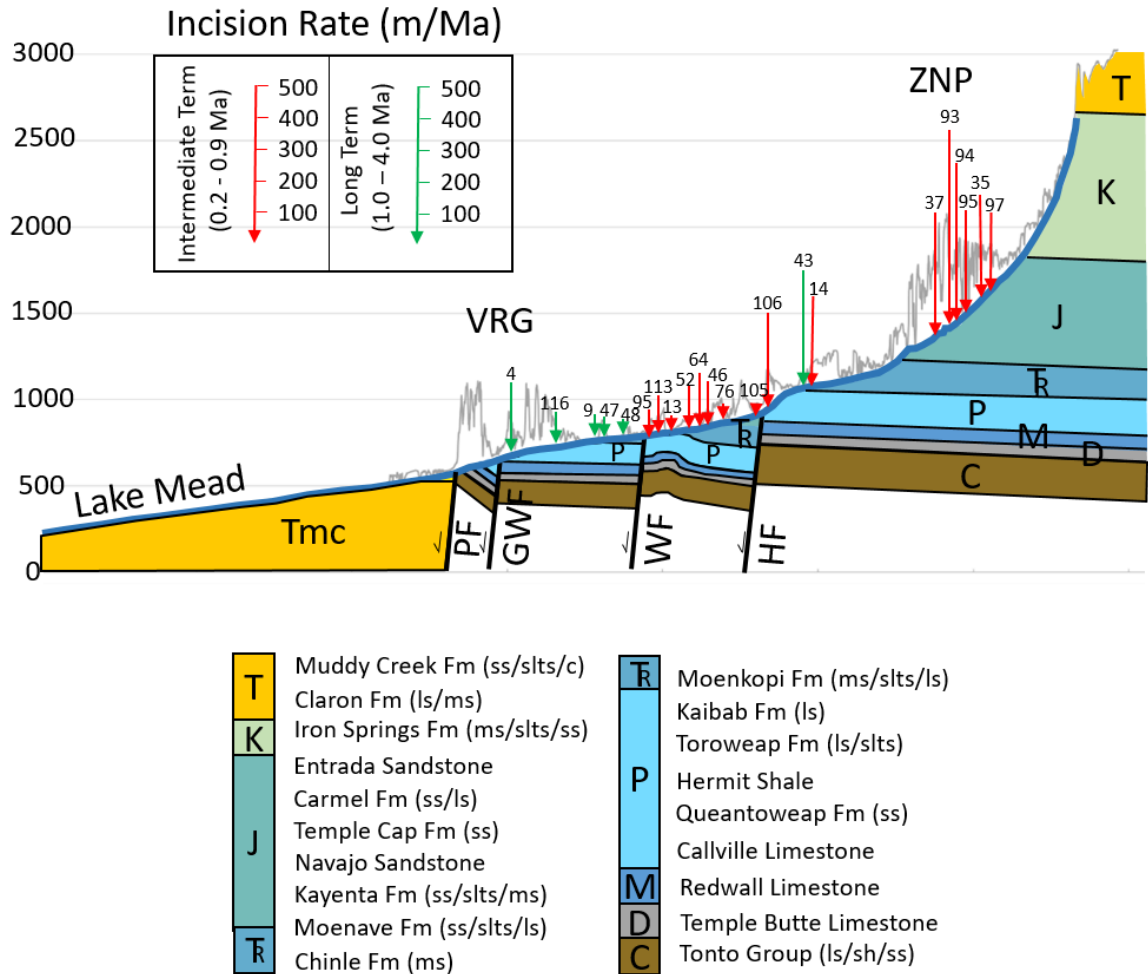
Figure 8. North Fork Virgin River profile with the substrate lithology as it flows across major normal faults. Gray line above the river profile represents the topography of the immediate landscape ~500 m from the river. Red and green arrows show intermediate (0.2-1.0 Ma) and long term incision rates (1.0-4.0 Ma), respectively. Numbers above each arrow correlate with the incision rate data point located in Appendix B. VRG—Virgin River Gorge; ZNP—Zion National Park; PF—Piedmont Fault; GWF—Grand Wash Fault; WF—Washington Fault; HF—Hurricane Fault.

faults. For example, Volcano Mountain lava flow (0.353 Ma) was emplaced across the Hurricane fault and provides an excellent example of fault-dampened incision. Incision rates in the hanging wall near the Hurricane fault decrease from 110 m/Ma at 5 km west of the fault (incision point 64), to 0 m/Ma at the fault (incision point 105) over the same time period. We use the term 'apparent' incision rates when flexure near the fault appears to account for variation in incision rates. Our observations are compatible with Crow et al. (2014) who noted such variations due to fault-related flexure are greatest within 5-10 km from the trace of the fault. Calculated incision rates of the same flow (Volcano Mountain) increase to 304 m/Ma on the upthrown footwall (incision point 106) directly east of the fault. But on the east side, the calculated incision rate of 304 m/Ma (incision point 106) is similar to the average regional block incision rates (338 m/Ma) of data points farther east, >5km away from the fault trace, suggesting limited footwall flexure where the VR crosses the Hurricane fault. In contrast, in La Verkin Creek tributary ~20 km north of the VR, apparent incision rates along the footwall of the Hurricane fault increase to 782 m/Ma (incision point 66) suggesting substantial footwall flexure at this location.

Given the large number of high quality incision points made possible by all the dated basalts in the Virgin River area (Appendix B), it is possible to separate out differences in average incision rate within blocks using only rates >5km away from major faults and regress these through time in each block (Fig. 9A). Average incision rates, excluding local fault related deformation and headwater erosion effects, show a regional increase in average incision rates eastward from block to block from 23 m/Ma in the Lake Mead block, to 85 m/Ma in the combined St. George and Hurricane block, to 338

m/Ma in the Zion block (Fig. 9B).
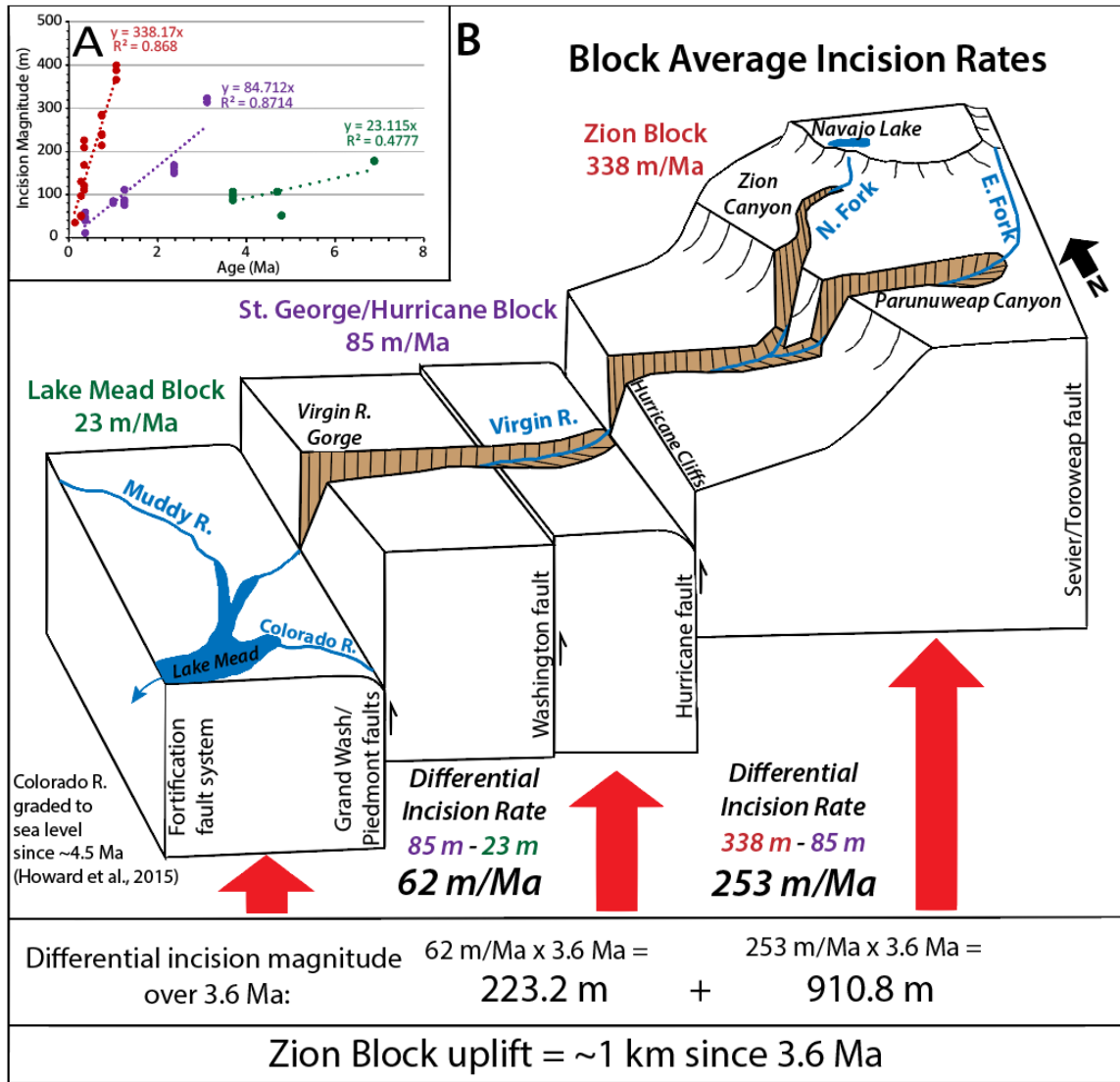
Figure 9. A 3D block model of the Virgin River as it flows across 4 structural blocks. Incision rates shown represent average incision rates of structural blocks within the Virgin drainage excluding data points within a 5 km distance to major faults. A) Data points used to calculate average incision of 3 blocks: Zion (Red), St. George and Hurricane combined (purple), and Lake Mead (green). Slope of trendlines were used as average incision rates. B) Simplified block diagram showing incision and epeirogenic uplift of each block.

Basalt paleoprofiles

Basalts flowed into and preserved segments of paleodrainages that inform the evolution of the tributary system for the VR. Grand Wash drains the eastern Virgin Mountains to the CR and was filled with basalt at 4.71 Ma (Beard et al., 2007). Basalts overlie gravels that are well rounded, with clasts similar to those found in the upper Muddy Creek conglomerate in the Virgin Depression, including yellow and purple quartzites that resemble clasts from the Canaan Peak Formation (Goldstrand, 1992, 1994). The paleoprofile of the Grand Wash basalts (Fig. 10) is quite similar to the present day profile of Grand Wash with a minor downstream divergence of the two profiles. However, Howard and Bohannon (2001) show that this basalt flow has been downfolded due to the formation of a hanging wall anticline along the Wheeler fault. This tributary incision rate, at incision points >5km away from the fault trace, varies from 11 m/Ma to 23 m/Ma and is compatible with the Lake Mead block average rate of (23 m/Ma).

The 3.7 Ma Black Rock Mountain basalt erupted from a vent near the divide between VR and paleo Grand Wash. It flowed northward into Virgin Gorge and southward into Grand Wash Trough in the hangingwall of Grand Wash fault (Fig. 11). The two profiles of Figure 11B compare north and south paleodrainages taken from the basalt flow and the nearest modern drainages. The profiles generally form concave up longitudinal profiles and the paleodivide, represented by multiple vents, has remained at a similar location and elevation for the past 3.7 Ma. The slope of the southern drainage has remained similar and there has been minor amounts of relief generation (~100 m) in the past 3.7 Ma giving tributary incision rates of 27 m/Ma compared to Lake Mead block average rate of 23 m/Ma seen in Figure 9. The slope of the northern drainage has
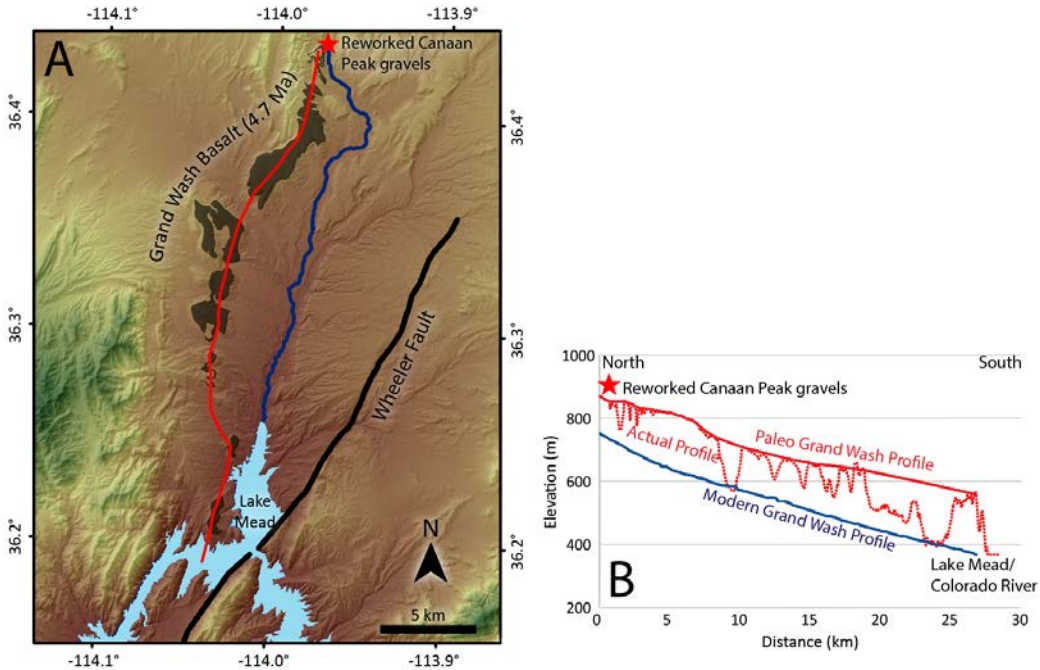
Figure 10. A) A DEM of lower Grand Wash Trough showing the extent of the Grand Wash basalt. B) A profile analysis showing the modern Grand Wash profile (blue) in comparison to a paleo Grand Wash profile (red), which was constructed using the top of the southward flowing Grand Wash basalt flow dated at 4.72 Ma.
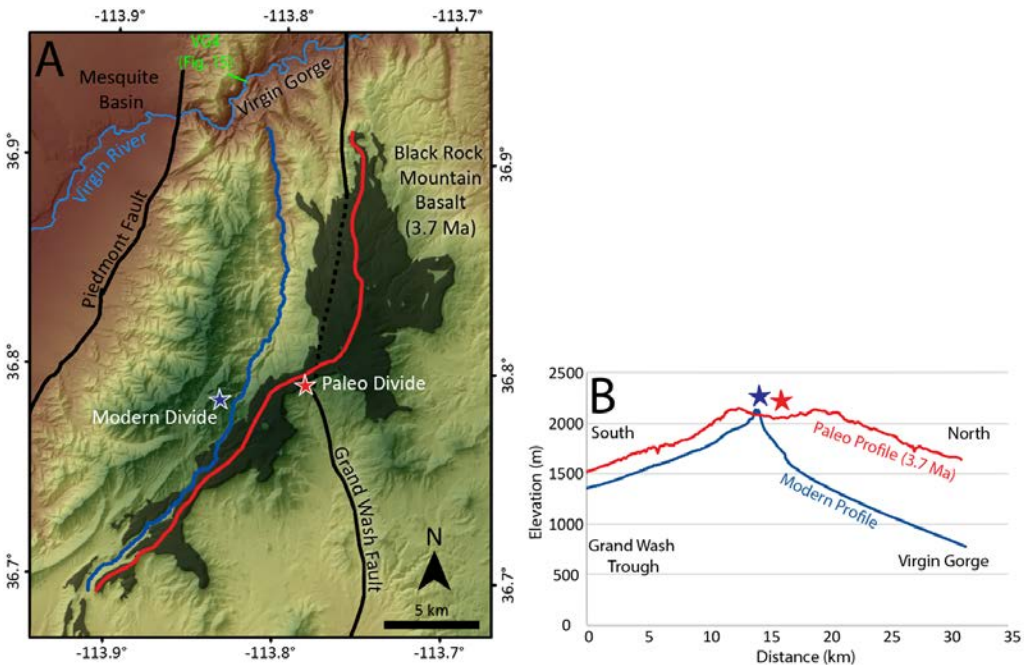
Figure 11. A) A DEM of the southern rim of the Virgin River Gorge showing the extent of the Black Rock Mountain basalt. B) A profile analysis showing the modern profile of Cottonwood Wash and Sullivan canyon (blue line) along with the current drainage divide (blue star), in comparison to a paleo profile (red line), which was constructed using the top of the south and north-flowing Black Rock Mountain basalt flow dated at 3.7 Ma. Notice the large difference in relief production between the north and south flowing tributaries from 3.7 Ma to present.

steepened with high amounts of relief generation (~850 m) in the past 3.7 Ma and average incision rates of 230 m/Ma indicating substantial footwall uplift adjacent to the Grand Wash fault in this locality as this rate is about 3 times the block average (85 m/Ma) shown in Figure 9.

Provenance Analysis

The upper Muddy Creek conglomerate (first arriving VR gravels) consists of yellow and purple quartzite, volcanics, carbonates, black chert, and chert litharenite. These gravels overlie fine-grained sediments of the Muddy Creek Formation and record the birth of a major high-energy VR system entering the Mesquite basin (Williams, 1996; Forrester, 2009; Muntean, 2012). In one location, these gravels appear to be "interbedded" with a small outcrop (about 15 x 15 meters) of 4.1 Ma basalt near Mesquite, NV (Williams, 1996) leading to the tentative assignment of this age to the birth of the Virgin River.

Age distribution plots (Fig. 12B) of zircons show distinctly different curves between lower Muddy Creek (sandstone and siltstone) and upper Muddy Creek paleo-VR (conglomerate and sandstone) samples (Forrester, 2009; Muntean, 2012). The lower Muddy Creek curve has a much broader peak ~ 20 Ma with small peaks at 14, 17, and 19 Ma. The upper Muddy Creek zircon samples show a sharp peak around 20 Ma with a few younger grains at 13 Ma. Potential sources of these zircon grains are listed in Figure 12A. A Kolmogorov-Smirnov (K-S) test (Dickinson and Gehrels, 2008) between the two datasets gives a calculated p-value of 0.00036 indicating a >95% confidence level that the parent sources of the upper and lower Muddy Creek deposits are statistically

distinguishable. Therefore, the upper and lower Muddy Creek deposits came from different sources. Potential source locations along with detrital zircon/sanidine sample locations are mapped in Figure 13.

We analyzed detrital sanidine from three samples of first-arriving VR gravels of which DZ analyses at two of these locations have previously been published (Fig. 12). An age distribution curve of the 3 combined DS samples shows four distinct peaks at 13.72 Ma, 18.68 Ma, 20.56 Ma and 23.8 Ma (Fig. 12C). The precise ages of the two highest peaks shows evidence for two different sources as opposed to the single peak at ~19 Ma shown by the detrital zircon data (Fig. 12B). Two grains at about 5.9 Ma gives a maximum depositional age of these first arriving VR gravels. Additional observations found within the 3 detrital sanidine samples show a potential change of provenance between the base and top of the upper Muddy Creek Formation (Appendix H). Performing a K-S test on these two datasets also gives a p-value <0.05 which suggests a >95% confidence level that the parent sources are statistically different.

INTERPRETATIONS

Profile Analysis

Of the 19 identified knickpoints, six of them (B, D, L, M, O and Q) are interpreted to represent steady-state knickpoints caused by repeated young slip across major faults. Knickpoints C, F, G, N, and S are interpreted to represent lithologically controlled steps in the longitudinal profile; C at the resistant Kaibab Formation within the Virgin Anticline, F at the contact of Kayenta and Navajo Formations, and G, N, and S reflecting basalts in the channel. Knickpoint H formed as a result of the Sentinel landslide, ~4.8 ka (Grater, 1945; Castleton, 2016). Knickpoint H may also hide a

Figure 12. Detrital Provenance Analysis. A) A compilation of potential igneous sources local to the Virgin River region (modified from Dickinson et al., 2014). Ages compiled from multiple sources: Indian Peak Caldera – Best et al., (1993, 2013); Caliente Caldera – Best et al., (1993, 2013); Kane Springs Wash Caldera – Novak (1984); Marysvale Volcanics – Rowley et al. (1994); Pine Valley – Hacker et al. (2007), Biek et al., (2010). B) Age distribution plot of previously published detrital zircon grains (Muntean, 2012; Forrester, 2009) separated into two curves, upper and lower Muddy Creek Formation, which show a change in headwater source through time. C) An age distribution plot of 328 detrital sanidine grains (this study) of the upper Muddy Creek formation. More precise ages from $^{40}Ar/^{39}Ar$ dating of sanidines clarifies that the single peak of detrital zircon data at 19-20 Ma is actually from two distinct sources at 18.68 and 20.56 Ma.
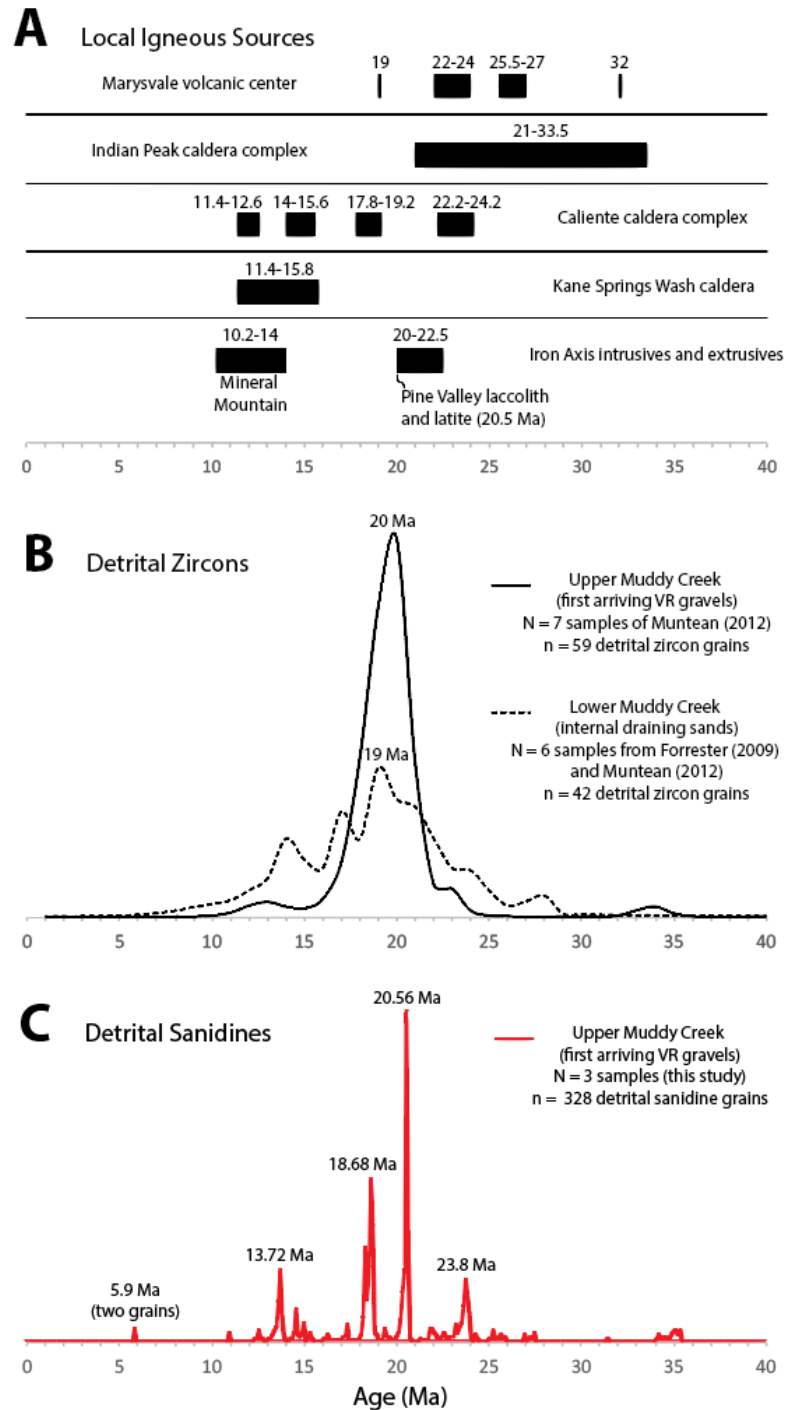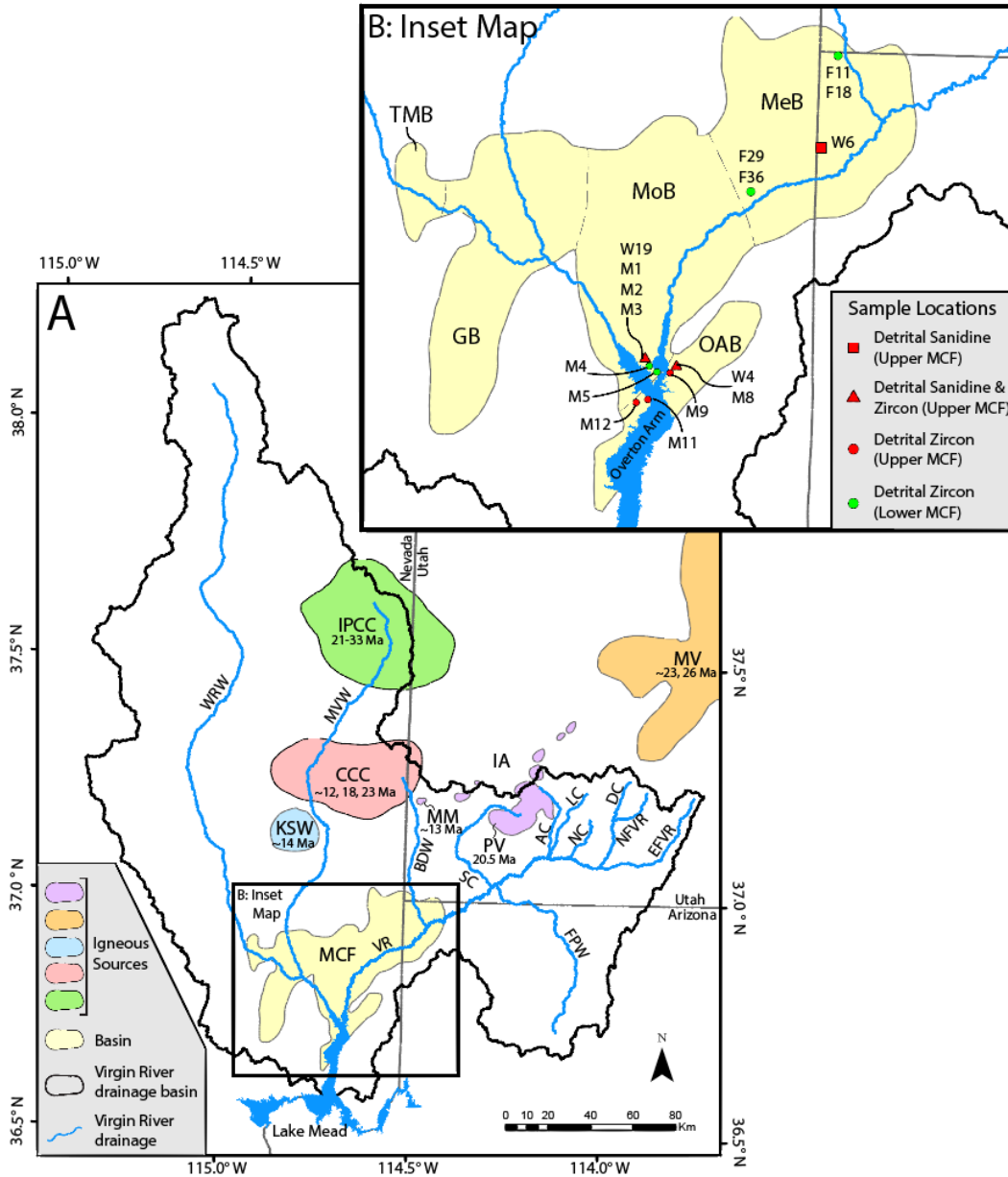
Figure 13. Detrital analysis of the Muddy Creek Formation. A) Regional map showing the locations of potential igneous sources found within the Muddy Creek Formation. IPCC – Indian Peak Caldera Complex; CCC – Caliente Caldera Complex; KSW – Kane Springs Wash caldera; MM – Mineral Mountain; PV – Pine Valley laccolith; IA – Iron Axis intrusives and extrusives; MV – Marysvale Volcanics; MCF – Muddy Creek formation. Tributaries include: WRW – White River Wash, MVW – Meadow Valley Wash, BDW – Beaver Dam Wash, SC – Santa Clara River, FPW – Fort Pearce Wash, AC – Ash Creek, LC – La Verkin Creek, NC – North Creek, DC – Deep Creek, NF – North Fork Virgin River, and EF – East Fork Virgin River. B) Inset map of the Muddy Creek formation showing the locations of key detrital samples from Forrester (2009) (F11, F18, F29, F36), Muntean (2012) (M1-M5, M8-M9, M11-M12) and this study (W4, W6, W19). The Muddy Creek formation fills five separate basins in this region: TMB – Table Mesa basin, GB – Glendale basin, MoB – Mormon basin, OAB – Overton Arm basin, MeB – Mesquite basin.

knickpoint similar to F, which should be found on the North Fork Virgin River (Appendix I). Three knickpoints (K, P, and R) within this study are anthropogenic in nature and represent dams at Ash Creek, Gunlock, and Baker Reservoirs, respectively.

Possible tectonic influences on channel steepness include both faults and epeirogenic uplift above mantle low velocity zones. Fault-related knickpoints across the Hurricane and Toroweap faults are not seen in Grand Canyon (Karlstrom et al., 2012; Crow et al., 2014) possibly due to higher stream power of the CR and/or lower recent slip rates. Landslides are common in rapidly uplifting environments however, we assume their effects to tributary profiles and incision rates at the millions of year's timescale to be minor in this region. The largest known landslide in the Zion Plateau area is the Sentinel landslide (Grater, 1945; Castleton, 2016). Castleton (2016) shows the knickpoint produced by the Sentinel landslide has greatly reduced in the last 4.8 ka as the Virgin River has incised through ~130 meters of the original ~180 meters of debris. VR tributary profiles show evidence of a disequilibrium landscape with deeply incised slot canyons and convex-up knickpoints on the Zion Plateau. Deep, narrow canyons form where the Virgin River North and East Forks incise through the resistant, cliff forming, Navajo Sandstone. Rock erodibility clearly influences channel steepness (Pederson and Tressler, 2012; Bursztyn et al., 2015). However, our k_{sn} results show a much stronger correlation with low velocity mantle (Fig. 6). Therefore, we propose that both rock type and ongoing uplift above upwelling mantle influence the Virgin River profiles with the latter being the dominant driver for the observed difference in steepness between North Fork/Deep Creek and East Fork tributaries (Fig. 4c; Crow, 2012).

Magmatic Sweep

The migration path of basaltic volcanism followed a general northeast direction at a rate of ~18 km/Ma (18 mm/yr) from the Lake Mead basalts to the East Fork Virgin River basalts. This parallels the general southwest vector of North American absolute plate motion at a similar rate of ~20 mm/yr relative to the asthenosphere (Minster and Jordan, 1978; Gordon and Jurdy, 1986). The correlation of steepest normalized stream gradients with underlying low velocity mantle and the sweep of young basaltic volcanism that involves mixed lithosphere and asthenosphere sources (Crow et al., 2011) leads us to interpret that the sweep of magmatism is related to upwelling asthenosphere, lithospheric removal/modification, basalt extraction, and buoyancy-driven uplift above zones of low velocity mantle.

Differential Incision

Spatially variable and temporally quasi-steady incision rates is a key observation that is helpful in determining potential drivers of differential incision. We interpret the observed quasi-steady incision rates through time to represent persistent regional uplift. Temporally unstable incision rates would suggest transient knickpoints that would be better explained by geomorphic controls. We observe transient knickpoints only at headwater locations as the Virgin River extends its reach into the uplifting Zion Plateau. However, incision rates show quasi-steady incision within each structural block at all downstream reaches after the headwater transience has passed through. (Fig. 9A)

Decreased apparent incision rates within 5 km of major normal faults (most pronounced on the down-dropping hanging wall) are interpreted to represent flexural responses such as hanging wall anticlines. Once these effects are "removed", summing

the differential incision between blocks multiplied by the duration of fault slip (3.6 Ma for initiation of Hurricane Fault; Billingsley and Workman, 2000) gives a total magnitude of CP incision of 1134 m (62 m x 3.6 Ma + 253 m x 3.6 Ma = 1134 m; Fig. 9) in the past 3.6 Ma. This assumes steady incision rates over 3.6 Ma in all three blocks, which is supported in Lake Mead and St George/Hurricane blocks by the incision rate data through time (inset to Fig. 9). Steady incision of the Zion block is only demonstrated for the past ~1 Ma. The Lava Point basalt flow (1.06 Ma) gives an incision rate of ~400 m/Ma. Biek et al. (2003) projected the Virgin River profile upstream from this point to find the elevation of the ancestral Virgin River near Zion Lodge in Zion National Park would be about halfway between the base and top of the present Zion Canyon. Assuming a steady incision rate, they inferred that headward erosion could have formed the present Zion Canyon in the past two million years while a similar canyon extended downstream near Virgin, UT. Assuming the Zion block has only been incised for 2 Ma gives us a minimum incision magnitude of 730 m (62 m x 3.6 Ma + 253 m x 2 Ma = 730 m).

We report differential incision magnitudes over 3.6 and 2.0 Ma time spans as maximum (1134 m) and minimum (730 m) values, respectively, while suggesting 1134 m of incision as the more accurate magnitude. Using a 2 Ma age as the amount of time at which these uplift rates have existed might only be appropriate at the present day Zion Canyon location. However, our goal is to discover the amount of time in which incision/uplift has been occurring throughout the Zion block. With the assumption that differential uplift will not occur without faulting, uplift of the Zion block has a maximum age, constrained by the Bundyville basalt (Billingsley and Workman, 2000), of 3.6 Ma. With both the Lake Mead and St. George/Hurricane blocks containing somewhat constant

rates through time, we also assume uplift of the Zion block has been constant through time. If steady uplift/incision at 338 m/Ma (Fig. 9) occurred since 3.6 Ma and the VR headward eroded into the block at 3.6 Ma, then there should be a total of 1216 m (338 m/Ma x 3.6 Ma) of total incision where the VR first entered the Zion block at the Hurricane fault. The amount of total incision magnitude since 3.6 Ma would decrease upstream as the stream has headward eroded since then. With the present river at an elevation of ~940 m as it crosses the Hurricane fault, this would suggest the VR first incised though rock that is now at an uplifted elevation of ~2156 m (940m + 1216m). The Jurassic Carmel formation lies at this elevation ~20 km west of the Hurricane fault at the 'West Temple' (Fig. 1), which is the uppermost stratigraphic layer of the southernmost Zion Canyon. The Carmel and overlying Iron Springs formations are the uppermost stratigraphic layers found immediately west of the Hurricane fault. Therefore, an ancestral 'Zion Canyon' may have initiated at the Hurricane fault at 3.6 Ma as the ancestral VR eroded into the Zion block at the stratigraphic level of the Carmel formation and has since migrated upstream. We report differential incision magnitudes over 3.6 and 2.0 Ma time spans as maximum (1134 m) and minimum (730 m) values, respectively, while suggesting 1134 m of incision as the more accurate magnitude.

The upstream decrease in incision rates along tributary headwaters is interpreted as a record of headward erosion through resistant basalt flows (Fig. 14). The gradient of the flow is similar to the upstream reaches of the river. Greater incision magnitudes at downstream reaches of the flow are due to greater amounts of time in which the stream has been incising the softer underlying sedimentary strata. With time, the transient knickpoint migrates upstream through the basalt flow and establishes the downstream

gradient and bedrock incision rates.
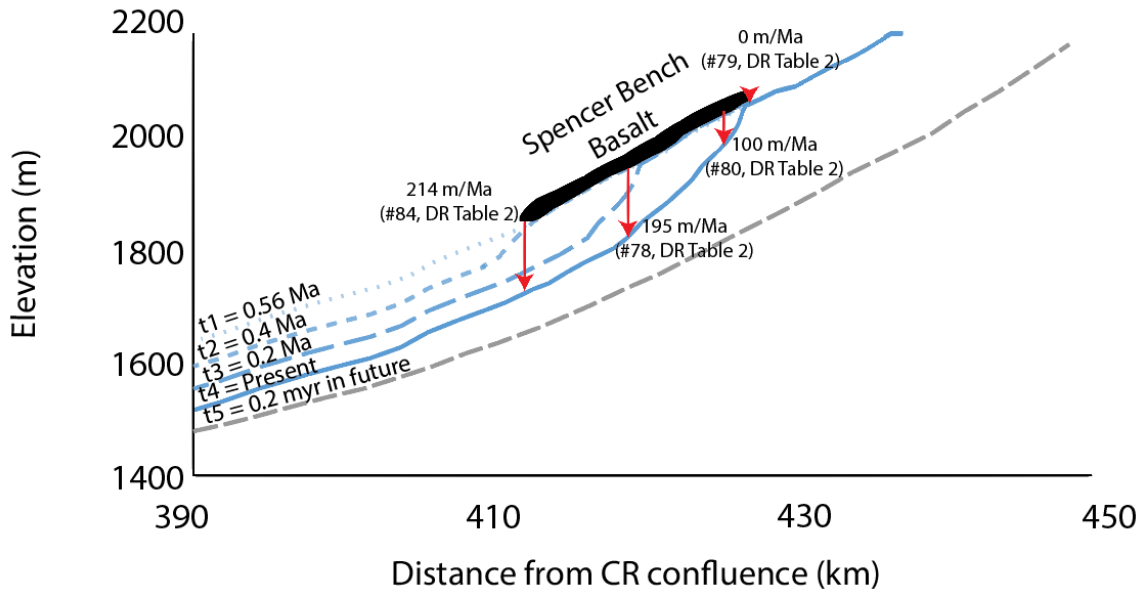
Figure 14. Time steps of hypothesized profiles explaining the local differential incision in the upstream extent of East Fork Virgin River. t1) The Spencer Bench basalt (0.57 Ma) enters into the EF drainage damming the channel and eventually causing the stream to flow on top of resistant basalt. t2) A knickpoint forms in the river profile due to decreased incision at the basalt but continued incision downstream. t3) Increased incision begins at the lower extent of the flow and the knickpoint propagates upstream undercutting the basalt. t4) The present river profile with high incision rates downstream due to more time eroding underlying less-resistant strata and no incision upstream because the river has not yet incised through the basalt. t5) The knickpoint will migrate upstream quicker in less resistant material and will eventually be erased.

Thus, our interpretation of the combined datasets is that a young (~ 4 Ma) Virgin River is headwardly eroding into an uplifting Zion Plateau. Differential incision magnitudes are a proxy for differential uplift across faults and across the region. Because incision rates can be shown to be quasi-steady over the past ~6 Ma, differential incision rates are also a proxy for differential uplift. Both the upper crustal faulting and the sweep of magmatism implicate tectonic influences on VR evolution and both are interpreted here to be manifestations of mantle modification processes that are driving melt

44

extraction and buoyancy modification near a step in the lithosphere-asthenosphere

boundary that is located beneath the SW Colorado Plateau.

The alternative end member interpretation is that the VR is incising into a

previously uplifted landscape but with no accompanying uplift of the Colorado Plateau

(Pederson et al., 2013). In this case, integration of its trunk stream to the Gulf of

California about 6-5 Ma provided a lower base level for incision of Grand Canyon and

for headward propagation of the VR. Using the 4 Ma age and measured magnitudes of

incision across the profile, this interpretation might reconstruct the pre-4 Ma Grand Wash

Cliffs/CP. Then, similar to Pelletier (2010), a headward wave of incision progressively

incises into the CP. Evolving profiles show a migrating knickpoint with fastest incision

rates as the knickpoint passes (Cook et al., 2009; Abbott et al., 2015). This hypothesis

predicts non-steady rather than steady incision in all reaches of the river which is falsified

by the observed quasi-steady incision over millions of years all along the profile,

excluding the headwater transience (Fig. 9). The no-uplift interpretation provides no way

to explain documented fault slips, the sweep of basaltic volcanism, or association of steep

stream profiles underlying low velocity mantle and hence is less satisfactory at the

systems level.

Another modeling approach is to look at relief generation and carving of deep

canyons. Relief is primarily generated through two processes that commonly interplay

with one another, river incision and fault displacement. Darling and Whipple (2015)

analyzed topographic profiles of interfluves starting at the locations of major relief

generators, the Colorado River and the Grand Wash fault. Relaxation of knickpoints in

profiles across the previously uplifted 17 Ma Grand Wash cliffs produced lower gradients

than the steep gradients found at the edges of Grand Canyon supporting a young western

Grand Canyon. We perform a similar analysis in this study to analyze the Virgin River as

a relief generator. Figure 15 shows a Virgin Gorge interfluve profile (VG4) starting at the

relief generator (Virgin River) and a profile perpendicular to Grand Wash fault (GWF1)

have similar lithologies but vary greatly with respect to profile relaxation (transect

locations found in Figs. 1 and 11). This suggests that the Virgin River incised the Virgin

Gorge long after relief along the Grand Wash fault was generated, inferring a young

canyon/river similar in age to the Grand Canyon. Two different Virgin Gorge interfluve

profiles (VG3 and VG4) show young relief generation however, the soft Hermit shale in

VG3 allowed increased erosion and relaxation of the profile.
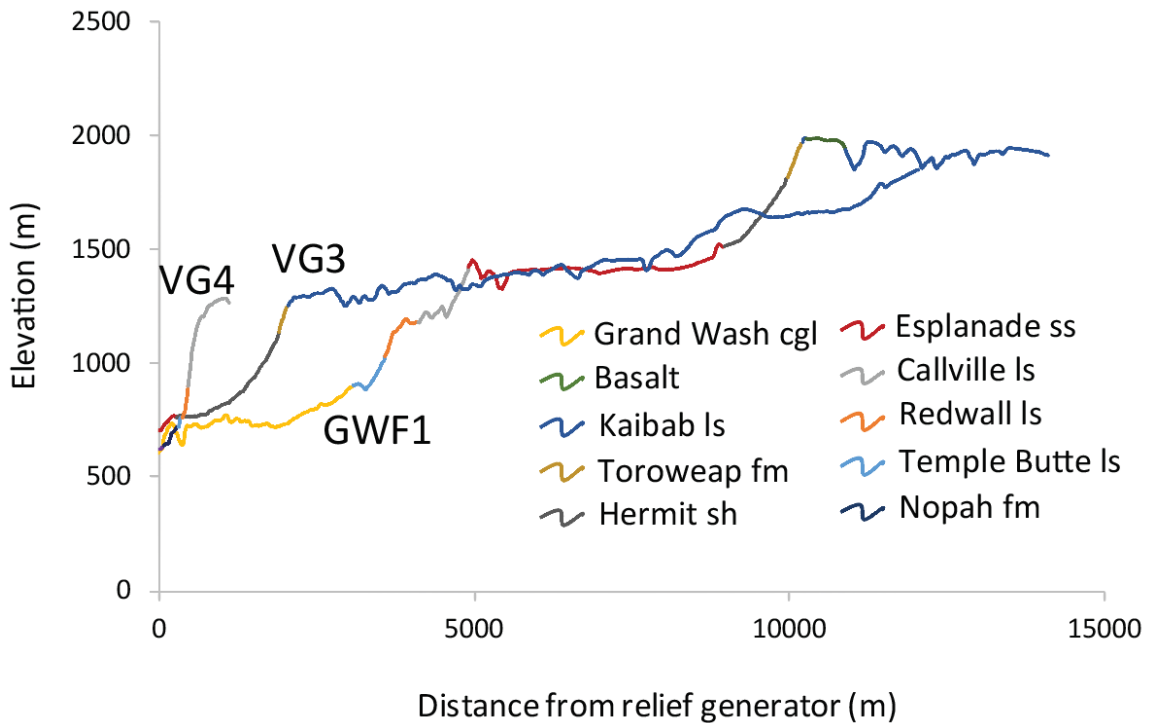
Figure 15. Topographic profiles of interfluves starting at major relief generators. GWF1—profile edited from Darling and Whipple (2015) to show differing rock formations along the profile starting at Grand Wash fault and going east across the Grand Wash Cliffs. VG3 and VG4—interfluve profiles starting at the Virgin River within the Virgin River Gorge. Note similar rock types between VG4 and GWF1 with discordant profile concavities.

Basalt paleoprofiles

The downstream divergence of Grand Wash profiles (Fig. 10) supports the hypothesis of regional active uplift relative to base level causing steeper modern river profiles, since base level (CR) has been graded to sea level since ~4.5 Ma (Howard et al., 2015). Howard et al. (2015) argue for 145-230 m of regional offset across the Black Mountains, located ~15 km west of the CR-VR confluence (Fig. 1), in the past 4 Ma (Ryan Crow, personal communication, 2018). We interpret this offset as an upper crustal accommodation to epeirogenic uplift. A potential complication related to this offset is that as this uplift occurred downstream of the CR-VR confluence post CR-VR integration, a transient knickpoint may have existed as a contributing driver of VR incision. However, we observe no evidence suggesting any transient knickpoint in our ~6 Ma record of incision rates (Fig. 9A). The Grand Wash basalt flow lies within the fault-dampened zone of the Wheeler fault and is therefore downfolded below the original elevation (Howard and Bohannon, 2001). If the flow is progressively downfolded as it nears the Wheeler fault than the paleoprofile shown in Fig. 10 had an even shallower gradient at the time of basalt deposition (4.7 Ma) which would infer even greater downstream divergence between the paleo and modern Grand Wash profiles and further support our interpretation of active regional uplift.

The 3.7 Ma Black Rock Mountain paleoprofile analysis (Fig. 11) shows similar results. At the time of this flow, the northern and southern drainages had very similar slopes which may infer similar base levels, uplift rates, and/or drainage areas. The stark contrast in relief generation between the northern and southern profiles since 3.7 Ma is explained by the northern profile's connection to the VR (local base level). Since 3.7

Ma, the VR greatly increased its drainage area and scale while the southern drainage has remained the same. With the initiation of the Hurricane fault at 3.6 Ma, the VR has also experienced a large increase in active headwater uplift, relative to smaller amounts of regional uplift observed in the Lake Mead block. The uplifting headwaters steepened the river profiles and increased stream power, which then generated the observed relief.

Provenance Analysis

Provenance analysis is important for interpreting when and how the VR became integrated. The well-rounded, far-traveled clasts found in Grand Wash Trough beneath a 4.7 Ma basalt are interpreted to represent reworked Canaan Peak gravels from the eastern flank of Pine Valley Mountains. We interpret the yellow volcanics and the chert litharenites to be derived from the Delfonte volcanics of southeastern California and Eleana Formation of Nevada, respectively. The combination of yellow volcanics, chert litharenites, black argillites with white quartz veins, and maroon and yellow quartzite clasts are diagnostic of the Canaan Peak Formation (Goldstrand 1992, 1994). This would suggest a paleo-river (ancestral Virgin?) entering Grand Wash Trough from the north around 4.7 Ma and perhaps entering the newly established Colorado River. Evidence of similar clasts found near Mesquite, NV suggest an ancestral Virgin exited the Virgin Gorge <4.1 Ma based upon the dated basalt of Williams (1996).

Age distribution plots of detrital zircons with sharp peaks around 19 Ma was interpreted by Dickinson et al. (2014) to propose that the ~4 Ma arrival of the VR had headwaters in the Pine Valley laccolith (20.5 Ma; Hacker et al., 2007). Dickinson et al. (2014) proposed that the distribution plots would have a much broader peak if the source was from Basin and Range igneous centers such as the Indian Peak and Caliente caldera

complexes since they have a much wider range of ages (~33-11 Ma; Best et al., 1993, 2013) (Fig. 12A and 13). The rest of the DZ spectrum is undiagnostic but suggests derivation from Mesozoic and Paleozoic strata (Appendix J). We interpret our analysis of upper versus lower Muddy Creek detrital zircons to indicate a change in headwater location. The lower, internally drained, Muddy Creek had a source in the northern Basin and Range igneous centers (primarily the Caliente caldera complex) which is supported by a broader peak (Fig. 12B). The upper Muddy Creek, first arriving VR gravels, shows a sharp peak at ~20 Ma indicating the capture of an ancestral VR through the VR Gorge with headwaters at Pine Valley Mountains (20.5 Ma). Alternate explanations for this analysis may include a zircon grain picking bias or small sample size of grains within this age range.

The more robust and precise dataset of detrital sanidine ages allows us to pinpoint source regions and resolve previous conflicts with a peak at 19 Ma as discussed in Dickinson et al. (2014). An age distribution curve of the upper Muddy Creek detrital sanidine grains shows two distinct peaks at 18.68 Ma and 20.56 Ma. We interpret the 20.56 Ma age to represent the influx of Pine Valley laccolith and latite (20.5 Ma; Hacker et al., 2007) sediments located east of Grand Wash fault. Other peaks at 18.68 Ma and 23.8 Ma represent the Caliente caldera complex (Best et al., 1993, 2013) while the 13.72 Ma peak is sourced from Mineral Mountain (14-10.2 Ma; Hacker et al., 2007), part of the Iron Axis intrusives and extrusives (Fig. 13). Therefore, the rapidly arriving far-traveled gravels that represent the upper Muddy Creek, had a mixed source of the Caliente Caldera complex and Mineral Mountain from Beaver Dam wash and the Pine Valley laccolith from an ancestral VR. The large peak of Pine Valley age grains found among

the lowest (first-arriving) gravels within the upper Muddy Creek is interpreted to indicate a headward eroding tributary from Mesquite Basin had tapped into a well-established drainage system with headwaters in the high elevation Pine Valley laccolith. A small headward eroding stream into the Pine Valley laccolith would show a gradual increase of 20.5 Ma age grains from lower (KCW17-4 and KCW17-6) to stratigraphically higher Muddy Creek samples (KCW17-19), which is not seen (Appendix H). The two youngest grains (~5.9 Ma) act as a much younger maximum depositional constraint then the previously published youngest detrital zircon grains of ~11 Ma (Muntean, 2012). This proves the Virgin River Gorge to be a relatively young canyon, similar in age to the Grand Canyon.

DISCUSSION

Evolution of the Virgin River

Our model for Virgin River evolution (Fig. 16) accommodates the following constraints/observations. 1) Zircons suggest CP (or CP equivalent formations of the BR) derived sediments enter the Virgin Depression/Overton Arm basins by at least 6 Ma (Muntean, 2012; Dickinson et al, 2014). 2) A paleo-river (likely the paleo VR) entered the GWT from the north 4.7 Ma, depositing reworked Canaan Peak gravels from an inferred source east of Pine Valley Mountains (this study). 3) A sharp contact exists in the Overton Arm, Mormon and Mesquite basins between two informally termed units, lower and upper Muddy Creek Formations. Lower Muddy Creek Formation is fine-grained siltstone interpreted as internally drained basin deposits. Upper Muddy Creek Formation contains coarse gravel that represent the arrival of the Virgin River (Williams, 1996; Swenberg, 2012) at 6-4 Ma (Dickinson et al., 2014; this study). 4) The northward

and southward outflows of the Black Rock Mountain basalt (3.7 Ma) suggests an ancestral river gorge and drainage divide similar to today's, existed 3.7 Ma (Fig. 11, this study). 5) A 3 Ma tuff intercalated with Muddy Creek Formation in Glendale Basin, west of Mormon Mesa, suggests the Basin and Range tributaries (White River and Meadow Valley Wash) did not become integrated with the Virgin River until after 3 Ma (Dickinson et al., 2014). 6) Differential incision data suggest a headward progression with slow incision rates since 6-4 Ma near the CR-VR confluence suggesting stable base level since then; incision rates increase upstream in steps across faults. 7) The shape of the modern VR watershed (Fig. 1) is unique with two distinct lobes, west and east, which appear to have been two separate drainage basins divided by the Beaver Dam and Virgin Mountains until integration through the Virgin Gorge. 8) The pattern of S-flowing (fault controlled tributaries) entering an east-propagating mainstem is suggested by modern geometries (Fig. 1).

Pre-5 Ma landscape

Figure 16 is a summary of our interpretation of the birth and evolution of the Virgin River system. Prior to the integration of the Colorado River to the Gulf of California and the incision of Grand Canyon, the Lake Mead Region consisted of large internally drained basins throughout the late Miocene (Fig. 16A). Basins relevant to this research include Grand Wash Trough, Virgin Depression (Mesquite and Mormon basins), Overton Arm, Temple Bar, Greggs, and Glendale basins. These basins formed at the major onset of extension ~17 Ma, in the resultant half-grabens of the Grand Wash, Piedmont, Bitter Ridge-Hamblin Bay, South Virgin-White Hills, Wheeler Ridge, and California Wash faults respectively (Faulds et al., 2016). The Hualapai Limestone
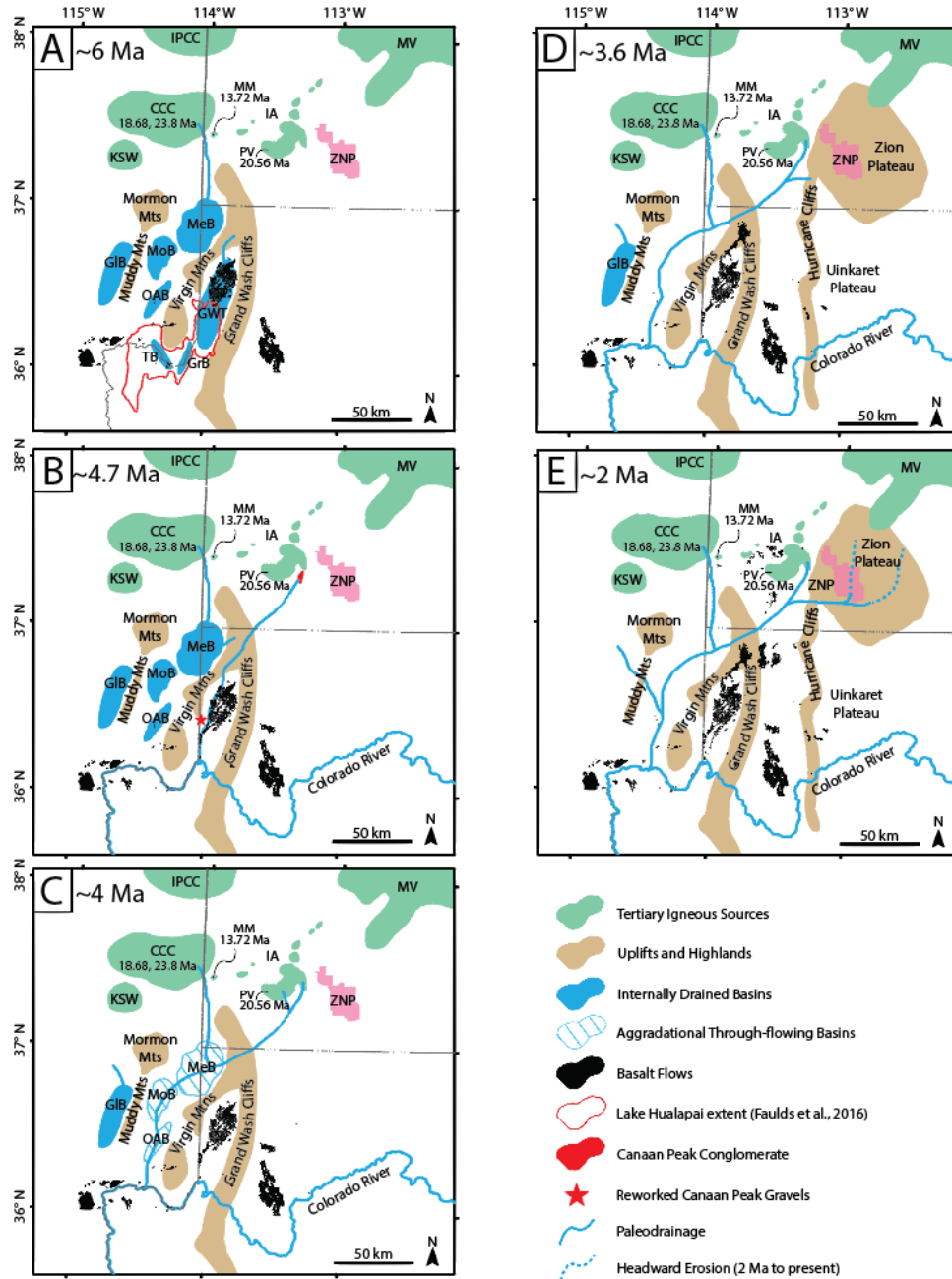
Figure 16. Interpreted paleo-drainage reconstructions of the Virgin River fluvial system at multiple time steps (A-E) from internally drained basins at ~6 Ma (A) to a through-flowing Virgin River with headwaters on the Zion Plateau at ~2 Ma (E). This figure illustrates the role of headward erosion and stream capture of a "Grand Wash River" which formed the current path of the Virgin River through the Virgin Gorge. CCC—Caliente Caldera complex; GlB— Glendale Basin; GrB—Greggs Basin; GWT—Grand Wash Trough; IA—Iron Axis intrusives and extrusives; IPCC—Indian Peak Caldera complex; KSW—Kane Springs Wash Caldera; MeB—Mesquite Basin; MM—Mineral Mountain; MoB—Mormon Basin; MV—Marysvale Volcanics; OAB—Overton Arm Basin; PV—Pine Valley; TB—Temple Basin; ZNP—Zion National Park. Labeled ages correlate with peaks found in the detrital sanidine age distribution curve (Figure 12C) and indicate interpreted sources from which the peaks originated.

provides a record of a spring fed lake (Lake Hualapai) in Grand Wash trough that persisted from 13 until the 6-4.5 Ma arrival of the CR (Spencer et al., 2001; Crossey et al., 2015). The Grand Wash cliffs were the major topographic feature providing relief in the area; the Pine Valley Mountains acted as the major topographic feature in the north. The Pine Valley laccolith formed during the early Miocene (20.5 Ma) as magma was emplaced within the Claron Formation, causing a rapid generation of relief (Biek et al., 2010). Detailed mapping shows evidence of slope oversteepening that lead to massive Miocene gravity slides being shed from the Pine Valley laccolith (Hacker, 1998; Hacker et al., 2002, 2007).

Integration and birth of the Virgin River

Figure 16B shows the earliest significant drainages off the Pine Valley laccolith is manifested by reworked Canaan Peak gravels found beneath the 4.7 Ma Grand Wash basalt in Grand Wash (see Fig. 10). Thick deposits of gypsum in the northern GWT suggest internal drainage until about 5 Ma (Faulds et al., 2016). A stream entering Grand Wash from the north likely eroded headwardly until reaching the Canaan Peak Formation exposed on the southeastern flanks of the Pine Valley Mountains. Also, note a stream flowing from the north into the Mesquite Basin, bringing in ~24-11 Ma detrital zircon grains from the Caliente Caldera complex. Figure 16C shows establishment of the present course of the VR about 4 Ma. We interpret the Virgin Gorge to be the result of headward erosion from the Virgin Depression, across the Piedmont and Grand Wash faults. By ~4 Ma, a headwardly eroding incipient Virgin River taps into and captures the Grand Wash drainage causing the rapid arrival of Canaan Peak gravels at the mouth of the Virgin River Gorge and within the Overton Arm basin. From 4.0 to 3.6 Ma, the large influx of

sediment from incision of the Virgin Gorge causes major aggradation within the Mesquite, Mormon, and Overton Arm basins similar to the Bullhead Alluvium located in the lower Colorado River (Howard et al., 2015). At about 3.6 Ma (Fig. 16D), slip along the Hurricane fault initiates as an upper crustal response to asthenospheric upwelling beneath the edge of the Colorado Plateau, as tracked by the onset of migrating basaltic volcanism. Combined footwall uplift and epeirogenic doming uplifts the headwaters, increases stream power and triggers a transition from aggradation to incision within the Virgin River drainage. By 2 Ma (Fig. 16E), the mainstem of the upper VR has incised headwardly across the Hurricane fault and continues to propagate eastward into the uplifting Zion Plateau.

Therefore, a few conclusions can be drawn from the proposed paleogeographic evolution. First, recent/ongoing differential uplift of the Zion Plateau is the major driver for drainage evolution in this region in the last 5 Ma. Second, headward erosion was the primary mechanism for the birth of the present day Virgin River and the transition from internally drained basins to a major through flowing drainage system.

Mechanisms for uplifts

The sweep of basalts found within the Virgin drainage acts as an amazing link between observed differential incision at the surface and subsurface mantle activity through time. Tomographic data of upper mantle velocities at 80 km depth show a low velocity ring around the western CP boundary and a high velocity anomaly known as the Escalante anomaly (Schmandt and Humphreys, 2010). These low mantle velocities are suggestive of the presence of partial melt in buoyant, hot, and rheologically weaker mantle (Sine et al., 2008; Schmandt and Humphreys, 2010). Low mantle velocities

underlie the majority of the northeastern portion of the VR drainage system including the entirety of Zion National Park. Figure 17 shows a correlation between low velocity mantle and increased incision rates. Our incision rates collected along the East Fork Virgin River plot higher than expected. The heights used at this location were calculated from the base of the basalt flow. However, if the thick cliffs below the basalt flow are well indurated quaternary gravels, instead of a Mesozoic conglomerate, than incision rates would be much lower (~50 m/Ma) when calculated from the base of the gravels as reported by Darling (2016). We interpret this data to suggest that mantle buoyancy is a contributor to differential incision and therefore differential surface uplift.
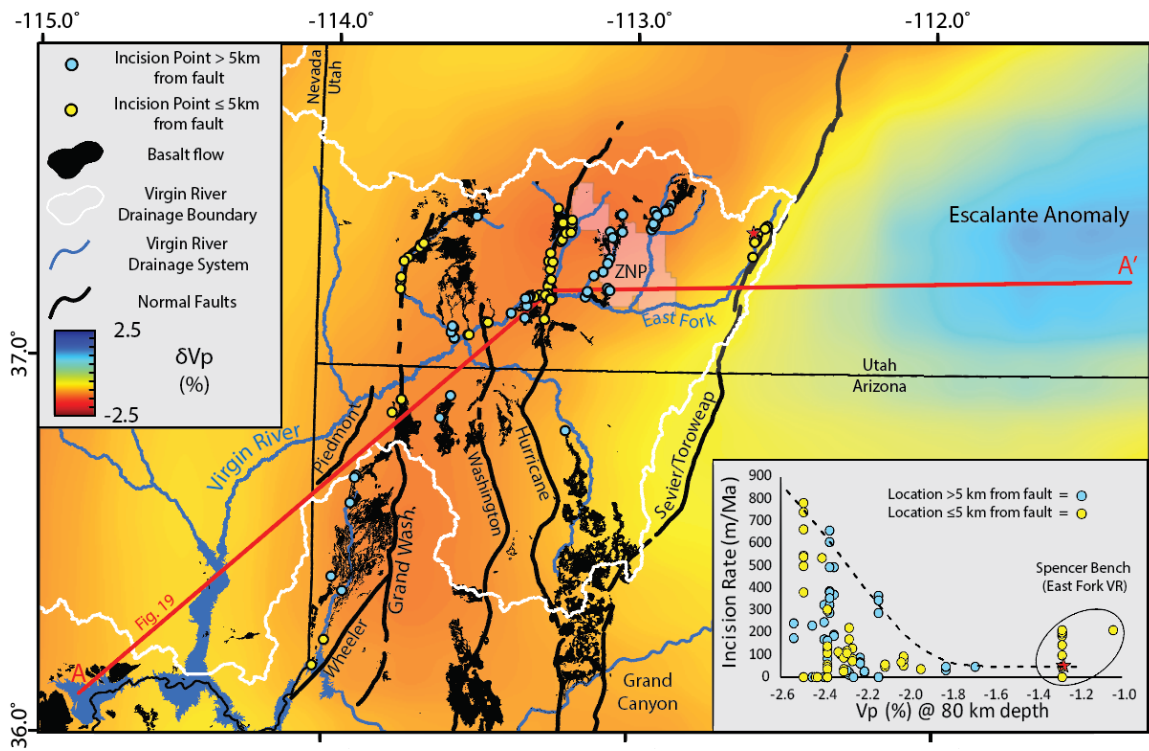
Figure 17. Blue-red scale background raster of p-wave mantle velocities (%) at a depth of 80 km (Schmandt and Humphreys, 2010). Blue data points represent locations of all calculated incision rates. An inset wedge plot shows a correlation among increasing incision rates with decreasing mantle velocity. The Spencer Bench basalt located along East Fork Virgin River do not fit the general trend. Heights along the East Fork Virgin River were measured from the base of the basalt (blue points). The red star shows an incision rate calculated from the base of what was interpreted to be Quaternary gravels below the basalt (See text; Darling, 2016). The dashed line shows a general curve of maximum incision rates, using the lower incision rate calculated by Darling (2016).

Details of mantle mechanism that could be driving uplift are incompletely understood, but lithospheric delamination and edge-driven convection have both been proposed. The preferred mechanism must be able to explain both the inward migration of basaltic magmatism toward the center of the Colorado Plateau (Best et al., 1980; Wenrich et al., 1995; Roy et al., 2009; Crow et al., 2011) and increase in asthenospheric melts through time, and to the east (Crow et al., 2011).

Delamination below the Escalante anomaly was supported by Levander et al. (2011). This model suggests thermochemical convection as upwelling mantle generates an intrusion of basaltic partial melts into the base of the CP increasing negative buoyancy and thermally weakening the mantle lithosphere. Decreased viscosity and increased density of the mantle lithosphere allows a 'drip' to form and delaminate the mantle lithosphere and perhaps some of the lower crust. The failure within the lowermost crust along a localized surface, as observed in the receiver function images (Fig. 3 of Levander et al., 2011), allows for the replacement of lithospheric mantle and lower crust with hot buoyant asthenosphere. The introduction of asthenosphere as the mantle lithosphere continues to tear away (delaminate) from the lower crust is suggested to explain the observed migration of magmatism. However, the dipping structure in the PdS receiver function image (Fig. 3 of Levander et al., 2011) opens to the northeast and therefore infers that the hot asthenosphere first encounters the thinned lithosphere in the northeast and migrates to the southwest. Thus, in detail, this model (Fig. 4 of Levander et al., 2011) does not support the direction of migration observed at the surface.

A second model explaining uplift of the Colorado Plateau proposes small-scale upper mantle edge-driven convection. The Colorado Plateau lithosphere is assumed to
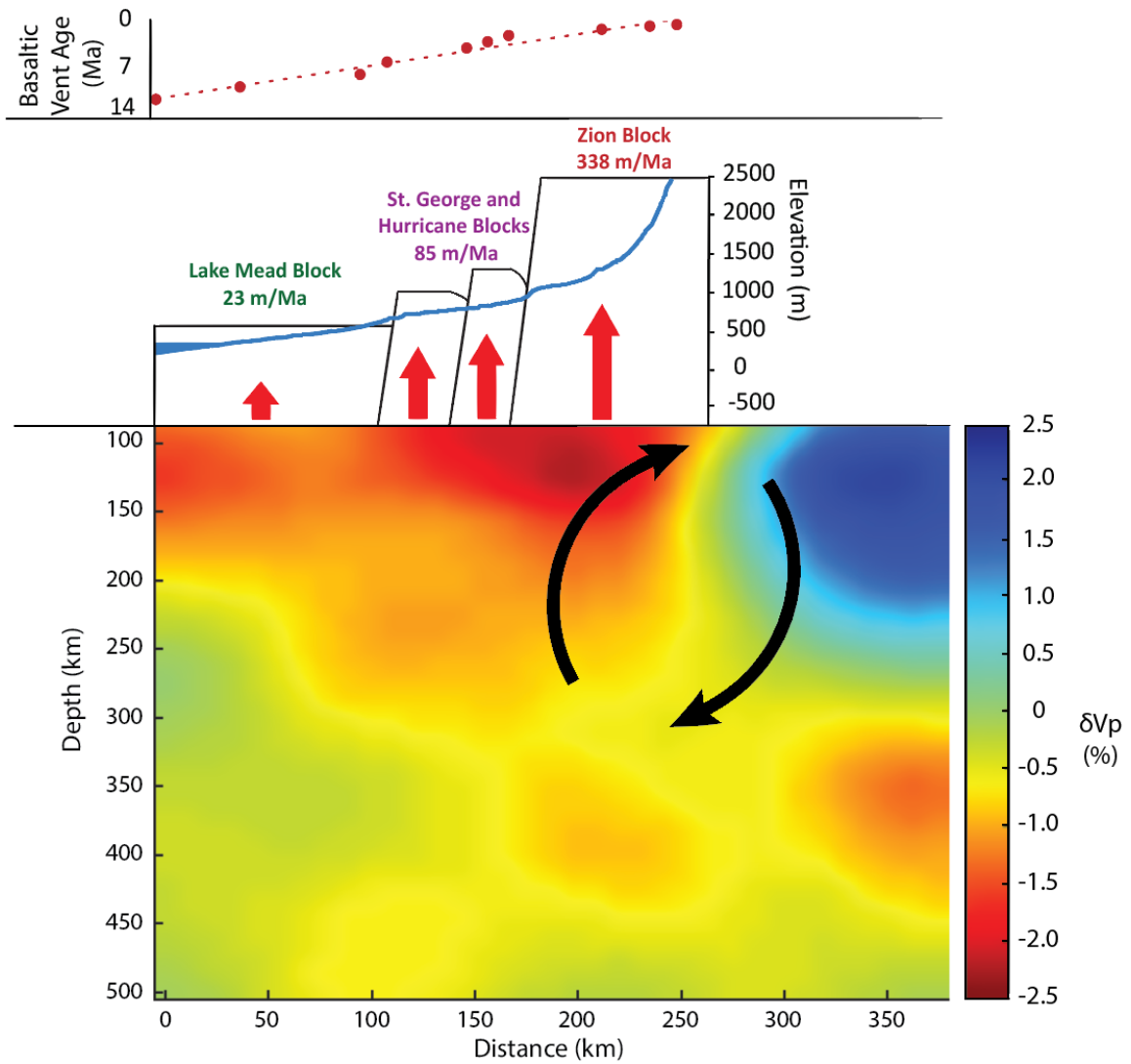
Figure 18. Tomographic cross-section of the general path of the Virgin River (Fig. 17). Low mantle velocities underlie the high k$_{sn}$ headwaters of North Fork Virgin River. A plot of oldest vents shows the spatial migration of basaltic volcanism through time. Black arrows represent upper mantle convection, which is the suggested mantle-driven mechanism of differential uplift in this study.

have a thickness of 120-140 km whereas the Basin and Range lithosphere has a thickness of 60-80 km (West et al., 2004). Van Wijk et al. (2010) use numerical modeling of an assumed step in lithospheric thicknesses to better understand the convective processes that take place. A thermally induced Rayleigh-Taylor instability forms at the large step with hot asthenosphere juxtaposed with colder mantle lithosphere. The hydrated and weakened mantle lithosphere begins to drip off the base of the Colorado Plateau and thinned lithosphere is replaced by hot buoyant asthenosphere, which drives surface uplift. The edge driven convection model applied to a thicker Colorado Plateau lithosphere as it moves SW over warm asthenosphere may best explain the northeastward migration of magmatism and increased uplift of the Zion Plateau (Fig. 18).

CONCLUSIONS

The differential incision history of the 5-4 Ma Virgin River drainage system is interpreted to provide evidence for ~730-1100 m of surface uplift of the CP. Documentation of quasi-steady incision for each reach, and removal of local effects of fault-dampened incision directly adjacent to faults, allow us to equate differential incision magnitude with uplift magnitude. Averaged incision rates show an eastward propagating stair-stepping increase across structural blocks: 23 m/Ma in the Lake Mead block (local base level), 85 m/Ma in the St. George and Hurricane blocks, and 338 m/Ma in the Zion block (headwaters). Differences in incision magnitude accumulate upstream to ~730-1100 m of uplift in the western CP relative to the CR-VR confluence depending on whether Zion block has been incising for 2 or 3.6 Ma. Thus, ~25-40% of the total surface uplift of the CP since 70 Ma occurred in the past 6-5 Ma (Karlstrom et al., 2012). Increased incision rates and oversteepened channel segments (ex. North Fork Virgin

River) correlate better with areas of underlying low velocity mantle than with variances in substrate lithology or precipitation. An observed NE-propagation of basaltic magmatism migrated at rates of ~18 km/Ma, similar to North American absolute plate motion (~20 km/Ma). We conclude that NE-propagating upper mantle convection drove differential uplift of the western CP in the past 5 Ma and that the birth and evolution of the VR provide evidence for large-scale landscape response to mantle-driven uplift.

List of Appendices

Appendix A: Compilation of dated basalts

Appendix B: Incision rates of the Virgin River Region

Appendix C: Detrital sanidine ^{40}Ar/^{39}Ar geochronology data

Appendix D: Observing headward erosion

Appendix E: Basin and Range tributary profiles

Appendix F: Contour map of all basaltic vents

Appendix G: Map of incision rates

Appendix H: Age distribution plots of detrital sanidine grains <40 Ma

Appendix I: Small-scale Virgin River drainage evolution

Appendix J: Age distribution plots of all detrital sanidine grains

APPENDIX A: COMPILATION OF DATED BASALTS

Flow	Unit Symbol	Sample	Latitude	Longitude	Age (Ma)	Dating Method	Quad	Reference
Santa Clara	Qbs	SC100605-1	37.1503	-113.6564	0.027 ± 0.0003	^{14}C	St. George	Willis et al. (2006)
Crater Hill	Qbc	ZP1501	37.2116	-113.1057	0.101 ± 0.08	Ar-Ar	Springdale West	UGS and NMGRL (2007b)
Crater Hill	Qbc	-	37.1681*	-113.0683*	0.122 ± 0.015	OSL	Springdale West	Biek et al (2010)
Radio Tower	Qbrt	H11299-4	37.1981	-113.2889	0.142 ± 0.06	Ar-Ar	Hurricane	Biek (2003b)
East Reef	Qber	VR122-2	37.2081	-113.3431	0.203 ± 0.16	Ar-Ar	Hurricane	Biek et al 2010
Grapevine Wash	Qbg	ZP-0502	37.3381	-113.1169	0.223 ± 0.03	Ar-Ar	The Guardian Angels	Willis and Hylland (2002)
Cinder Pits	Qbcp	VR123-5	37.1819	-113.3186	0.243 ± 0.02	Ar-Ar	Hurricane	Biek (2003b)
Grapevine Wash	Qbg	ZP-0606	37.2789	-113.0961	0.263 ± 0.01	Ar-Ar	The Guardian Angels	Willis and Hylland (2002)
Grapevine Wash	Qbg	ZP-0607	37.2800	-113.0961	0.263 ± 0.03	Ar-Ar	The Guardian Angels	Willis and Hylland (2002)
Crater Hill	Qbc	ZP1501	37.2116	-113.1057	0.282 ± 0.08	Ar-Ar	Springdale West	UGS unpublished data
Grapevine Wash	Qbg	ZP-0503	37.3500	-113.1069	0.294 ± 0.02	Ar-Ar	The Guardian Angels	Willis and Hylland (2002)
Grapevine Wash	Qbg	ZP-0605	37.2981	-113.0989	0.314 ± 0.04	Ar-Ar	The Guardian Angels	Willis and Hylland (2002)
Crater Hill	Qbc	VR41-02	37.1746	-113.0834	0.312 ± 0.07	Ar-Ar	Springdale West	UGS unpublished data
Crater Hill	Qbc	VR41-03	37.1802	-113.0848	0.322 ± 0.13	Ar-Ar	Springdale West	UGS unpublished data
Volcano Knoll	Qbvk	CP71900-6	37.4217	-112.9292	0.344 ± 0.03	Ar-Ar	Cogswell Point	Biek and Hylland (2007)
Little Creek	Qblc	LD98-1	37.0813*	-113.1518*	0.349 ± 0.015	Ar-Ar	Little Creek Mountain	Downing (2000)
Volcano Mountain	Qbv2	6 15	37.1879*	-113.2749*	0.358 ± 0.04	Ar-Ar	Hurricane	Sanchez(1995)
Virgin Flats	Qbvf	CP71900-1	37.4131	-112.9756	0.375 ± 0.02	Ar-Ar	Cogswell Point	Biek and Hylland (2007)
Divide	Qbd	TD12999-1	37.0719	-113.2981	0.415 ± 0.08	Ar-Ar	The Divide	Hayden (2004a)
Gould Wash	Qbgw	VR41-08	37.1258	-113.2491	0.423 ± 0.21	Ar-Ar	Little Creek Mountain	Biek et al 2010
Saddle Mountain	Qbsm	VY122001-3	37.3123	-113.6399	0.476 ± 0.12	Ar-Ar	Veyo	Biek et al 2010
Spencer Bench	Qb	-	37.3821*	-112.5673*	0.570 ± 0.02	Ar-Ar	Orderville	Schiefelbein (2002)
Dammeron Valley East	Qbde	VY122001-4	37.3095	-113.5641	0.598 ± 0.02	Ar-Ar	Veyo	Biek et al 2010
Lark Canyon	Qbla	CEQ-18	37.4036	-113.6132	0.614 ± 0.04	Ar-Ar	Central East	Biek et al 2010
Graham Ranch (Sage)	Qgrb	-	36.4700	-113	0.635 ± 0.24	K-Ar	Heaton Knolls	Jackson (1990)
Baker Dam	Qbbd	VY8301-3	37.3484	-113.6701	0.674 ± 0.04	Ar-Ar	Veyo	Biek et al 2010
Pine Valley	Qbpv	CEQ-14	37.4080	-113.5292	0.674 ± 0.07	Ar-Ar	Central East	UGS and NMGRL (2007a)
Veyo	Qbve3	VY111902-7	37.2748	-113.7049	0.699 ± 0.04	Ar-Ar	Veyo	UGS and NMGRL (2007b)
Baker Dam	Qbbd	VY8301-1	37.3330	-113.6933	0.694 ± 0.14	Ar-Ar	Veyo	Biek et al 2010
Horse Knoll	Qbhk	CP62001-3	37.4369	-112.8811	0.739 ± 0.02	Ar-Ar	Cogswell Point	Biek and Hylland (2007)
Hornet Point	Qbhp	CP83100-3	37.4526	-112.9993	0.750 ± 0.05	Ar-Ar	Cogswell Point	Biek and Hylland (2007)
Pintura	Qbp	ACG-1	37.2833	-113.2833	0.821 ± 0.1	Ar-Ar	Pintura	Lund et al. (2001)
Antelope Knoll	Qab	23-B91	36.8014*	-113.2066*	0.83 ± 0.28	K-Ar	Antelope Knoll	Wenrich et al. (1995)
Pintura	Qbp	BR-1	37.4107	-113.2144	0.851 ± 0.03	Ar-Ar	Kolob Arch	Lund and Everitt (1998)
Pintura	Qbp	MH-1	37.3653	-113.2361	0.881 ± 0.04	Ar-Ar	Smith Mesa	Lund et al. (2001)
Washington	Qbw	HJ11299-2	37.1589	-113.4719	0.881 ± 0.04	Ar-Ar	Harrisburg Junction	Biek (2003a)
Pintura	Qbp	AC-1	37.4031	-113.2364	0.891 ± 0.05	Ar-Ar	Kolob Arch	Lund and Everitt (1998)
Pintura	Qbp	VR113-4	37.2431	-113.2969	0.902 ± 0.02	Ar-Ar	Hurricane	Biek (2003b)
Central West	Qvcw	VY8301-6	37.3721	-113.6617	0.926 ± 0.07	Ar-Ar	Veyo	Biek et al (2010)
Ivans Knoll	Qbi	H11299-2	37.1720	-113.352	0.983 ± 0.07	Ar-Ar	Hurricane	Biek (2003b)
Washington	Qbw	VR40-07	37.1378	-113.4718	0.986 ± 0.02	Ar-Ar	Harrisburg Junction	Biek (2003a)
Magotsu Creek	Qbmc	VY11702-1	37.2808	-113.7613	0.993 ± 0.03	Ar-Ar	Gunlock	UGS and NMGRL (2008)
Magotsu Creek	Qbmc	VY8301-7	37.3671	-113.6856	1.006 ± 0.09	Ar-Ar	Veyo	Biek et al (2010)
Little Tanks Basalt	Qlb	25-B91	36.5444	-113.3778	1.0 ± 0.4	K-Ar	Little Tanks	Wenrich et al. (1995)
Lava Point	Qblp	ZP-0601	37.3872	-113.0386	1.033 ± 0.03	Ar-Ar	Kolob Resevoir	Biek (2007b)
Grass Knoll	Qbgk	SMQ-1	37.2742	-113.6059	1.027 ± 0.36	Ar-Ar	Saddle Mountain	Biek et al (2010)
Ivans Knoll	Qbi	VR123-11	37.1261	-113.3639	1.043 ± 0.02	Ar-Ar	Hurricane	Biek (2003b)
Horse Ranch Mountain	Qbhr	KA92600-1	37.4786	-113.1589	1.043 ± 0.06	Ar-Ar	Kolob Arch	Biek (2007a)
Kolob Peak	Qbkp	KR81200-1	37.4225	-113.0672	1.064 ± 0.05	Ar-Ar	Kolob Resevoir	Biek (2007b)
Lava Point	Qblp	VR41-01c	37.2113	-113.1468	1.067 ± 0.01	Ar-Ar	Virgin	Biek et al (2010)
Remnants	Qbr	TD11699-3	37.1050	-113.3261	1.074 ± 0.03	Ar-Ar	The Divide	Hayden (2004)
Ivans Knoll	Qbi	VR41-06	37.1284	-113.2971	1.067 ± 0.16	Ar-Ar	Hurricane	Biek (2003b)
Lava Point	Qblp	ZP-0602	37.3861	-113.04	1.094 ± 0.02	Ar-Ar	Kolob Resevoir	Biek (2007b)
Grass Valley Reservoir	Qbgvr	CEQ-8	37.4032	-113.5178	1.087 ± 0.13	Ar-Ar	Central East	Biek et al (2010)
Grass Valley	Qbgv	VR42-03	37.0747	-113.3244	1.097 ± 0.09	Ar-Ar	The Divide	Biek et al (2010)
Big Sand	Qbb	VR42-09	37.1631	-113.6103	1.137 ± 0.05	Ar-Ar	Santa Clara	Biek et al (2010)
Lava Point	Qblp	ZP-0405	37.3740	-113.06	1.155 ± 0.14	Ar-Ar	The Guardian Angels	Willis and Hylland (2002)
Cedar Bench	Qbcb	VR42-08	37.2195	-113.6314	1.167 ± 0.03	Ar-Ar	Santa Clara	Biek et al (2010)
Cedar Bench	Qbcb	VR40-05	37.1047	-113.594	1.238 ± 0.01	Ar-Ar	St. George	Biek et al (2010)
East Mesa	Qeb	20-B91	36.9184*	-113.4156*	1.4 ± 0.25	K-Ar	Yellowhorse Flat	Wenrich et al. (1995)
Lava Ridge	Qbl	VR40-06	37.1121	-113.551	1.419 ± 0.01	Ar-Ar	St. George	Higgins (2003)
Little Creek Peak	Qbli	VR43-01	37.3556	-113.0727	1.449 ± 0.04	Ar-Ar	The Guardian Angels	Willis and Hylland (2002)
West Mesa	Qwb	21-B91	36.8834*	-113.4389*	1.6 ± 0.3	K-Ar	Yellowhorse Flat	Wenrich et al. (1995)

APPENDIX A (CONT.): COMPILATION OF DATED BASALTS

Flow	Unit Symbol	Sample	Latitude	Longitude	Age (Ma)	Dating Method	Quad	Reference
Gunlock	Qbgd	VR40-01	37.2381	-113.7744	1.620 ± 0.07	Ar-Ar	Shivwits	Biek et al (2010)
Gunlock	Qbgd	VY8301-9	37.3230	-113.668	1.641 ± 0.02	Ar-Ar	Veyo	UGS and NMGRL (2008)
Gunlock	Qbgd	VY8301-10	37.3245	-113.6664	1.661 ± 0.02	Ar-Ar	Veyo	Biek et al (2010)
Little Black Mountain	Qb	27-B92	36.9920	-113.5	1.7 ± 0.4	K-Ar	Yellowhorse Flat	Wenrich et al. (1995)
Central West	Qvcw	VY11802-7	37.3711	-113.6719	1.793 ± 0.09	Ar-Ar	Veyo	Biek et al (2010)
Granite Wash	Tbgw	VY11802-1	37.3667	-113.6306	1.996 ± 0.02	Ar-Ar	Veyo	UGS and NMGRL (2008)
Aqueduct Hill	Tbah	VY8301-4	37.3504	-113.6719	2.006 ± 0.04	Ar-Ar	Veyo	UGS and NMGRL (2008)
Basalt flow undivided	Tb	01RB-068	37.4452*	-113.6363*	2.249 ± 0.05	Ar-Ar	Central West	UGS and NMGRL (2008)
Twin Peaks	Tbt	VR40-04	37.1129	-113.5991	2.355 ± 0.02	Ar-Ar	St. George	Biek et al (2010)
Seegmiller Mountain	Tsb	PED-32-66	36.8460	-113.641	2.35 ± 0.31	K-Ar	Wolf Hole Mountain	Reynolds et al (1986)
Twin Peaks	Tbt	VR40-12	37.1425	-113.5687	2.385 ± 0.02	Ar-Ar	Washington	Biek et al (2010)
Twin Peaks	Tbt	VR40-10	37.2224	-113.5664	2.446 ± 0.02	Ar-Ar	Washington	Biek et al (2010)
Seegmiller Mountain	Tsb	PED-33-66	36.8460	-113.643	2.44 ± 0.51	K-Ar	Wolf Hole Mountain	Reynolds et al (1986)
Mount Logan Basalt	Tmlb	PED-43-66	36.3515	-113.2017	2.63 ± 0.34	K-Ar	Mount Logan	Reynolds et al (1986)
Wolf Hole Mountain	Twb	29-B91	36.9009*	-113.6154*	3.1 ± 0.4	K-Ar	Wolf Hole Mountain	Wenrich et al. (1995)
Grand Wash Bay basalt	Tgb	UAKA 89-24	36.2722	-113.9845	3.24 ± 0.05	K-Ar	Lake Mead	Damon et al. (1996)
Mt. Trumbull Basalt	Tmb	PED-42-66	36.3978	-113.1544	3.47 ± 0.63	K-Ar	Mt. Trumbull NW	Best et al. (1980)
Black Rock Canyon	Tbrb	19-B91	36.8988*	-113.371*	3.5 ± 0.6	K-Ar	White Pockets	Wenrich et al. (1995)
Bundyville Basalt	Tbb	PED-40-66	36.4082	-113.2917	3.6 ± 0.18	K-Ar	Jones Hill	Reynolds et al (1986)
Hobble Basalt Flow	Thb	18-B91	36.6003*	-113.7661*	3.6 ± 0.54	K-Ar	St. George Canyon	Wenrich et al. (1995)
Mt. Trumbull Basalt	Tmb	PED-42-66	36.3978	-113.1544	3.67 ± 0.09	K-Ar	Mt. Trumbull NW	Best et al. (1980)
Black Rock Mountain	Tbb	28-B91	36.7781	-113.7418	3.7 ± 0.6	K-Ar	Purgatory	Wenrich et al. (1995)
Diamond Butte Basalt	Tdb	24-B91	36.5640	-113.35	4.3 ± 0.6	K-Ar	Little Tanks	Wenrich et al. (1995)
Sandy Point	Tbsp	JF-97-76	36.1147	-114.1113	4.48 ± 0.03	Ar-Ar	Meadview North	Faulds et al. (2001)
Whitmore Hill Vent	Twb	4-B86	36.1400	-113.227	4.56 ± 0.12	K-Ar	Whitmore Rapids	Wenrich et al. (1995)
Pakoon Springs Basalt	Tb	UAKA 89-23	36.4000	-113.933	4.7 ± 0.07	K-Ar	Pakoon Springs	Damon et al. (1996)
Grand Wash	Tgb	K06-286.5-R-1	36.2013	-114.0327	4.72 ± 0.17	Ar-Ar	Lake Mead	Crow et al. (in prep)
Grand Wash	Tgb	H98AR-23-1	36.3676	-114.012	4.78 ± 0.03	Ar-Ar	Lake Mead	Beard et al. (2007)
Cottonwood Basalt (top)	Tb	PED-35-66	36.6270	-113.8897	4.73 ± 0.18	K-Ar	Cane Springs	Reynolds et al (1986)
Poverty Mountain Basalt	Tpb	PED-39-66	36.4310	-113.558	4.75 ± 0.26	K-Ar	Poverty Spring	Best et al. (1980)
Fortification Hill Basalt	Tfb	87-38-143-LN	36.0505	-114.677	5.42 ± 0.13	K-Ar	Lake Mead	Feurbach et al. (1991)
Fortification Hill Basalt	Tfb	F8-42-82-LN	36.0770	-114.5955	5.43 ± 0.16	K-Ar	Lake Mead	Feurbach et al. (1991)
Fortification Hill Basalt	Tfb	87-38-142-LN	36.0532	-114.6817	5.73 ± 0.13	K-Ar	Lake Mead	Feurbach et al. (1991)
Fortification Hill Basalt	Tfb	F7-38-13-LN	36.0625	-114.6822	5.89 ± 0.18	K-Ar	Lake Mead	Feurbach et al. (1991)
Muddy Creek Volcanics	Tmv	87-10-129-LN	36.4120	-114.3838	6.02 ± 0.39	K-Ar	Lake Mead	Feurbach et al. (1991)
Dellenbaugh Basalt	Tsb	PED-38-66	36.1530	-113.583	6.78 ± 0.15	K-Ar	Castle Peak	Reynolds et al (1986)
Cottonwood Basalt (base)	Tb	PED-34-66	36.6270	-113.8893	6.87 ± 0.2	K-Ar	Cane Springs	Best et al. (1980)
Mt. Dellenbaugh Basalt	Tsb	PED-37-66	36.1090	-113.542	7.06 ± 0.49	K-Ar	Mt. Dellenbaugh	Reynolds et al (1986)
Callville Mesa Volcanics	Tcm4	F8-24-85-LN	36.1642	-114.7325	8.49 ± 0.2	K-Ar	Lake Mead	Feurbach et al. (1991)
Snap Point Basalt	Tsgb	SP-80-1	36.1730	-113.811	9.07 ± 0.8	K-Ar	Snap Canyon East	Reynolds et al (1986)
Gold Butte	Tbgb	K-97-12-3E-1	36.2662	-114.2539	9.39 ± 0.05	Ar-Ar	Lake Mead	Beard et al. (2007)
Hamblin Volcanics	Tvh	11-714-71	36.1865	-114.6542	10.19 ± 0.07	Ar-Ar	Lake Mead	Anderson et al. (1994)
Callville Mesa Volcanics	Tcm1	F8-24-100-LN	36.1720	-114.7083	10.46 ± 0.23	K-Ar	Lake Mead	Feurbach et al. (1991)
Tertiary Basalt Undivided	Tvc	KT8250	36.1881	-114.4949	11.1 ± 1.1	K-Ar	Lake Mead	Thompson (1985)
Callville Mesa Volcanics	Tcm	TV92-5	36.1745	-114.8125	11.55 ± 0.14	Ar-Ar	Lake Mead	Harlan et al. (1998)
Hamblin Volcanics	Tvhu	12-801-17	36.1826	-114.6778	11.85 ± 0.03	Ar-Ar	Lake Mead	Anderson et al. (1994)
Tertiary Basalt Undivided	Tyb	K-97-12-4F-1	36.2663	-114.3918	12.23 ± 0.07	Ar-Ar	Lake Mead	Beard et al. (2007)
Tertiary Basalt Undivided	Tyb	K-97-12-5G-2	36.2897	-114.3696	12.33 ± 0.07	Ar-Ar	Lake Mead	Beard et al. (2007)
River Mountains Basalt	Trmb	JF-92-07	36.1043	-114.9222	12.292 ± 0.02	Ar-Ar	Lake Mead	Faulds et al. (1999)
Lovell Wash Basalt	Thlb	TV92-7	36.1775	-114.8145	13.33 ± 0.1	Ar-Ar	Lake Mead	Harlan et al. (1998)
Patsy Mine Volcanics	Tpm	92-MIL-4	36.0111	-114.75	14.333 ± 0.03	Ar-Ar	Lake Mead	Faulds et al. (1999)

* = estimated location

Note: All Ar-Ar ages were recalculated using a Fish Canyon monitor age of 28.201 Ma (Kuiper et al., 2008) and a decay constant of 5.463E-10/yr (Min et al., 2000)

APPENDIX B: Incision Rates of the Virgin River Region

	Flow	River/Tributary	Incision Point Latitude	Incision Point Longitude	Strath Elevation (m)	River Elevation (m)	Strath Height (m)	Height Method	Age (Ma)	Error (Ma)	Dating Method	Dated Sample Number	Incision Rate (m/Ma)	Incision Rate Error (m/Ma)	Preferred /Approx	Structural Block	Age Reference
1	Antelope Knoll	Fort Pearce Wash	36.8411	-113.2175	1460	1419	41	Topo/GE	0.83	0.28	K-Ar	-	49	+43 -21	Approx	Zion	Billingsley (1994)
2	Black Rock Mtn	Sullivan Canyon	36.8779	-113.7917	1450	1022	428	Topo/GE	3.7	0.6	K-Ar	28-B91	116	+26 -18	Approx	St. George	Billingsley (1990, 1993)
3	Black Rock Mtn	Mtn Sheep Wash	36.9125	-113.7622	1632	997	635	Topo/GE	3.7	0.6	K-Ar	28-B91	172	+36 -26	Approx	St. George	Billingsley (1990, 1993)
4	Black Rock Mtn	Virgin River	36.9125	-113.7622	1507**	678	829	Topo/GE	3.7	0.6	K-Ar	28-B91	224	+47 -34	Approx	St. George	Billingsley (1990, 1993)
5	Black Rock Mtn	Cottonwood Wash	36.70817	-113.9049	1518	1420	98	Topo/GE	3.7	0.6	K-Ar	28-B91	26	+8 -6	Approx	Lake Mead	Billingsley (1990, 1993)
6	Black Rock Mtn	Cottonwood Wash	36.70188	-113.9097	1480	1393	87	Topo/GE	3.7	0.6	K-Ar	28-B91	24	+8 -6	Approx	Lake Mead	Billingsley (1990, 1993)
7	Black Rock Mtn	Cottonwood Wash	36.6347	-113.9219	1274	1166	108	Laser Range	3.7	0.6	K-Ar	28-B91	29	+6 -5	Approx	Lake Mead	Billingsley (1990, 1993)
8	Cedar Bench	Santa Clara River	37.0794	-113.5926	860	778	82	Topo/GE	1.238	0.01	Ar-Ar	VR40-05	66	±9	Approx	St. George	Biek et al (2010)
9	Cedar Bench	Virgin River	37.0799	-113.5926	860	771	89	Topo/GE	1.238	0.01	Ar-Ar	VR40-05	72	±9	Approx	St. George	Biek et al (2010)
10	Cedar Bench	Virgin River	37.1062	-113.5950	882	771	111	Laser Range	1.238	0.01	Ar-Ar	VR40-05	90	±2	Preferred	St. George	Biek et al (2010)
11	Cedar Bench	Virgin River					76	Publication	1.238	0.01	Ar-Ar	VR40-05	61	±9	Approx	St. George	Willis and Biek(2001)
12	Crater Hill	Coal Pits Wash	37.2216	-113.0873	1314	1314	0	Topo/GE	0.122	0.015	OSL	-	0	+93 -73	Preferred	Zion	Biek et al (2010)
13	Crater Hill	Coal Pits Wash	37.2159	-113.0800	1275	1275	0	Topo/GE	0.122	0.015	OSL	-	0	+93 -73	Preferred	Zion	Biek et al (2010)
14	Crater Hill	Virgin River	37.197	-113.1609	1113	1078	35	Laser Range	0.122	0.015	OSL	-	287	+59 -46	Preferred	Zion	Biek et al (2010)
15	Gould Wash	Frog Hollow	37.1349	-113.2944	1127	1091	36	Topo/GE	0.423	0.21	Ar-Ar	VR41-08	85	+133 -44	Approx	Zion	Biek et al (2010)
16	Gould Wash	Frog Hollow	37.1354	-113.2951	1123	1067	56	Topo/GE	0.423	0.21	Ar-Ar	VR41-08	132	+181 -60	Approx	Zion	Biek et al (2010)
17	Grand Wash	Grand Wash	36.26969	-113.9952	501	394	107	Topo/GE	3.24	0.05	K-Ar	UAKA 89-24	33	±4	Approx	Lake Mead	Damon et al. (1996)
18	Grand Wash	Grand Wash	36.43815	-113.9767	819	767	52	Laser Range	4.78	0.03	Ar-Ar	H98AR-23-1	11	±0.5	Approx	Lake Mead	Beard et al. (2007)
19	Grand Wash	Grand Wash					178	Publication	6.87	0.2	K-Ar	PED-34-66	26	±2	Approx	Lake Mead	Hamblin et al. (1981)
20	Grand Wash	Colorado River	36.2013	-114.0327	495	261	234	Publication	4.72	0.17	Ar-Ar	K06-286.5-R-1	50	±2	Preferred	Lake Mead	Crow et al. (in prep.)
21	Grand Wash	Grand Wash	36.4008	-113.9407	745	638	107	Topo/GE	4.7	0.07	K-Ar	UAKA 89-23	23	+3 -2	Approx	Lake Mead	Damon et al. (1996)
22	Grapevine Wash	North Creek	37.2998	-113.0823	1692	1562	130	Topo/GE	0.263	0.01	Ar-Ar	ZP-0606	494	+59 -55	Approx	Zion	Willis and Hylland (2002)
23	Grapevine Wash	North Creek	37.2876	-113.0885	1459	1408	51	Topo/GE	0.263	0.01	Ar-Ar	ZP-0606	194	+47 -44	Approx	Zion	Willis and Hylland (2002)
24	Grapevine Wash	North Creek	37.2648	-113.1037	1337	1239	98	Topo/GE	0.263	0.01	Ar-Ar	ZP-0606	373	+54 -50	Approx	Zion	Willis and Hylland (2002)
25	Grapevine Wash	North Creek	37.2541	-113.1339	1221	1172	49	Topo/GE	0.263	0.01	Ar-Ar	ZP-0606	186	+47 -43	Approx	Zion	Willis and Hylland (2002)
26	Gunlock	Santa Clara River	37.2291	-113.7752	1112	1034	78	Topo/GE	1.62	0.07	Ar-Ar	VR40-01	48	+9 -8	Preferred	St. George	Biek et al (2010)
27	Gunlock	Santa Clara River	37.2068	-113.7757	1100	1006	94	Topo/GE	1.62	0.07	Ar-Ar	VR40-01	58	+9 -8	Preferred	St. George	Biek et al (2010)
28	Gunlock	Santa Clara River	37.2378	-113.7745	1133	1047	86	Topo/GE	1.62	0.07	Ar-Ar	VR40-01	53	+9 -8	Preferred	St. George	Biek et al (2010)
29	Horse Knoll	Deep Creek	37.4037	-112.9324	1946	1707	239	Topo/GE	0.739	0.02	Ar-Ar	CP62001-3	323	+23 -22	Approx	Zion	Biek and Hylland (2007)
30	Horse Knoll	Spring Run Gulch	37.4467	-112.8822	2321	2321	0	Topo/GE	0.739	0.02	Ar-Ar	CP62001-3	0	+14 -13	Approx	Zion	Biek and Hylland (2007)
31	Horse Knoll	Spring Run Gulch	37.4374	-112.8902	2271	2144	127	Topo/GE	0.739	0.02	Ar-Ar	CP62001-3	172	+19 -18	Approx	Zion	Biek and Hylland (2007)
32	Horse Knoll	Spring Run Gulch	37.4308	-112.8981	2210	1970	240	Topo/GE	0.739	0.02	Ar-Ar	CP62001-3	325	+23 -22	Approx	Zion	Biek and Hylland (2007)
33	Horse Knoll	Corral Canyon	37.4316	-112.8889	2228	2228	0	Topo/GE	0.739	0.02	Ar-Ar	CP62001-3	0	+14 -13	Approx	Zion	Biek and Hylland (2007)
34	Horse Knoll	Corral Canyon	37.4286	-112.9002	2116	2116	0	Topo/GE	0.739	0.02	Ar-Ar	CP62001-3	0	+14 -13	Approx	Zion	Biek and Hylland (2007)
35	Horse Knoll	Deep Creek	37.4114	-112.9241	1978	1764	214	Topo/GE	0.739	0.02	Ar-Ar	CP62001-3	290	+22 -21	Approx	Zion	Biek and Hylland (2007)
36	Horse Knoll	Deep Creek	37.3837	-112.9458	1870	1585	285	Topo/GE	0.739	0.02	Ar-Ar	CP62001-3	386	+25 -23	Approx	Zion	Biek and Hylland (2007)
37	Horse Knoll	Deep Creek	37.3796	-112.9448	1865	1581	284	Topo/GE	0.739	0.02	Ar-Ar	CP62001-4	384	+25 -23	Approx	Zion	Biek and Hylland (2007)
38	Ivans Knoll	Virgin River	37.1698	-113.3546	926**	846	80	Topo/GE	0.983	0.07	Ar-Ar	H11299-2	81	+17 -15	Approx	Hurricane	Biek (2003b)
39	Ivans Knoll	Virgin River	37.1378	-113.3601	911**	832	79	Topo/GE	1.043	0.02	Ar-Ar	VR123-11	76	±11	Approx	Hurricane	Biek (2003b)
40	Ivans Knoll	Virgin River					85	Publication	0.983	0.07	Ar-Ar	H11299-2	86	±16	Approx	Hurricane	Willis and Biek(2001)

APPENDIX B (cont.): Incision Rates of the Virgin River Region

	Flow	River/Tributary	Incision Point Latitude	Incision Point Longitude	Strath Elevation (m)	River Elevation (m)	Strath Height (m)	Height Method	Age (Ma)	Error (Ma)	Dating Method	Dated Sample Number	Incision Rate (m/Ma)	Incision Rate Error (m/Ma)	Preferred /Approx	Structural Block	Age Reference
41	Ivans Knoll	Virgin River	-	-	-	-	85	Publication	1.043	0.02	Ar-Ar	VR123-11	81	+10 -12	Approx	Hurricane	Willis and Biek(2001)
42	Kolob Peak	Kolob Creek	37.4177	-113.0428	2424	2424	0	Topo/GE	1.064	0.05	Ar-Ar	KR81200-1	0	+10 -9	Approx	Zion	Biek (2007b)
43	Lava Point	Virgin River	37.2102	-113.1539	1467**	1078	389	Topo/GE	1.067	0.01	Ar-Ar	VR41-01c	365	±13	Approx	Zion	Biek (2007b)
44	Lava Point	Virgin River	-	-	-	-	400	Publication	1.067	0.01	Ar-Ar	VR41-01c	375	±13	Approx	Zion	Willis and Biek(2001)
45	Lava Point	North Creek	37.2114	-113.1542	1459	1091	368	Topo/GE	1.067	0.01	Ar-Ar	VR41-01c	345	±13	Approx	Zion	Biek (2007b)
46	Lava Point	North Creek	37.3719	-113.0420	2379	2123	256	Topo/GE	1.094	0.02	Ar-Ar	ZP-0602	234	+14 -13	Approx	Zion	Biek (2007b)
47	Lava Ridge	Virgin River	37.0891	-113.5473	830	778	52	Topo/GE	1.419	0.01	Ar-Ar	VR40-06	37	±7	Approx	St. George	Biek et al (2010)
48	Lava Ridge	Virgin River	37.0896	-113.5438	816	778	38	Laser Range	1.419	0.01	Ar-Ar	VR40-06	27	±2	Preferred	St. George	Biek et al (2010)
49	Lava Ridge	Virgin River	-	-	-	-	52	Publication	1.419	0.01	Ar-Ar	VR40-06	37	±7	Approx	St. George	Willis and Biek(2001)
50	Little Creek Pk	Pine Spring Wash	37.3714	-113.0824	2446	2189	257	Topo/GE	1.449	0.04	Ar-Ar	VR43-01	177	±12	Approx	Zion	Willis and Hylland (2002)
51	Little Creek Pk	Pine Spring Wash	37.356	-113.0739	2360	2008	352	Topo/GE	1.449	0.04	Ar-Ar	VR43-01	243	+14 -13	Approx	Zion	Willis and Hylland (2002)
52	Magotsu Creek	Santa Clara River	37.29	-113.7524	1207	1122	85	Topo/GE	0.993	0.03	Ar-Ar	VY11702-1	86	+13 -12	Approx	St. George	UGS and NMGRL (2008)
53	Magotsu Creek	Santa Clara River	37.2805	-113.7660	1185	1105	80	Topo/GE	0.993	0.03	Ar-Ar	VY11702-1	81	+13 -12	Approx	St. George	UGS and NMGRL (2008)
54	Magotsu Creek	Santa Clara River	37.3241	-113.7128	1298	1260	38	Topo/GE	0.993	0.03	Ar-Ar	VY11702-1	38	+12 -11	Approx	St. George	UGS and NMGRL (2008)
55	Pine Valley	Santa Clara River	37.405	-113.5277	1973	1973	0	Topo/GE	0.674	0.07	Ar-Ar	CEQ-14	0	+17 -14	Approx	St. George	UGS and NMGRL (2007a)
56	Pintura	Virgin River	-	-	-	-	58	Publication	0.902	0.02	Ar-Ar	VR113-4	64	+13 -12	Approx	Hurricane	Willis and Biek(2001)
57	Pintura	Ash Creek	37.2294	-113.2843	963	963	0	Topo/GE	0.902	0.02	Ar-Ar	VR113-4	0	±11	Approx	Hurricane	Biek (2003b)
58	Pintura	Ash Creek	37.2681	-113.2798	1057	1057	0	Topo/GE	0.902	0.02	Ar-Ar	VR113-4	0	±11	Approx	Hurricane	Biek (2003b)
59	Pintura	Ash Creek	37.2901	-113.2856	1113	1113	0	Topo/GE	0.902	0.02	Ar-Ar	VR113-4	0	±11	Approx	Hurricane	Biek (2003b)
60	Pintura	Ash Creek	37.3115	-113.2792	1166	1166	0	Topo/GE	0.821	0.1	Ar-Ar	ACG-1	0	+14 -11	Approx	Hurricane	Lund et al. (2001)
61	Pintura	Ash Creek	37.3927	-113.2402	1361	1361	0	Topo/GE	0.891	0.05	Ar-Ar	AC-1	0	+12 -11	Approx	Hurricane	Lund and Everitt (1998)
62	Pintura	Ash Creek	37.4309	-113.2572	1472	1472	0	Topo/GE	0.891	0.05	Ar-Ar	AC-1	0	+12 -11	Approx	Hurricane	Lund and Everitt (1998)
63	Pintura	La Verkin Creek	37.2225	-113.2851	997	943	54	Topo/GE	0.902	0.02	Ar-Ar	VR113-4	60	+13 -12	Approx	Hurricane	Biek (2003b)
64	Pintura	La Verkin Creek	37.241	-113.2752	1133	1034	99	Topo/GE	0.902	0.02	Ar-Ar	VR113-4	110	+14 -13	Approx	Hurricane	Biek (2003b)
65	Pintura	La Verkin Creek	37.2881	-113.2713	1552	1114	438	Topo/GE	0.821	0.1	Ar-Ar	ACG-1	533	+90 -70	Approx	Zion	Lund et al. (2001)
66	Pintura	La Verkin Creek	37.3428	-113.2465	1907	1218	689	Topo/GE	0.881	0.04	Ar-Ar	MH-1	782	+49 -45	Approx	Zion	Lund et al. (2001)
67	Pintura	La Verkin Creek	37.3478	-113.2416	1920	1265	655	Topo/GE	0.881	0.04	Ar-Ar	MH-1	743	+47 -43	Approx	Zion	Lund et al. (2001)
68	Pintura	La Verkin Creek	37.3656	-113.2300	1919	1332	587	Topo/GE	0.881	0.04	Ar-Ar	MH-1	666	+44 -40	Approx	Zion	Lund et al. (2001)
69	Pintura	La Verkin Creek	37.3797	-113.2102	1896	1415	481	Topo/GE	0.881	0.04	Ar-Ar	MH-1	546	+38 -35	Approx	Zion	Lund et al. (2001)
70	Pintura	La Verkin Creek	37.3915	-113.2104	1912	1471	441	Topo/GE	0.881	0.04	Ar-Ar	MH-1	501	+36 -33	Approx	Zion	Lund et al. (2001)
71	Pintura	La Verkin Creek	37.4006	-113.2104	1915	1578	337	Topo/GE	0.881	0.04	Ar-Ar	MH-1	383	+30 -27	Approx	Zion	Lund et al. (2001)
72	Pintura	La Verkin Creek	37.3675	-113.2128	1805	1330	475	Topo/GE	0.881	0.04	Ar-Ar	MH-1	539	+38 -34	Approx	Zion	Lund et al. (2001)
73	Pintura	La Verkin Creek	37.2035	-113.2845	957	914	43	Topo/GE	0.902	0.02	Ar-Ar	VR113-4	48	±12	Approx	Hurricane	Biek (2003b)
74	Radio Tower	Virgin River	37.1998	-113.3131	896	896	0	Topo/GE	0.142	0.06	Ar-Ar	H11299-4	0	+122 -50	Approx	Hurricane	Biek (2003b)
75	Radio Tower	Virgin River	-	-	-	-	21	Publication	0.142	0.06	Ar-Ar	H11299-4	148	+230 -93	Approx	Hurricane	Willis and Biek(2001)
76	Radio Tower	Virgin River	37.1997	-113.2935	913	908	5	Laser Range	0.142	0.06	Ar-Ar	H11299-4	35	+50 -20	Preferred	Hurricane	Biek (2003b)
77	Spencer Bench	EF Virgin River	37.3739	-112.5902	2003	1898	105	Topo/GE	0.57	0.02	Ar-Ar	-	184	+25 -23	Approx	Zion	Schiefelbein (2002)
78	Spencer Bench	EF Virgin River	37.3586	-112.5948	1963	1852	111	Topo/GE	0.57	0.02	Ar-Ar	-	195	+25 -24	Approx	Zion	Schiefelbein (2002)
79	Spencer Bench	EF Virgin River	37.3937	-112.5586	2053	2053	0	Topo/GE	0.57	0.02	Ar-Ar	-	0	+18 -17	Approx	Zion	Schiefelbein (2002)
80	Spencer Bench	EF Virgin River	37.3915	-112.5617	2064	2007	57	Laser Range	0.57	0.02	Ar-Ar	-	100	±7	Approx	Zion	Schiefelbein (2002)

APPENDIX B (cont.): Incision Rates of the Virgin River Region

	Flow	River/Tributary	Incision Point Latitude	Incision Point Longitude	Strath Elevation (m)	River Elevation (m)	Strath Height (m)	Height Method	Age (Ma)	Error (Ma)	Dating Method	Dated Sample Number	Incision Rate (m/Ma)	Incision Rate Error (m/Ma)	Preferred /Approx	Structural Block	Age Reference
81	Spencer Bench	EF Virgin River	37.3918	-112.5596	2052	2026	26	Laser Range	0.57	0.02	Ar-Ar	-	46	±5	Approx	Zion	Schiefelbein (2002)
82	Spencer Bench	EF Virgin River	37.3559	-112.5954	1950	1836	114	Laser Range	0.57	0.02	Ar-Ar	-	200	+11 -10	Approx	Zion	Schiefelbein (2002)
83	Spencer Bench	EF Virgin River	37.351	-112.6005	1946	1826	120	Laser Range	0.57	0.02	Ar-Ar	-	211	±11	Approx	Zion	Schiefelbein (2002)
84	Spencer Bench	EF Virgin River	37.3115	-112.6059	1863	1741	122	Topo/GE	0.57	0.02	Ar-Ar	-	214	+26 -24	Approx	Zion	Schiefelbein (2002)
85	Spencer Bench	EF Virgin River	37.3875	-112.5669	2073	1990	83	Topo/GE	0.57	0.02	Ar-Ar	-	146	+24 -22	Approx	Zion	Schiefelbein (2002)
86	Spencer Bench	EF Virgin River	37.3673	-112.5939	-	-	30	Publication	0.57	0.02	Ar-Ar	-	53	±18	Preferred	Zion	Darling (2016)
87	Twin Peaks	Santa Clara River	37.0954	-113.6035	954**	789	165	Topo/GE	2.355	0.02	Ar-Ar	VR40-04	70	±5	Approx	St. George	Biek et al (2010)
88	Twin Peaks	Virgin River	37.0952	-113.6035	923**	769	154	Topo/GE	2.355	0.02	Ar-Ar	VR40-04	65	±5	Approx	St. George	Biek et al (2010)
89	Twin Peaks	Virgin River	-	-	-	-	168	Publication	2.355	0.02	Ar-Ar	VR40-04	71	±5	Approx	St. George	Willis and Biek(2001)
90	Twin Peaks	Virgin River	37.1113	-113.5999	923**	772	151	Topo/GE	2.355	0.02	Ar-Ar	VR40-05	64	±5	Preferred	St. George	Biek et al (2010)
91	Veyo	Santa Clara River	37.3179	-113.7151	1312	1246	66	Topo/GE	0.699	0.04	Ar-Ar	VV111902-7	94	+21 -19	Approx	St. George	UGS and NMGRL (2007b)
92	Veyo	Santa Clara River	37.3287	-113.7025	1344	1298	46	Topo/GE	0.699	0.04	Ar-Ar	VV111902-7	66	+19 -17	Approx	St. George	UGS and NMGRL (2007b)
93	Volcano Knoll	Deep Creek	37.3887	-112.9361	1849	1622	227	Topo/GE	0.344	0.03	Ar-Ar	CP71900-6	660	+95 -80	Approx	Zion	Biek and Hylland (2007)
94	Volcano Knoll	Deep Creek	37.3901	-112.9343	1842	1632	210	Topo/GE	0.344	0.03	Ar-Ar	CP71900-6	610	+90 -76	Approx	Zion	Biek and Hylland (2007)
95	Volcano Knoll	Deep Creek	37.3955	-112.9395	1854	1684	170	Topo/GE	0.344	0.03	Ar-Ar	CP71900-6	494	+79 -66	Approx	Zion	Biek and Hylland (2007)
96	Volcano Knoll	Deep Creek	37.4284	-112.9351	1926	1840	86	Topo/GE	0.344	0.03	Ar-Ar	CP71900-6	250	+56 -47	Approx	Zion	Biek and Hylland (2007)
97	Volcano Knoll	Deep Creek	37.4186	-112.9279	1898	1786	112	Topo/GE	0.344	0.03	Ar-Ar	CP71900-6	326	+63 -53	Approx	Zion	Biek and Hylland (2007)
98	Volcano Knoll	Deep Creek	37.4174	-112.9275	-	-	122	Publication	0.344	0.03	Ar-Ar	CP71900-6	355	+66 -55	Approx	Zion	Crow (2012)
99	Volcano Mtn	Virgin River	37.1939	-113.3300	933	883	50	Topo/GE	0.358	0.04	Ar-Ar	6 15	140	+50 -40	Approx	Hurricane	Sanchez(1995)
100	Volcano Mtn	Virgin River	37.1972	-113.3444	912	873	39	Topo/GE	0.358	0.04	Ar-Ar	6 15	109	+46 -37	Approx	Hurricane	Sanchez(1995)
101	Volcano Mtn	Virgin River	37.194	-113.3472	913	871	42	Topo/GE	0.358	0.04	Ar-Ar	6 15	117	+47 -38	Approx	Hurricane	Sanchez(1995)
102	Volcano Mtn	Virgin River	37.1916	-113.3500	926	866	60	Topo/GE	0.358	0.04	Ar-Ar	6 15	168	+54 -43	Approx	Hurricane	Sanchez(1995)
103	Volcano Mtn	Virgin River	37.1894	-113.3596	911	863	48	Topo/GE	0.358	0.04	Ar-Ar	6 15	134	+49 -39	Approx	Hurricane	Sanchez(1995)
104	Volcano Mtn	Virgin River	37.1497	-113.4059	844	832	12	Topo/GE	0.358	0.04	Ar-Ar	6 15	34	+36 -29	Approx	Hurricane	Sanchez(1995)
105	Volcano Mtn	Virgin River	37.1906	-113.2759	934	934	0	Topo/GE	0.358	0.04	Ar-Ar	6 15	0	+32 -25	Preferred	Hurricane	Sanchez(1995)
106	Volcano Mtn	Virgin River	37.1878	-113.2732	1044	935	109	Topo/GE	0.358	0.04	Ar-Ar	6 15	304	+71 -57	Approx	Zion	Sanchez(1995)
107	Volcano Mtn	Virgin River	37.1905	-113.2709	1042	935	107	Topo/GE	0.358	0.04	Ar-Ar	6 15	299	+71 -56	Approx	Zion	Sanchez(1995)
108	Volcano Mtn	Virgin River	37.188	-113.2757	1044	934	110	Laser Range	0.358	0.04	Ar-Ar	6 15	307	+46 -37	Approx	Zion	Sanchez(1995)
109	Volcano Mtn	Virgin River	-	-	-	-	125	Publication	0.358	0.046	Ar-Ar	6 15	349	+86 -66	Approx	Zion	Willis and Biek(2001)
110	Volcano Mtn	Virgin River	-	-	-	-	52	Publication	0.358	0.045	Ar-Ar	6 15	145	+54 -42	Approx	Hurricane	Willis and Biek(2001)
111	Washington	Virgin River	37.1255	-113.4904	890	800	90	Topo/GE	0.986	0.02	Ar-Ar	VR40-07	91	±12	Preferred	Hurricane	Biek (2003a)
112	Washington	Virgin River	37.1235	-113.4822	918	802	116	Topo/GE	0.986	0.02	Ar-Ar	VR40-07	118	+13 -12	Approx	Hurricane	Biek (2003a)
113	Washington	Virgin River	-	-	-	-	107	Publication	0.881	0.04	Ar-Ar	HF11299-2	121	+16 -18	Approx	Hurricane	Willis and Biek(2001)
114	Washington	Virgin River	37.1235	-113.4822	-	-	107	Publication	0.986	0.02	Ar-Ar	VR40-07	109	+13 -12	Approx	Hurricane	Willis and Biek(2001)
115	Wolf Hole Mtn	Black Rock Gulch	36.867	-113.6333	1540	1216	324	Topo/GE	3.1	0.4	K-Ar	-	105	+19 -15	Approx	St. George	Billingsley (1993)
116	Wolf Hole Mtn	Virgin River	36.9265	-113.6000	1053**	739	314	Topo/GE	3.1	0.4	K-Ar	-	101	+19 -14	Approx	St. George	Billingsley (1993)

* = datapoint used in calculating block average incision rate (Fig. 10)

** = projected height

Red = Data points used in calculation of average block incision rates (see text)

Black = 'Apparent' incision rates; ≤ 5 km from major fault; not used in block average incision rates

65

APPENDIX C

Detrital Sanidine 40Ar/39Ar geochronology data

ID	Power (watts)	$^{40}Ar/^{39}Ar$	$^{37}Ar/^{39}Ar$	$^{36}Ar/^{39}Ar$ (x 10^{-3})	$^{39}Ar_K$ (x 10^{-15} mol)	K/Ca	$^{40}Ar*$ (%)	Age (Ma)	±1s (Ma)
KCW17-19, Sanidine, J=0.001896±0.03%, IC=1.0245±0.000773, NM-293D, Lab#=65988, Argus VI									
05	2.0	1.766	0.0075	0.2247	1.028	67.9	96.3	5.863	0.024
53	2.0	3.298	0.0199	0.3718	1.455	25.6	96.7	11.008	0.023
107	2.0	4.151	0.0169	1.706	1.265	30.1	87.9	12.586	0.033
119	2.0	4.364	0.0362	1.624	0.668	14.1	89.0	13.411	0.057
20	2.0	3.977	0.0223	0.2055	0.834	22.9	98.5	13.518	0.032
91	2.0	4.374	0.0108	1.432	0.612	47.1	90.3	13.634	0.070
06	2.0	7.244	0.0325	11.13	3.442	15.7	54.6	13.652	0.049
58	2.0	8.275	0.0264	14.58	3.063	19.3	47.9	13.695	0.052
49	2.0	4.138	0.0316	0.5679	1.180	16.2	96.0	13.707	0.028
145	2.0	4.004	0.0227	0.0975	1.348	22.5	99.3	13.721	0.021
71	2.0	4.259	0.0027	0.0792	3.795	187.6	99.5	14.612	0.009
136	2.0	4.813	0.0028	1.688	1.372	179.4	89.6	14.882	0.040
36	2.0	4.643	0.0011	1.024	0.919	464.7	93.5	14.974	0.037
04	2.0	4.481	0.0009	0.4099	2.332	579.9	97.3	15.039	0.016
35	2.0	5.181	0.0051	0.6346	2.432	99.6	96.4	17.219	0.018
08	2.0	5.105	0.0057	0.2335	2.098	90.2	98.7	17.368	0.017
38	2.0	5.164	0.0062	0.3919	1.620	82.9	97.8	17.409	0.022
117	2.0	5.407	0.0120	0.4631	1.055	42.6	97.5	18.175	0.033
56	2.0	5.353	0.0043	0.2056	2.122	119.1	98.9	18.246	0.018
97	2.0	5.427	0.0117	0.4521	0.731	43.8	97.6	18.253	0.049
96	2.0	5.593	0.0067	0.9344	1.159	76.7	95.1	18.333	0.034
16	2.0	5.416	0.0099	0.3126	1.572	51.5	98.3	18.356	0.026
54	2.0	5.365	0.0065	0.1291	1.377	78.3	99.3	18.365	0.024
01	2.0	5.442	0.0069	0.3655	2.274	73.5	98.0	18.393	0.019
86	2.0	5.449	0.0076	0.3471	4.502	67.5	98.1	18.436	0.010
03	2.0	5.472	0.0075	0.3283	1.919	68.3	98.2	18.533	0.020
51	2.0	5.453	0.0077	0.2483	0.872	66.2	98.7	18.547	0.037
59	2.0	5.535	0.0067	0.5214	2.271	76.4	97.2	18.553	0.019
114	2.0	5.532	0.0067	0.4912	1.401	75.6	97.4	18.573	0.028
80	2.0	5.434	0.0085	0.1539	1.397	60.2	99.2	18.581	0.023
11	2.0	5.569	0.0074	0.6067	4.009	69.0	96.8	18.582	0.014
88	2.0	5.576	0.0116	0.6104	1.342	44.1	96.8	18.603	0.029
23	2.0	5.617	0.0110	0.7373	1.124	46.5	96.1	18.615	0.035
68	2.0	8.104	0.0101	9.126	3.662	50.5	66.7	18.643	0.048
45	2.0	5.710	0.0053	1.007	5.272	95.5	94.8	18.660	0.012
93	2.0	5.554	0.0130	0.4779	1.043	39.2	97.5	18.664	0.034
17	2.0	5.461	0.0050	0.1495	2.130	101.2	99.2	18.674	0.018
48	2.0	5.446	0.0055	0.0925	2.720	92.3	99.5	18.680	0.013
141	2.0	5.562	0.0060	0.4839	3.806	85.5	97.4	18.682	0.013
104	2.0	5.499	0.0074	0.2697	1.618	69.3	98.6	18.685	0.022
76	2.0	5.444	0.0084	0.0744	4.131	60.7	99.6	18.695	0.010
15	2.0	5.527	0.0057	0.3539	6.706	89.6	98.1	18.696	0.009
99	2.0	5.547	0.0108	0.4096	0.763	47.1	97.8	18.707	0.042
74	2.0	5.484	0.0055	0.1943	4.941	92.3	99.0	18.708	0.009
75	2.0	5.471	0.0069	0.1232	4.165	73.7	99.3	18.739	0.009
30	2.0	5.490	0.0051	0.1745	0.762	100.8	99.1	18.749	0.040
108	2.0	5.482	0.0046	0.1350	7.304	111.4	99.3	18.761	0.007
40	2.0	5.669	0.0050	0.7503	2.702	102.8	96.1	18.780	0.017
95	2.0	5.776	0.0123	1.087	1.673	41.5	94.4	18.807	0.030
34	2.0	5.485	0.0075	0.0879	2.765	68.1	99.5	18.819	0.014
09	2.0	5.627	0.0054	0.5701	3.183	94.2	97.0	18.820	0.015

APPENDIX C (cont.)

Detrital Sanidine 40Ar/39Ar geochronology data (continued)

ID	Power (watts)	$^{40}Ar/^{39}Ar$	$^{37}Ar/^{39}Ar$	$^{36}Ar/^{39}Ar$ (x 10^{-3})	$^{39}Ar_K$ (x 10^{-15} mol)	K/Ca	$^{40}Ar^*$ (%)	Age (Ma)	±1s (Ma)
124	2.0	5.946	0.0188	0.2133	0.781	27.2	99.0	20.282	0.044
148	2.0	5.966	0.0085	0.2457	0.652	60.0	98.8	20.313	0.053
85	2.0	5.938	0.0209	0.1351	1.069	24.5	99.4	20.333	0.031
22	2.0	8.993	0.0193	10.46	3.623	26.4	65.6	20.344	0.045
19	2.0	6.054	0.0328	0.4788	2.417	15.6	97.7	20.384	0.018
125	2.0	5.944	0.0238	0.0892	1.691	21.4	99.6	20.399	0.022
120	2.0	5.981	0.0200	0.2118	1.036	25.5	99.0	20.404	0.035
62	2.0	5.977	0.0258	0.1912	1.486	19.8	99.1	20.412	0.023
122	2.0	6.018	0.0159	0.2989	1.490	32.1	98.6	20.441	0.024
25	2.0	6.862	0.0204	3.146	2.103	25.0	86.5	20.450	0.033
110	2.0	6.074	0.0219	0.4520	1.853	23.3	97.8	20.478	0.022
02	2.0	5.992	0.0189	0.1649	2.810	27.0	99.2	20.487	0.014
146	2.0	6.483	0.0239	1.792	2.676	21.4	91.9	20.524	0.022
139	2.0	6.376	0.0208	1.413	2.071	24.5	93.5	20.540	0.026
33	2.0	6.040	0.0165	0.2538	1.759	31.0	98.8	20.560	0.022
109	2.0	6.027	0.0164	0.1745	2.892	31.2	99.2	20.597	0.014
60	2.0	6.432	0.0080	0.2884	1.279	63.5	98.7	21.868	0.028
47	2.0	6.477	0.0127	0.3648	2.455	40.2	98.4	21.946	0.018
65	2.0	6.446	0.0102	0.1637	3.687	49.9	99.3	22.042	0.012
78	2.0	6.903	0.0103	0.5184	1.682	49.4	97.8	23.251	0.026
92	2.0	7.247	0.0075	1.301	1.902	68.0	94.7	23.637	0.026
63	2.0	7.004	0.0071	0.3563	2.991	72.3	98.5	23.760	0.016
103	2.0	6.951	0.0060	0.1340	2.681	84.9	99.4	23.802	0.014
98	2.0	6.984	0.0068	0.1172	1.827	75.5	99.5	23.935	0.021
102	2.0	7.094	0.0071	0.4157	9.178	72.0	98.3	24.008	0.008
57	2.0	7.168	0.0114	0.3402	0.961	44.8	98.6	24.338	0.039
101	2.0	7.373	0.0077	0.3593	3.581	66.4	98.6	25.020	0.015
130	2.0	7.972	0.0055	2.105	2.186	92.2	92.2	25.304	0.028
73	2.0	7.551	0.0065	0.4590	4.195	78.0	98.2	25.528	0.013
64	2.0	7.505	0.0073	0.2621	3.173	70.0	99.0	25.570	0.015
90	2.0	7.730	0.0096	0.7267	1.568	53.3	97.2	25.871	0.031
82	2.0	9.211	0.0056	0.1535	2.647	90.5	99.5	31.508	0.019
138	2.0	10.03	0.0090	0.2088	0.822	56.8	99.4	34.250	0.055
50	2.0	10.38	0.0053	0.2509	2.031	96.3	99.3	35.411	0.028
89	2.0	24.91	-0.1789	48.45	0.013	-	42.5	36.3	11.6
100	2.0	21.56	0.0126	0.6495	0.838	40.4	99.1	72.67	0.28
129	2.0	23.30	0.0097	0.7862	0.908	52.8	99.0	78.34	0.27
133	2.0	23.43	0.0195	0.6342	0.649	26.1	99.2	78.90	0.36
144	2.0	23.77	0.0019	1.704	0.758	268.0	97.9	79.00	0.35
116	2.0	23.59	0.0084	0.6273	0.866	60.9	99.2	79.46	0.30
132	2.0	23.64	0.0078	0.5006	2.270	65.3	99.4	79.74	0.10
72	2.0	23.62	0.0117	0.3840	1.136	43.5	99.5	79.78	0.26
41	2.0	23.61	0.0118	0.3315	1.144	43.1	99.6	79.82	0.23
121	2.0	23.85	0.0077	1.013	1.859	66.1	98.7	79.94	0.12
105	2.0	23.69	0.0094	0.2805	1.866	54.2	99.7	80.12	0.15
18	2.0	23.69	0.0099	0.1178	2.826	51.7	99.9	80.30	0.10
46	2.0	23.74	0.0060	0.2006	2.390	85.7	99.8	80.354	0.100
137	2.0	23.74	0.0034	0.2007	3.643	150.9	99.8	80.365	0.070
135	2.0	23.76	0.0044	0.1770	3.127	117.1	99.8	80.467	0.081
26	2.0	23.86	0.0078	0.2516	2.050	65.0	99.7	80.72	0.13
84	2.0	25.43	0.0031	5.110	1.448	163.0	94.1	81.17	0.24
115	2.0	27.50	0.0063	0.6516	0.645	80.5	99.3	92.38	0.48

APPENDIX C (cont.)

Detrital Sanidine 40Ar/39Ar geochronology data (continued)

ID	Power	$^{40}Ar/^{39}Ar$	$^{37}Ar/^{39}Ar$	$^{36}Ar/^{39}Ar$	$^{39}Ar_K$	K/Ca	$^{40}Ar^*$	Age	±1s
	(watts)			(x 10^{-3})	(x 10^{-15} mol)		(%)	(Ma)	(Ma)
43	2.0	27.75	0.0078	0.1622	2.405	65.2	99.8	93.68	0.14
81	2.0	27.99	0.0058	0.1784	2.249	87.7	99.8	94.47	0.15
131	2.0	30.24	0.0015	6.871	0.783	332.1	93.3	95.35	0.41
70	2.0	29.48	0.0067	0.8992	0.517	76.0	99.1	98.65	0.60
126	2.0	50.12	0.0196	1.273	1.538	26.1	99.3	164.97	0.35
07	2.0	49.89	0.0225	0.4686	1.878	22.7	99.7	164.98	0.35
106	2.0	55.62	0.0077	0.8133	6.788	66.6	99.6	182.73	0.23
55	2.0	63.79	0.0038	0.7618	1.836	135.4	99.6	208.26	0.44
44	2.0	67.54	0.0106	1.258	1.306	48.1	99.5	219.40	0.55
13	2.0	69.53	0.0494	1.674	3.734	10.3	99.3	225.17	0.45
140	2.0	87.33	0.0121	0.7097	1.183	42.1	99.8	279.81	0.64
10	2.0	93.70	0.0148	10.26	1.718	34.6	96.8	290.37	0.90
52	2.0	93.96	0.0051	10.97	2.307	100.1	96.6	290.51	0.73
79	2.0	92.93	0.0096	3.930	2.654	53.0	98.8	293.60	0.89
28	2.0	93.30	0.0059	4.181	1.108	87.0	98.7	294.48	0.73
142	2.0	93.53	0.0116	0.3583	1.471	43.9	99.9	298.51	0.41
112	2.0	100.8	0.0078	19.68	1.305	65.1	94.2	303.0	1.0
143	2.0	101.5	0.0071	14.50	1.098	71.7	95.8	309.66	0.77
127	2.0	105.6	0.0078	6.424	1.170	65.5	98.2	328.55	0.94
66	2.0	108.4	0.0045	2.741	2.133	113.2	99.3	339.9	1.1
61	2.0	115.6	0.0143	19.39	1.826	35.7	95.0	346.3	1.4
32	2.0	117.0	0.0096	13.66	1.616	53.2	96.6	355.3	1.4
67	2.0	128.6	0.0024	9.728	1.188	212.4	97.8	391.37	0.92
27	2.0	207.2	0.0147	0.4597	1.277	34.8	99.9	606.3	1.9
37	2.0	252.0	0.0100	23.17	1.372	50.9	97.3	698.7	3.6
123	2.0	284.9	0.0350	1.966	0.900	14.6	99.8	789.3	7.0
111	2.0	321.7	0.0507	9.629	0.131	10.1	99.1	865.6	10.0
77	2.0	328.3	0.0056	2.914	0.800	91.2	99.7	884.0	5.7
147	2.0	344.1	0.0304	1.092	0.863	16.8	99.9	918.7	4.3
87	2.0	414.3	0.0105	0.6991	0.815	48.4	100.0	1060.8	5.1
118	2.0	454.2	0.0147	2.550	0.592	34.6	99.8	1135.7	6.7
12	2.0	472.4	0.0094	1.558	0.659	54.1	99.9	1169.8	5.9
94	2.0	509.0	0.0272	1.101	0.639	18.8	99.9	1236.0	6.1
31	2.0	510.2	0.0416	0.6280	0.124	12.3	100.0	1238.4	15.9
24	2.0	534.1	0.0055	0.7368	0.124	92.0	100.0	1279.9	13.8
42	2.0	545.7	0.0104	0.5656	0.136	49.2	100.0	1300.0	13.8
Mean age ± 2s			n=139	MSWD=78263.58		71.8 ±143.1		20.0	1.1

KCW17-4, Sanidine, J=0.0018708±0.04%, IC=1.001982±0.0011492, NM-293L, Lab#=66084, Argus VI

ID	Power	$^{40}Ar/^{39}Ar$	$^{37}Ar/^{39}Ar$	$^{36}Ar/^{39}Ar$	$^{39}Ar_K$	K/Ca	$^{40}Ar^*$	Age	±1s
101	2.25	1.763	0.0063	0.0892	1.998	81.4	98.5	5.910	0.016
157	2.25	4.810	0.0381	3.096	0.377	13.4	81.0	13.27	0.11
74	2.25	5.691	0.0280	5.695	1.299	18.2	70.4	13.653	0.053
112	2.25	4.228	0.0263	0.7083	1.337	19.4	95.1	13.688	0.031
02	2.25	6.772	0.0238	9.309	1.575	21.5	59.4	13.696	0.069
82	2.25	4.238	0.0196	0.6896	2.923	26.0	95.2	13.741	0.015
159	2.25	4.558	0.0368	1.739	0.696	13.9	88.8	13.779	0.058
121	2.25	5.125	0.0282	3.603	0.957	18.1	79.2	13.830	0.048
10	2.25	4.265	0.0214	0.6905	0.362	23.8	95.2	13.830	0.094
87	2.25	4.299	0.0237	0.7676	0.607	21.6	94.8	13.869	0.056
56	2.25	4.708	0.0213	2.147	1.901	24.0	86.5	13.874	0.034
49	2.25	5.695	0.0102	5.452	1.840	50.2	71.7	13.905	0.044
29	2.25	4.695	0.0033	1.395	2.055	156.0	91.2	14.579	0.025

68

APPENDIX C (cont.)

Detrital Sanidine 40Ar/39Ar geochronology data (continued)

ID	Power (watts)	$^{40}Ar/^{39}Ar$	$^{37}Ar/^{39}Ar$	$^{36}Ar/^{39}Ar$ (x 10^{-3})	$^{39}Ar_K$ (x 10^{-15} mol)	K/Ca	$^{40}Ar*$ (%)	Age (Ma)	±1s (Ma)
110	2.25	5.783	0.0024	4.953	1.974	208.8	74.7	14.704	0.039
05	2.25	5.025	0.0183	1.770	0.811	27.8	89.6	15.326	0.057
141	2.25	4.537	0.0139	0.1143	2.460	36.7	99.3	15.331	0.016
122	2.25	7.540	0.0070	7.347	1.105	72.5	71.2	18.268	0.072
130	2.25	5.470	0.0070	0.1526	0.526	72.9	99.2	18.456	0.068
136	2.25	6.697	0.0067	4.165	2.909	76.5	81.6	18.597	0.029
169	2.25	6.033	0.0072	1.904	3.153	71.3	90.7	18.612	0.021
24	2.25	5.629	0.0077	0.5037	1.481	66.2	97.4	18.643	0.028
111	2.25	6.126	0.0078	2.185	3.147	65.6	89.5	18.645	0.023
80	2.25	5.713	0.0098	0.7382	1.921	52.3	96.2	18.694	0.024
57	2.25	6.303	0.0060	2.735	4.570	84.6	87.2	18.695	0.020
55	2.25	6.235	0.0055	2.501	10.081	92.7	88.1	18.695	0.014
115	2.25	5.543	0.0107	0.1368	0.988	47.7	99.3	18.719	0.035
139	2.25	5.546	0.0099	0.1428	1.036	51.4	99.3	18.726	0.036
42	2.25	5.893	0.0096	1.302	1.254	53.0	93.5	18.739	0.035
35	2.25	5.590	0.0059	0.2705	1.291	86.8	98.6	18.745	0.030
06	2.25	5.592	0.0089	0.2744	1.449	57.4	98.6	18.749	0.028
38	2.25	6.668	0.0067	3.886	4.612	76.5	82.8	18.776	0.022
160	2.25	5.670	0.0091	0.5076	1.876	55.8	97.4	18.778	0.022
37	2.25	5.738	0.0052	0.7367	8.996	97.3	96.2	18.778	0.008
07	2.25	5.639	0.0054	0.3947	1.958	94.8	97.9	18.785	0.022
84	2.25	5.647	0.0058	0.4134	4.194	87.5	97.8	18.794	0.012
163	2.25	5.754	0.0076	0.7461	2.089	67.3	96.2	18.824	0.024
153	2.25	5.774	0.0099	0.7851	1.131	51.3	96.0	18.854	0.038
21	2.25	6.025	0.0070	1.512	0.879	73.1	92.6	18.976	0.047
31	2.25	8.227	0.0441	8.751	0.068	11.6	68.6	19.20	0.60
105	2.25	5.786	0.0061	0.2813	2.154	84.0	98.6	19.397	0.017
63	2.25	6.689	0.0246	2.646	0.247	20.7	88.3	20.10	0.16
161	2.25	6.167	0.0350	0.6484	0.294	14.6	96.9	20.33	0.13
72	2.25	6.074	0.0179	0.2811	0.294	28.5	98.7	20.38	0.13
120	2.25	6.170	0.0242	0.5377	1.074	21.1	97.5	20.449	0.040
58	2.25	10.36	0.0230	14.67	5.728	22.1	58.1	20.481	0.035
28	2.25	6.120	0.0244	0.3297	0.958	20.9	98.4	20.486	0.038
48	2.25	6.349	0.0215	1.061	1.250	23.7	95.1	20.530	0.036
34	2.25	6.583	0.0220	1.812	1.247	23.2	91.9	20.570	0.038
23	2.25	6.389	0.0230	1.148	2.246	22.2	94.7	20.577	0.025
158	2.25	6.407	0.0189	1.205	1.868	26.9	94.5	20.579	0.026
166	2.25	6.346	0.0392	1.003	1.963	13.0	95.4	20.581	0.027
104	2.25	6.192	0.0150	0.4745	1.516	34.0	97.8	20.584	0.026
79	2.25	6.494	0.0209	1.493	0.797	24.4	93.2	20.590	0.054
167	2.25	6.116	0.0201	0.2040	1.857	25.3	99.0	20.596	0.023
62	2.25	6.220	0.0233	0.5574	1.608	21.9	97.4	20.597	0.028
30	2.25	6.118	0.0193	0.2092	0.654	26.5	99.0	20.598	0.057
81	2.25	6.407	0.0163	1.178	1.502	31.4	94.6	20.608	0.032
162	2.25	6.248	0.0218	0.6385	1.396	23.4	97.0	20.611	0.031
97	2.25	6.089	0.0173	0.0978	1.858	29.5	99.5	20.612	0.021
04	2.25	6.107	0.0211	0.1541	2.230	24.2	99.3	20.616	0.019
94	2.25	6.780	0.0160	2.428	2.549	31.9	89.4	20.619	0.027
44	2.25	6.180	0.0198	0.3998	1.871	25.8	98.1	20.619	0.024
102	2.25	6.172	0.0224	0.3725	1.137	22.8	98.2	20.620	0.035
92	2.25	6.108	0.0177	0.1495	1.869	28.8	99.3	20.625	0.022
156	2.25	6.090	0.0131	0.0853	0.853	38.8	99.6	20.626	0.045

APPENDIX C (cont.)

Detrital Sanidine 40Ar/39Ar geochronology data (continued)

ID	Power (watts)	$^{40}Ar/^{39}Ar$	$^{37}Ar/^{39}Ar$	$^{36}Ar/^{39}Ar$ (x 10^{-3})	$^{39}Ar_K$ (x 10^{-15} mol)	K/Ca	$^{40}Ar^*$ (%)	Age (Ma)	±1s (Ma)
32	2.25	6.114	0.0170	0.1676	1.532	30.0	99.2	20.627	0.025
15	2.25	6.151	0.0112	0.2915	2.150	45.7	98.6	20.627	0.021
113	2.25	6.088	0.0154	0.0740	2.610	33.1	99.7	20.631	0.015
109	2.25	6.320	0.0357	0.8643	0.742	14.3	96.0	20.634	0.051
116	2.25	6.193	0.0167	0.4246	4.552	30.5	98.0	20.637	0.012
151	2.25	6.399	0.0215	1.121	0.778	23.7	94.8	20.638	0.059
145	2.25	6.134	0.0272	0.2146	2.360	18.8	99.0	20.651	0.018
20	2.25	6.225	0.0162	0.5130	1.075	31.5	97.6	20.656	0.038
03	2.25	6.295	0.0184	0.7497	1.700	27.7	96.5	20.656	0.029
148	2.25	6.097	0.0166	0.0799	1.428	30.8	99.6	20.657	0.027
59	2.25	6.104	0.0238	0.1041	2.212	21.5	99.5	20.657	0.018
26	2.25	6.233	0.0228	0.5412	3.181	22.3	97.5	20.658	0.016
150	2.25	6.093	0.0249	0.0600	1.658	20.5	99.7	20.664	0.022
149	2.25	6.138	0.0151	0.2098	2.015	33.8	99.0	20.666	0.021
117	2.25	6.098	0.0233	0.0741	1.275	21.9	99.7	20.667	0.028
140	2.25	6.108	0.0171	0.1053	2.530	29.8	99.5	20.669	0.016
108	2.25	6.210	0.0264	0.4481	1.505	19.3	97.9	20.674	0.028
27	2.25	6.115	0.0180	0.1213	0.836	28.3	99.4	20.676	0.043
138	2.25	6.133	0.0151	0.1720	1.817	33.7	99.2	20.685	0.022
69	2.25	6.103	0.0274	0.0720	2.121	18.6	99.7	20.689	0.018
89	2.25	6.145	0.0137	0.1969	1.412	37.3	99.1	20.703	0.026
119	2.25	6.127	0.0172	0.1178	2.073	29.6	99.5	20.721	0.019
155	2.25	10.27	0.0205	14.14	2.649	24.9	59.3	20.723	0.052
107	2.25	6.293	0.0164	0.6504	3.939	31.1	97.0	20.749	0.014
114	2.25	6.573	0.0141	0.2058	2.395	36.3	99.1	22.142	0.044
14	2.25	8.251	0.0046	5.464	1.837	110.1	80.4	22.56	0.14
147	2.25	7.586	0.0147	2.731	0.894	34.6	89.4	23.05	0.14
52	2.25	7.244	0.0179	1.352	0.816	28.5	94.5	23.27	0.14
90	2.25	7.279	0.0153	1.384	0.851	33.3	94.4	23.35	0.11
100	2.25	7.752	0.0170	2.952	0.622	29.9	88.8	23.38	0.19
103	2.25	7.556	0.0117	2.166	1.389	43.6	91.5	23.51	0.11
51	2.25	7.337	0.0125	1.373	1.209	40.9	94.5	23.558	0.088
65	2.25	7.044	0.0181	0.3557	1.082	28.2	98.5	23.586	0.094
152	2.25	8.518	0.0091	5.283	1.714	56.4	81.7	23.64	0.12
106	2.25	7.075	0.0023	0.3917	1.766	225.8	98.4	23.650	0.050
123	2.25	7.213	0.0055	0.8121	0.417	92.1	96.7	23.70	0.23
71	2.25	7.206	0.0125	0.7297	1.286	40.9	97.0	23.759	0.084
91	2.25	7.223	0.0073	0.7828	1.565	70.1	96.8	23.759	0.070
17	2.25	7.070	0.0064	0.2617	1.332	79.4	98.9	23.763	0.077
165	2.25	7.124	0.0110	0.3917	1.944	46.3	98.4	23.817	0.058
98	2.25	7.165	0.0050	0.5003	1.748	103.0	97.9	23.845	0.066
18	2.25	7.215	0.0110	0.6394	3.400	46.3	97.4	23.877	0.042
08	2.25	7.168	0.0062	0.4769	2.697	82.9	98.0	23.879	0.044
154	2.25	7.168	0.0046	0.4534	3.327	111.6	98.1	23.903	0.028
66	2.25	7.224	0.0075	0.6135	3.862	67.9	97.5	23.934	0.036
01	2.25	7.160	0.0052	0.3509	2.725	98.5	98.6	23.979	0.041
99	2.25	7.653	0.0034	0.7377	1.083	151.3	97.2	25.258	0.091
164	2.25	8.228	0.0092	0.6104	1.551	55.7	97.8	27.328	0.073
46	2.25	10.40	0.0097	0.2671	1.432	52.3	99.2	34.990	0.093
73	2.25	10.44	0.0059	0.2837	1.492	86.4	99.2	35.097	0.087
133	2.25	14.53	0.0353	4.731	0.311	14.5	90.4	44.40	0.60
64	2.25	24.09	0.0126	0.4537	0.626	40.6	99.4	80.24	0.40

70

APPENDIX C (cont.)

Detrital Sanidine 40Ar/39Ar geochronology data (continued)

ID	Power	$^{40}Ar/^{39}Ar$	$^{37}Ar/^{39}Ar$	$^{36}Ar/^{39}Ar$	$^{39}Ar_K$	K/Ca	$^{40}Ar*$	Age	±1s
	(watts)			(x 10⁻³)	(x 10⁻¹⁵ mol)		(%)	(Ma)	(Ma)
125	2.25	24.37	0.0052	0.4110	4.429	97.5	99.5	81.184	0.068
76	2.25	28.36	0.0093	0.8645	1.642	55.0	99.1	93.77	0.16
83	2.25	29.81	0.0134	2.314	1.274	37.9	97.7	97.09	0.20
67	2.25	52.51	0.0165	2.675	2.951	30.9	98.5	169.05	0.20
144	2.25	53.89	0.0147	1.075	1.124	34.8	99.4	174.81	0.42
25	2.25	56.31	0.0084	0.8232	1.192	60.9	99.6	182.56	0.51
134	2.25	56.85	0.0079	1.786	3.093	64.8	99.1	183.36	0.52
12	2.25	58.57	0.0061	0.1856	2.353	83.5	99.9	190.14	0.30
19	2.25	80.07	0.0274	42.60	0.202	18.6	84.3	217.6	2.4
168	2.25	68.76	0.0106	1.839	1.377	48.0	99.2	219.82	0.41
77	2.25	68.88	0.0047	0.9198	1.336	109.5	99.6	221.03	0.54
68	2.25	68.81	0.0114	0.5120	2.417	44.8	99.8	221.18	0.59
170	2.25	69.41	0.0044	2.131	1.238	114.7	99.1	221.55	0.56
53	2.25	69.83	0.0035	2.123	0.681	143.9	99.1	222.82	0.92
135	2.25	69.87	0.0145	0.6299	0.812	35.2	99.7	224.29	0.87
78	2.25	71.02	0.0044	1.426	3.714	116.9	99.4	227.05	0.55
96	2.25	76.63	0.0146	0.3868	2.245	35.0	99.9	244.88	0.94
132	2.25	122.7	0.0127	4.673	0.824	40.1	98.9	374.41	0.87
Mean age ± 2s			n=135	MSWD=37499.29		50.2 ±74.2		19.40	0.96

KCW17-6, Sanidine, J=0.0018712±0.04%, IC=1±1E-20, NM-293L,
Lab#=66085, Argus VI

ID	Power	$^{40}Ar/^{39}Ar$	$^{37}Ar/^{39}Ar$	$^{36}Ar/^{39}Ar$	$^{39}Ar_K$	K/Ca	$^{40}Ar*$	Age	±1s
10	2.25	4.238	0.0253	0.8567	0.675	20.2	94.1	13.577	0.051
15	2.25	5.661	0.0247	5.550	2.306	20.7	71.0	13.699	0.039
51	2.25	4.610	0.0263	1.963	5.695	19.4	87.4	13.728	0.016
47	2.25	4.803	0.0257	2.610	2.088	19.9	84.0	13.734	0.030
46	2.25	4.192	0.0232	0.5366	1.290	22.0	96.3	13.741	0.028
07	2.25	4.605	0.0294	1.874	2.664	17.4	88.0	13.801	0.022
16	2.25	4.212	0.0275	0.5162	7.474	18.6	96.4	13.830	0.008
05	2.25	4.900	0.0046	2.318	2.465	110.4	86.0	14.351	0.022
52	2.25	5.499	0.0179	0.8633	0.233	28.5	95.4	17.85	0.14
22	2.25	5.484	0.0073	0.3734	6.064	69.6	98.0	18.286	0.009
55	2.25	5.476	0.0130	0.2925	0.568	39.4	98.4	18.342	0.054
24	2.25	5.464	0.0048	0.2115	4.337	105.2	98.9	18.382	0.009
42	2.25	5.487	0.0069	0.2350	5.097	73.4	98.7	18.434	0.009
18	2.25	5.613	0.0070	0.6627	9.980	72.5	96.5	18.435	0.008
25	2.25	5.447	0.0097	0.0920	11.856	52.4	99.5	18.444	0.004
43	2.25	5.869	0.0106	1.400	1.696	48.2	93.0	18.564	0.031
23	2.25	6.929	0.0046	4.971	5.119	111.3	78.8	18.577	0.024
29	2.25	5.735	0.0064	0.9274	5.144	79.6	95.2	18.583	0.012
49	2.25	5.736	0.0089	0.8746	5.357	57.1	95.5	18.640	0.012
13	2.25	5.657	0.0096	0.5642	4.679	53.4	97.1	18.684	0.011
17	2.25	5.654	0.0060	0.5450	12.048	85.6	97.2	18.689	0.006
54	2.25	5.532	0.0068	0.1228	1.652	74.7	99.4	18.702	0.021
33	2.25	5.903	0.0069	1.368	15.221	73.5	93.2	18.710	0.008
21	2.25	5.684	0.0065	0.5979	4.320	78.4	96.9	18.740	0.012
35	2.25	5.620	0.0110	0.3802	7.485	46.6	98.0	18.744	0.008
11	2.25	6.588	0.0249	2.226	0.485	20.5	90.0	20.177	0.086
32	2.25	6.201	0.0163	0.5772	7.483	31.4	97.3	20.517	0.009
38	2.25	6.133	0.0216	0.3327	2.145	23.6	98.4	20.530	0.020
36	2.25	6.755	0.0195	2.435	5.111	26.1	89.4	20.533	0.019
44	2.25	6.106	0.0221	0.2384	2.610	23.0	98.9	20.533	0.016
04	2.25	6.112	0.0194	0.2418	3.546	26.4	98.9	20.552	0.013

71

APPENDIX C (cont.)

Detrital Sanidine 40Ar/39Ar geochronology data (continued)

ID	Power	$^{40}Ar/^{39}Ar$	$^{37}Ar/^{39}Ar$	$^{36}Ar/^{39}Ar$	$^{39}Ar_K$	K/Ca	$^{40}Ar*$	Age	±1s
	(watts)			(x 10^{-3})	(x 10^{-15} mol)		(%)	(Ma)	(Ma)
31	2.25	6.104	0.0214	0.2123	3.921	23.8	99.0	20.553	0.011
19	2.25	6.249	0.0257	0.6957	4.655	19.9	96.7	20.561	0.014
48	2.25	6.353	0.0234	1.045	11.748	21.8	95.2	20.563	0.008
26	2.25	6.101	0.0201	0.1808	7.026	25.3	99.2	20.576	0.007
57	2.25	6.086	0.0201	0.1290	1.262	25.4	99.4	20.577	0.028
45	2.25	6.307	0.0203	0.8730	4.151	25.2	95.9	20.578	0.014
56	2.25	6.083	0.0220	0.1122	18.532	23.2	99.5	20.582	0.004
20	2.25	6.215	0.0235	0.5511	6.964	21.7	97.4	20.591	0.010
12	2.25	6.120	0.0214	0.2268	5.863	23.8	98.9	20.592	0.009
30	2.25	6.141	0.0192	0.2890	3.168	26.6	98.6	20.600	0.014
50	2.25	6.104	0.0219	0.1343	3.960	23.3	99.4	20.633	0.011
02	2.25	6.096	0.0168	0.0730	14.887	30.3	99.7	20.663	0.004
27	2.25	7.308	0.0156	3.032	0.248	32.6	87.7	21.81	0.28
37	2.25	7.108	0.0076	0.4282	2.745	66.9	98.2	23.732	0.043
09	2.25	7.035	0.0074	0.1484	7.567	69.3	99.4	23.763	0.019
34	2.25	7.100	0.0058	0.2781	8.401	87.5	98.8	23.855	0.018
28	2.25	7.220	0.0083	0.5758	11.374	61.8	97.7	23.963	0.019
01	2.25	8.060	0.0069	0.4150	10.694	74.4	98.5	26.961	0.018
40	2.25	8.190	0.0079	0.3127	7.909	65.0	98.9	27.502	0.020
06	2.25	12.69	0.0060	0.5759	5.560	85.5	98.7	42.359	0.040
03	2.25	24.64	0.0125	2.791	0.652	40.7	96.7	79.77	0.37
53	2.25	24.27	0.0061	0.1043	5.897	83.3	99.9	81.186	0.044
41	2.25	24.33	0.0052	0.0881	6.458	97.8	99.9	81.377	0.049
14	2.25	28.13	0.0095	0.3072	3.410	53.8	99.7	93.573	0.092
08	2.25	28.23	0.0216	0.2512	3.221	23.6	99.7	93.97	0.11
39	2.25	50.55	0.0065	0.5006	2.253	78.1	99.7	164.96	0.22
Mean age ± 2s			n=57	MSWD=129728.89		48.4 ±56.3		19.7	1.0

KCW17-6, Sanidine, J=0.0018716±0.04%, IC=1±1E-20, NM-293L, Lab#=66086, Argus VI

ID	Power	$^{40}Ar/^{39}Ar$	$^{37}Ar/^{39}Ar$	$^{36}Ar/^{39}Ar$	$^{39}Ar_K$	K/Ca	$^{40}Ar*$	Age	±1s
02	2.25	4.988	0.0122	4.390	0.275	41.7	74.0	12.58	0.14
56	2.25	6.561	0.0286	8.863	1.431	17.8	60.1	13.435	0.061
79	2.25	4.246	0.0220	0.8134	1.392	23.2	94.4	13.647	0.029
62	2.25	4.408	0.0224	1.252	2.526	22.8	91.6	13.758	0.020
64	2.25	4.361	0.0252	1.080	0.530	20.3	92.7	13.772	0.059
12	2.25	4.448	0.0205	1.373	2.063	24.9	90.9	13.773	0.023
09	2.25	4.137	0.0189	0.2966	1.183	26.9	97.9	13.796	0.025
74	2.25	4.566	0.0068	1.076	1.407	74.7	93.0	14.469	0.031
55	2.25	4.356	0.0065	0.2865	0.747	79.1	98.1	14.548	0.037
41	2.25	5.115	0.0199	1.125	1.090	25.6	93.5	16.288	0.033
58	2.25	5.521	0.0229	2.116	0.068	22.3	88.7	16.67	0.39
49	2.25	5.937	0.0097	2.920	0.301	52.6	85.5	17.28	0.12
68	2.25	5.970	0.0065	2.025	4.262	78.0	90.0	18.282	0.020
88	2.25	5.425	0.0077	0.1201	2.275	66.1	99.4	18.346	0.017
46	2.25	5.497	0.0088	0.3611	1.908	57.7	98.1	18.347	0.019
51	2.25	5.420	0.0085	0.0988	2.630	60.1	99.5	18.349	0.013
52	2.25	5.412	0.0083	0.0595	1.535	61.3	99.7	18.360	0.023
73	2.25	5.446	0.0086	0.1624	3.621	59.1	99.1	18.374	0.011
08	2.25	5.441	0.0110	0.1444	2.599	46.2	99.2	18.377	0.013
42	2.25	5.516	0.0075	0.3933	2.128	68.2	97.9	18.379	0.018
59	2.25	5.899	0.0073	1.686	2.951	70.1	91.6	18.385	0.021
80	2.25	5.537	0.0103	0.3978	0.900	49.7	97.9	18.447	0.040
18	2.25	5.474	0.0081	0.1712	1.898	62.7	99.1	18.459	0.018

Detrital Sanidine 40Ar/39Ar geochronology data (continued)

ID	Power (watts)	$^{40}Ar/^{39}Ar$	$^{37}Ar/^{39}Ar$	$^{36}Ar/^{39}Ar$ (x 10^{-3})	$^{39}Ar_K$ (x 10^{-15} mol)	K/Ca	$^{40}Ar*$ (%)	Age (Ma)	±1s (Ma)
15	2.25	5.494	0.0049	0.2093	1.470	104.1	98.9	18.489	0.023
47	2.25	5.809	0.0072	1.166	2.809	71.1	94.1	18.597	0.021
89	2.25	6.481	0.0058	3.407	2.276	87.6	84.5	18.632	0.033
57	2.25	5.630	0.0062	0.5254	6.456	82.2	97.2	18.632	0.008
30	2.25	6.321	0.0099	2.847	5.610	51.7	86.7	18.650	0.017
86	2.25	5.522	0.0075	0.1313	1.484	67.8	99.3	18.661	0.022
36	2.25	5.842	0.0102	1.214	3.192	49.9	93.9	18.663	0.017
19	2.25	5.849	0.0054	1.213	1.989	94.0	93.9	18.685	0.023
01	2.25	5.547	0.0089	0.1474	1.556	57.2	99.2	18.732	0.023
91	2.25	6.054	0.0357	1.183	0.124	14.3	94.3	19.42	0.27
06	2.25	6.046	0.0094	1.009	0.313	54.3	95.1	19.56	0.11
22	2.25	6.047	0.0247	0.3299	0.531	20.6	98.4	20.250	0.065
75	2.25	6.849	0.0241	2.972	1.222	21.2	87.2	20.320	0.047
87	2.25	6.558	0.0212	1.890	1.997	24.1	91.5	20.416	0.031
83	2.25	6.081	0.0244	0.2575	0.951	20.9	98.8	20.435	0.039
90	2.25	6.074	0.0247	0.1553	3.673	20.7	99.3	20.516	0.011
37	2.25	6.090	0.0225	0.1885	1.356	22.7	99.1	20.534	0.024
32	2.25	6.141	0.0194	0.3601	2.130	26.3	98.3	20.534	0.019
27	2.25	7.230	0.0234	4.047	1.588	21.8	83.5	20.535	0.042
66	2.25	6.073	0.0285	0.1284	2.070	17.9	99.4	20.539	0.018
34	2.25	6.065	0.0212	0.0977	1.362	24.0	99.6	20.542	0.025
54	2.25	6.131	0.0233	0.3185	1.258	21.9	98.5	20.542	0.029
70	2.25	6.087	0.0180	0.1636	3.474	28.3	99.2	20.547	0.013
72	2.25	6.130	0.0226	0.3096	3.121	22.6	98.5	20.549	0.014
16	2.25	6.073	0.0239	0.1178	1.606	21.4	99.5	20.550	0.021
25	2.25	6.068	0.0255	0.0856	1.434	20.0	99.6	20.562	0.025
43	2.25	6.051	0.0259	0.0286	2.403	19.7	99.9	20.564	0.015
60	2.25	6.086	0.0221	0.1439	0.716	23.1	99.3	20.565	0.047
10	2.25	6.101	0.0170	0.1751	2.175	29.9	99.2	20.585	0.017
03	2.25	6.100	0.0176	0.1683	2.992	29.0	99.2	20.587	0.015
26	2.25	6.070	0.0202	0.0539	6.862	25.3	99.8	20.601	0.007
07	2.25	7.116	0.0266	3.559	1.142	19.2	85.2	20.638	0.051
38	2.25	6.081	0.0151	0.0342	2.091	33.9	99.9	20.656	0.016
85	2.25	6.862	0.0028	1.584	0.282	183.8	93.2	21.75	0.23
84	2.25	6.758	0.0301	0.9815	1.502	17.0	95.7	22.006	0.084
13	2.25	6.653	0.0096	0.6080	4.699	53.2	97.3	22.018	0.027
63	2.25	6.747	0.0273	0.7171	0.529	18.7	96.9	22.23	0.18
61	2.25	6.785	0.0196	0.4309	1.916	26.0	98.1	22.646	0.053
65	2.25	6.993	0.0142	1.007	0.457	35.9	95.8	22.77	0.19
76	2.25	6.923	0.0101	0.1144	2.968	50.4	99.5	23.426	0.031
78	2.25	7.334	0.0044	1.269	3.805	117.3	94.9	23.658	0.043
67	2.25	7.412	0.0051	1.532	3.085	100.2	93.9	23.661	0.054
40	2.25	7.378	0.0105	1.401	1.813	48.8	94.4	23.678	0.076
31	2.25	7.502	0.0053	1.746	2.876	96.2	93.1	23.750	0.059
05	2.25	7.085	0.0060	0.3149	2.677	84.9	98.7	23.773	0.040
28	2.25	7.053	0.0069	0.1786	4.810	73.7	99.3	23.800	0.024
24	2.25	7.191	0.0087	0.5705	1.933	58.7	97.7	23.873	0.058
33	2.25	7.086	0.0074	0.1846	4.202	68.6	99.2	23.906	0.025
35	2.25	7.703	0.0051	0.4916	2.966	99.3	98.1	25.683	0.038
17	2.25	10.28	0.0040	0.3149	2.279	127.0	99.1	34.544	0.063
20	2.25	10.46	-0.0010	0.4478	1.316	-	98.7	35.02	0.12
48	2.25	10.41	0.0136	0.2412	0.747	37.5	99.3	35.05	0.16

APPENDIX C (cont.)

Detrital Sanidine 40Ar/39Ar geochronology data (continued)

| ID	Power	$^{40}Ar/^{39}Ar$	$^{37}Ar/^{39}Ar$	$^{36}Ar/^{39}Ar$	$^{39}Ar_K$	K/Ca	$^{40}Ar^*$	Age	±1s
	(watts)			($\times 10^{-3}$)	($\times 10^{-15}$ mol)		(%)	(Ma)	(Ma)
82	2.25	10.50	0.0068	0.4127	2.930	75.3	98.8	35.171	0.051
11	2.25	10.58	0.0078	0.5783	2.835	65.8	98.4	35.287	0.060
50	2.25	23.75	0.0140	0.5132	0.782	36.4	99.4	79.08	0.32
04	2.25	24.07	0.0063	1.440	0.809	81.6	98.2	79.24	0.33
71	2.25	23.81	0.0057	0.3707	0.786	89.1	99.5	79.42	0.29
45	2.25	24.51	0.0109	1.948	1.589	46.9	97.7	80.18	0.17
14	2.25	25.35	0.0063	0.6800	1.367	80.6	99.2	84.18	0.23
21	2.25	26.10	0.0156	0.9692	0.180	32.8	98.9	86.4	1.6
39	2.25	27.86	0.0216	0.3336	1.031	23.6	99.7	92.69	0.25
77	2.25	28.39	0.0265	0.7345	0.720	19.3	99.2	94.05	0.35
53	2.25	29.87	0.0148	0.8478	1.704	34.4	99.2	98.74	0.17
23	2.25	52.12	0.0083	4.738	2.773	61.7	97.3	165.97	0.24
69	2.25	66.80	0.0072	0.4518	3.855	70.8	99.8	215.21	0.31
29	2.25	68.75	0.0072	0.3446	1.118	70.6	99.9	221.24	0.58
81	2.25	71.73	0.0175	2.934	2.636	29.2	98.8	227.96	0.40
Mean age ± 2s		n=90		MSWD=30425.82		50.3 ±61.4		19.61	0.86

Notes
:

Isotopic ratios corrected for blank, radioactive decay, and mass discrimination, not corrected for interfering reactions.

Errors quoted for individual analyses include analytical error only, without interfering reaction or J uncertainties.

Mean age is weighted mean age of Taylor (1982). Mean age error is weighted error

  of the mean (Taylor, 1982), multiplied by the root of the MSWD where MSWD>1, and also

  incorporates uncertainty in J factors and irradiation correction uncertainties.

 Isotopic abundances after Steiger and Jäger (1977).

Ages calculated relative to FC-2 Fish Canyon Tuff sanidine interlaboratory standard at 28.201 Ma

Decay Constant (LambdaK (total)) = 5.543e-10/a

Correction factors:

  $(^{39}Ar/^{37}Ar)_{Ca}$ = 0.000758 ± 0.000007

  $(^{36}Ar/^{37}Ar)_{Ca}$ = 0.000286 ± 0.0000005

  $(^{38}Ar/^{39}Ar)_K$ = 0.013

  $(^{40}Ar/^{39}Ar)_K$ = 0.00873 ± 0.00017

APPENDIX D: OBSERVING HEADWARD EROSION
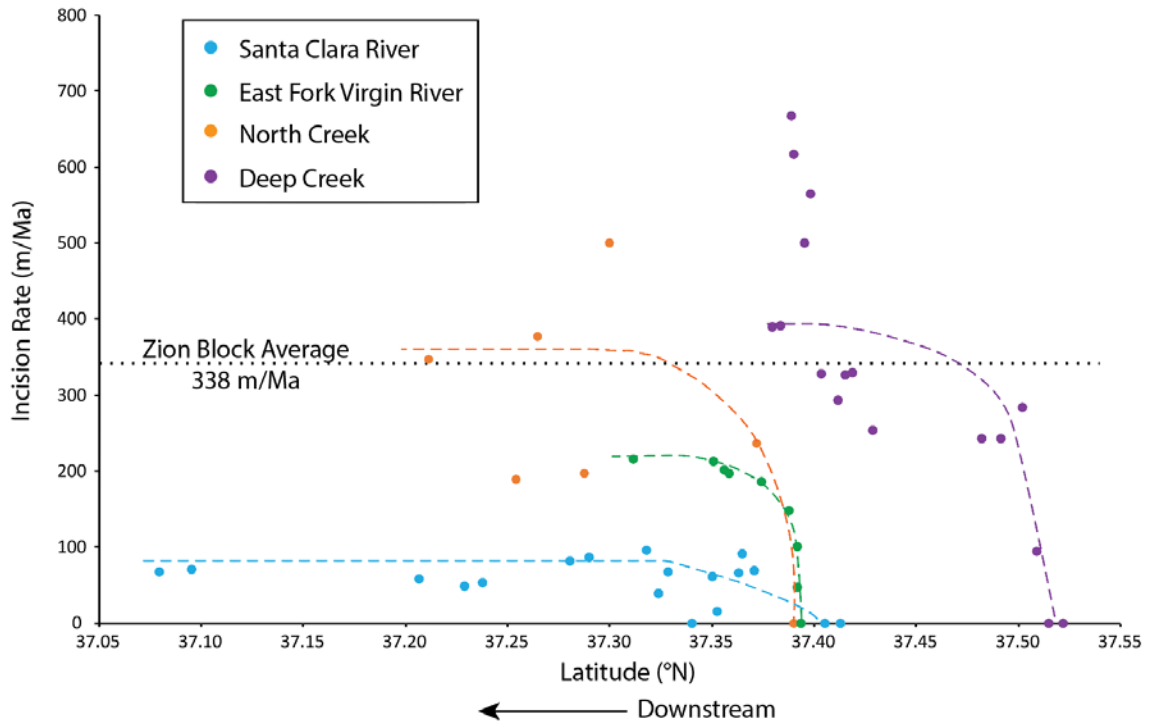
Appendix D. Plot of incision rates versus latitude along 4 tributaries of the Virgin River (Santa Clara River, East Fork Virgin River, North Creek, and Deep Creek) showing the headwater effect on incision rates. We use latitude as a proxy for location along the North-South tributary (headwaters are at higher latitudes). Incision rates at the headwaters are near 0 m/Ma. Incision rates rapidly increase downstream and then eventually level off to a steady rate. Outlying data points along North Creek (orange) are interpreted to show change along 2 small scale faults. Outliers on Deep Creek (purple) may be caused by errors in the DEM as these data points lie within the steep narrow slot canyons.

APPENDIX E: BASIN AND RANGE TRIBUTARY PROFILES

River profiles of White River Wash (WRW) and Meadow Valley Wash (MVW), located in the Basin and Range, consist of long shallow gradients and have broad convexities at similar elevations (~1500 m). Normalized channel steepness (k_{sn}) along the BR tributaries show low average values upstream of the broad knickpoints (~40 $m^{0.9}$) and generally increase downstream (~170 $m^{0.9}$). Similar results along Fort Pearce Wash of the CP-TZ tributaries show a large difference in average k_{sn} values upstream and downstream of knickpoint M, ~50 $m^{0.9}$ and ~215 $m^{0.9}$ respectively.

White River Wash and Meadow Valley Wash, located in the BR province, have very low gradients in comparison to the remaining tributaries. However, the k_{sn} analyses show that downstream extents of these two tributaries are relatively steep for the amount of upstream contributing area. We interpret the low gradient washes upstream of the broad convexities to represent pre-5 Ma gradients of internal drainages without recent uplift; steeper gradients downstream of these knickpoints may represent channel adjustments to integration of the BR tributaries with the VR at ~3 Ma.

APPENDIX F: CONTOUR MAP OF ALL BASALTIC VENTS
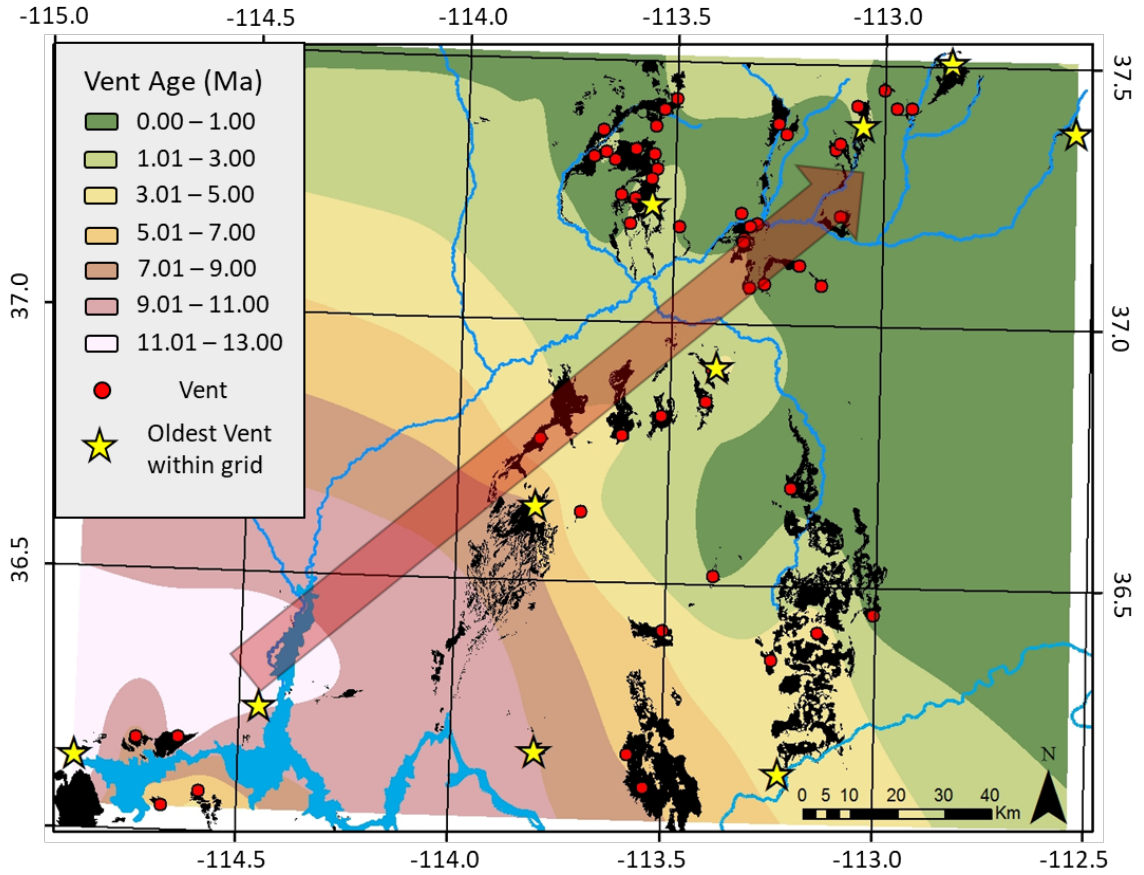
Appendix F. A contour map of all known vent ages throughout the southeastern Virgin River drainage system showing the migration path of basaltic volcanism. The contours were generated using the 'Topo to Raster' interpolation method in ArcGIS. Red dots represent all known vent locations while yellow stars represent the oldest vent age within each 0.5 x 0.5 degree grid.

APPENDIX G: MAP OF INCISION RATES
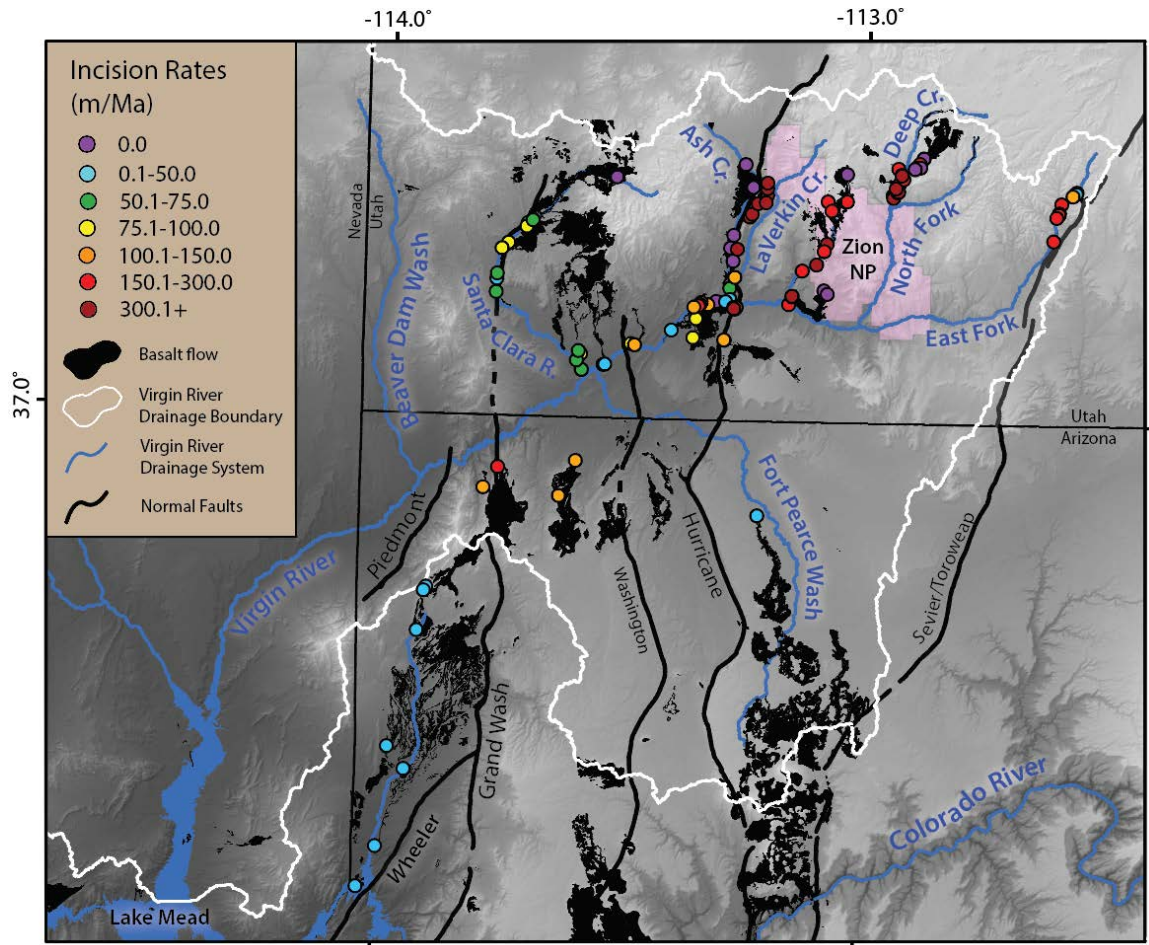
Appendix G. Digital elevation model and hillshade showing incision data point locations and rates.

APPENDIX H: AGE DISTRIBUTION PLOTS OF DETRITAL SANIDINE GRAINS <40 MA
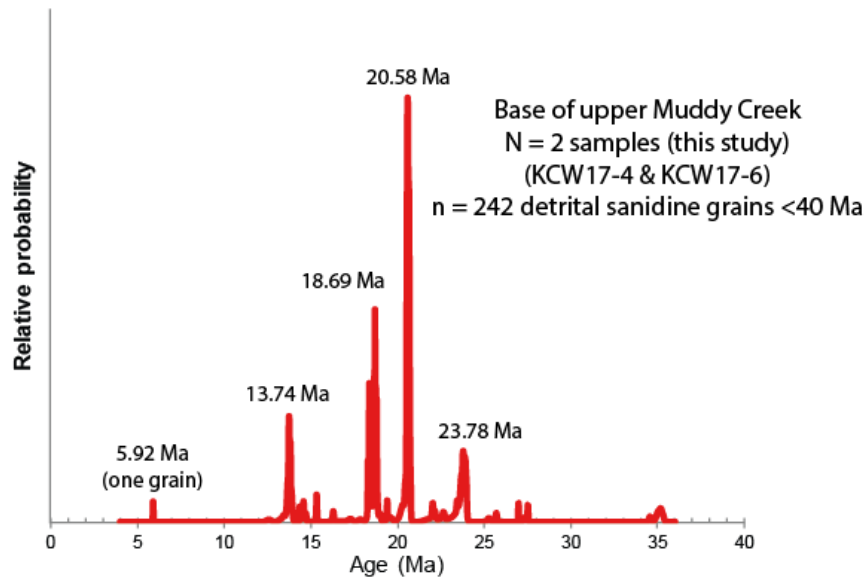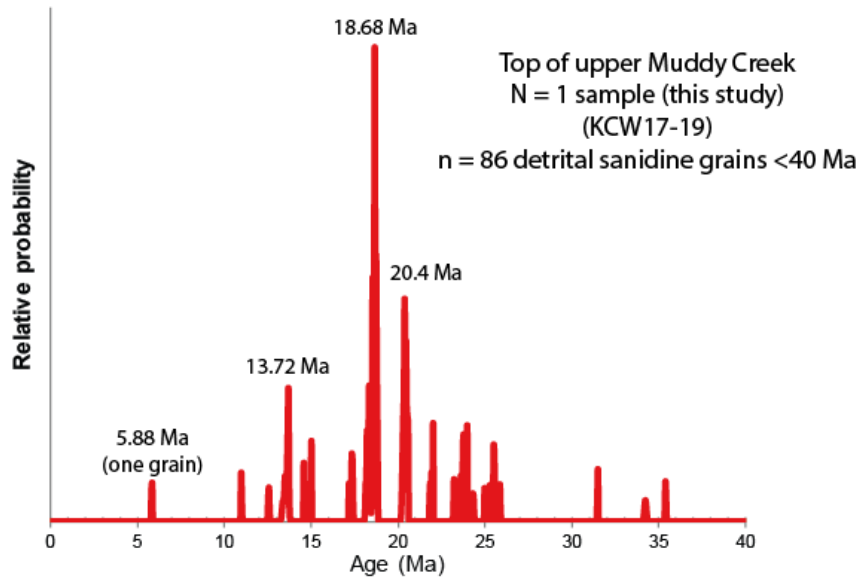
Appendix H. Age distribution plots of the top of the upper Muddy Creek formation (KCW17-19) and the base of the upper Muddy Creek formation (KCW17-4 and KCW17-6). The two plots are relatively similar with the only major difference being the change in highest peak age from 20.56 (base of upper Muddy Creek) to 18.68 (top of upper Muddy Creek). This can be explained by a dilution of Pine Valley grains (20.56 Ma) as the Virgin headwaters moved east across the Hurricane fault, away from the Pine Valley mountains.

APPENDIX I: SMALL-SCALE VIRGIN RIVER DRAINAGE EVOLUTION

Sentinel Landslide and Zion Narrows Knickpoint

The largest knickpoint unrelated to an active fault, knickpoint F, lies along the East Fork Virgin River at the contact between the less resistant Kayenta formation and the more resistant Navajo Sandstone. If this knickpoint formed due to differing lithologies, as was interpreted above, we would expect a knickpoint similar in scale to exist at the same contact along the North Fork Virgin River; however, we observe no knickpoint at this location. A hypothesis to explain the history and formation/erasing of North Fork knickpoints begins ~5 ka, prior to the Sentinel landslide. Before the landslide, the North Fork and East Fork rivers both consisted of lithologically controlled knickpoints at the contact between Kayenta and Navajo formations (~1350 m) similar to the present knickpoint F. About 4.8 ka, the Sentinel landslide dammed the North Fork about 10 km downstream of the Kayenta/Navajo contact, forming Sentinel Lake within Zion canyon (Grater, 1945; Castleton et al., 2016). Castleton et al. (2016) give an approximate stable water elevation of 1345 m based on lake sediments deposited up to a maximum elevation of 1315 m. However, they state the lake may have reached a maximum height of 1445 m at one point. The deposition of lake sediments may have diminished a previous lithological knickpoint along the North Fork and created a new one downstream at the location of the landslide, knickpoint H. If this hypothesis is true, the Sentinel rock avalanche not only formed the wide, flat valley bottom of Zion Canyon (Grater, 1945); but it also erased a steep knickpoint that existed at the entrance to the Narrows and allowed easy access to the Riverside Walk trail found in Zion National Park. Without the rock avalanche, visitors would have to scale a ~60 meter cliff to enter the narrows from

the bottom, similar to Parunuweap Canyon (Labyrinth Falls) of the East Fork Virgin River.

Santa Clara connection to Beaver Dam Wash

The Santa Clara river runs a unique course as it drains the northern flank of the Pine Valley mountains, wraps around the western flank and joins the Virgin River to the south (Fig. 1). This river also crosses the Gunlock fault two separate times. One hypothesis to explain this intriguing course begins >4 Ma. The Santa Clara river may have originated as a tributary to Beaver Dam Wash on the west side of the Beaver Dam mountains, headward eroding its way northeast and tapping into the Pine Valley laccolith >4Ma. Activity along Gunlock fault, west dropping normal fault, or stream capture by a headward eroding tributary of the Virgin River across the fault may have eventually caused the Santa Clara river to ultimately make a U-turn and flow southeast. To test this hypothesis, we could perform detrital sanidine analyses on lower Muddy Creek samples to see if Pine Valley grains (20.56 Ma) exist in the 4-6 Ma strata. If a 20.56 Ma peak exists in the lower Muddy Creek than this hypothesis would be supported.

APPENDIX J: AGE DISTRIBUTION PLOTS OF ALL DETRITAL SANIDINE GRAINS
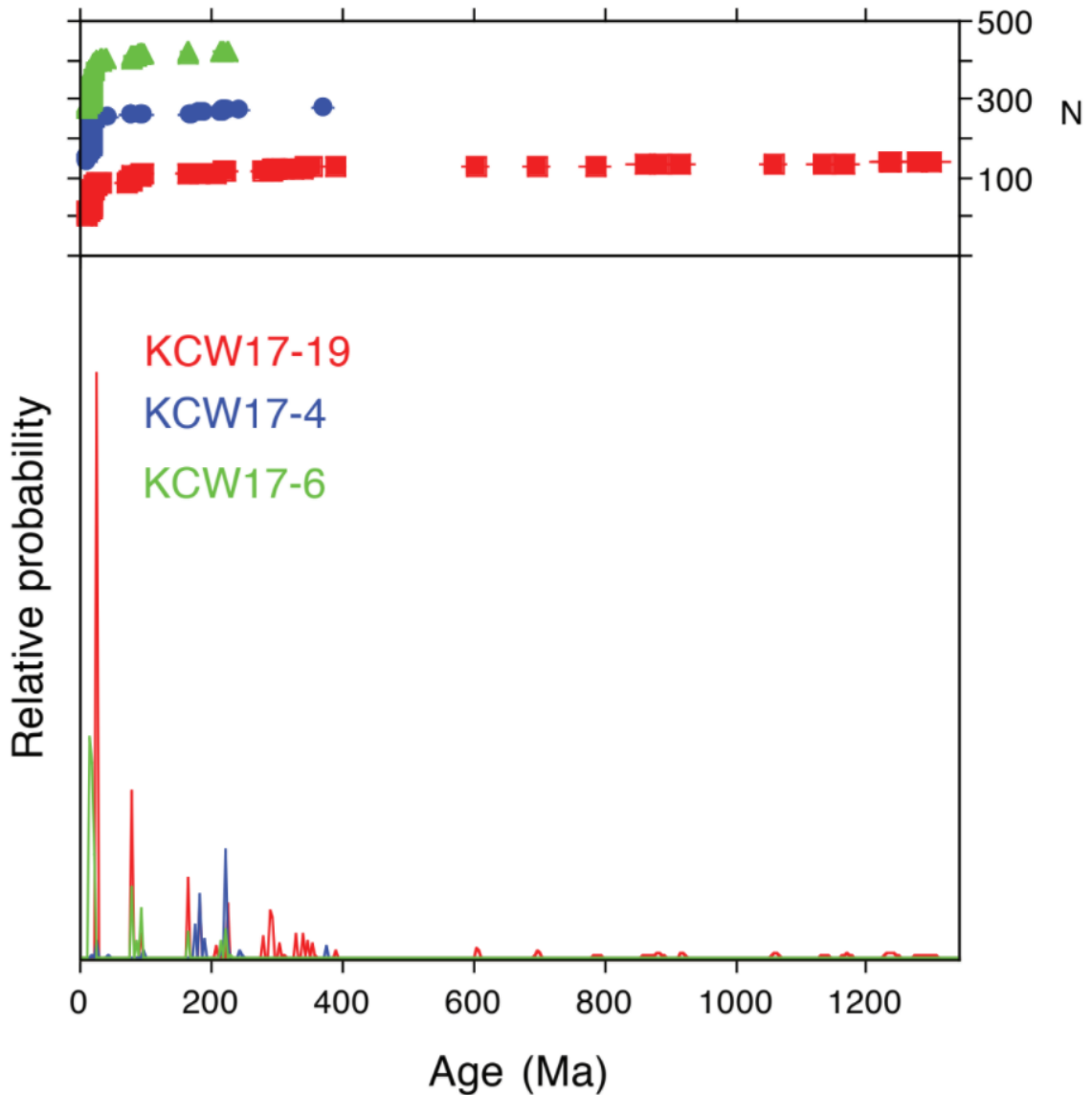
Appendix J. Age distribution plots showing all dated sanidine grains in the 3 samples dated in this study (KCW17-4, KCW17-6, and KCW17-19). Sample KCW17-19 (top of the upper Muddy Creek formation) is the only sample that contains Precambrian age grains. These older ages are expected to originate from the basement rocks that make up the core of the Virgin Mountains. These stratigraphically lower lying Precambrian rocks were not yet exhumed at the time of the first arrival of the Virgin River through the incipient Virgin Gorge. Hence, as incision of the gorge began, the youngest grains were deposited nearest the mouth of the Virgin Gorge (KCW17-6; Figure 13); and as incision of the gorge continued, older grains were deposited at higher stratigraphic levels within the Virgin Depression (KCW17-19; Figure 13).

REFERENCES CITED

Abbott, L.D., Lundstrom, C., and Traub, C., 2015, Rates of river incision and scarp

retreat in eastern and central Grand Canyon over the past half million years:

Evidence for passage of a transient knickzone: Geosphere, v. 11, no. 3, p. 1–22,

doi:10.1130/GES00978.1

Anderson, R.E., and Christenson, G.E., 1989, Quaternary faults, folds, and selected

volcanic features in the Cedar City 1°x2° quadrangle, Utah: Utah Geological and

Mineral Survey Miscellaneous Publication 89-6, 29 p.

Anderson, R.E., Barnhard, T.P., and Snee, L.W., 1994, Roles of plutonism, midcrustal

flow, tectonic rafting, and horizontal collapse in shaping the Miocene strain field of

the Lake Mead area, Nevada and Arizona: Tectonics, v. 13, p. 1381-1410.

Beard, L.S., Anderson, R.E., Block, D.L., Bohannon, R.G., Brady, R.J., Castor, S.B.,

Duebendorfer, E.M., Faulds, J.E., Felger, T.J., Howard, K.A., Kuntz, M.A., and

Williams, V.S., 2007, Preliminary geologic map of the Lake Mead 30' X 60'

quadrangle, Clark County, Nevada, and Mohave County, Arizona: U.S. Geological

Survey Open-File Report 2007-1010, 109 p., 3 plates, scale 1:100,000,

http://pubs.usgs.gov/of/2007/1010/.

Best, M.G., McKee, E.H., and Damon, P.E., 1980, Space-time-composition patterns of

Late Cenozoic mafic volcanism, southwestern Utah and adjoining areas: American

Journal of Science, v. 280, p. 1035-1050.

Best, M.G., Scott, R.B., Rowley, P.D., Swadley, W.C., Anderson, R.E., Grommé, S.C.,

Harding, A.E., Deino, A.L., Christiansen, E.H., Tingey, D.G., and Sullivan, K.M.,

1993, Oligocene–Miocene caldera complexes, ash-flow sheets, and tectonism in the

central and southeastern Great Basin, in Lahren, M.M., Trexler, J.H., Jr., and

Spinosa, C., eds., Crustal Evolution of the Great Basin and Sierra Nevada: Reno,

Nevada, Mackay School of Mines (University of Nevada)–Geological Society of

America (joint Cordilleran/Rocky Mountain Sections meeting) Field Trip

Guidebook, p. 285–311.

Best, M.G., Christiansen, E.H., Deino, A.L., Grommé, S., Hart, G.L., and Tingey, D.G.,

2013, The 36–18 Ma Indian Peak–Caliente ignimbrite field and calderas,

southeastern Great Basin, USA: Multicyclic supereruptions: Geosphere, v. 9, p. 864–

950, doi: 10 .1130/GES00902 .1 .

Biek, R.F., 2003a, Geologic map of the Harrisburg Junction quadrangle, Washington

County, Utah: Utah Geological Survey Map 191, 42 p., 2 plates, scale 1:24,000.

Biek, R.F., 2003b, Geologic map of the Hurricane quadrangle, Washington County, Utah:

Utah Geological Survey Map 187, 61 p., 2 plates, scale 1:24,000.

Biek, R.F., 2007a, Geologic map of the Kolob Arch quadrangle, Washington and Iron

Counties, Utah: Utah Geological Survey Map 225, 3 plates, scale 1:24,000.

Biek, R.F., 2007b, Geologic map of the Kolob Reservoir quadrangle, Washington and

Iron Counties, Utah: Utah Geological Survey Map 220, 2 plates, scale 1:24,000.

Biek, R.F., Willis, G.C., Hylland, M.D., and Doelling, H.H., 2003, Geology of Zion

National Park, Utah, in Sprinkel, D.A., Chidsey, T.C., and Anderson, P.B., editors,

Geology of Utah's parks and monuments: Utah Geological Association and Bryce

Canyon Natural History Association, Utah Geological Association Publication 28,

second edition, p. 107-137.

Biek, R.F., and Hylland, M.D., 2007, Geologic map of the Cogswell Point quadrangle,

Washington, Kane, and Iron Counties, Utah: Utah Geological Survey Map 221, 2
plates, scale 1:24,000.

Biek, R.F., Rowley, P.D., Hayden, J.M., Hacker, D.B., Willis, G.C., Hintze, L.F.,
Anderson, R.E., and Brown, K.D., 2010, Geologic map of the St. George and east
part of the Clover Mountains 30' x 60' quadrangles, Washington and Iron Counties,
Utah: Utah Geological Survey Map 242DM, 2 plates, 101 p., scale 1:100,000, GIS
data (printed map published in 2009 as Map 242).

Billingsley, G.H., 1990, Geologic map of the Purgatory quadrangle, northern Mohave
County, Arizona: U.S. Geological Survey Open-File Report 90-540, scale 1:24,000.

Billingsley, G.H., 1993, Geologic map of the Wolf Hole Mountain and vicinity, Mohave
County, northwestern Arizona: U.S. Geological Survey Miscellaneous Investigations
Series Map I-2296, scale 1:31,680, includes text and cross sections.

Billingsley, G.H., 1994, Geologic map of the Antelope Knoll quadrangle, northern
Mohave County, Arizona: U.S. Geological Survey Open-File Report 94-449, scale
1:24,000, 18 p.

Billingsley, G.H., and Workman, J.B., 2000, Geologic map of the Littlefield 30'x60'
quadrangle, Mohave County, northwestern Arizona: U.S. Geological Survey
Geologic Investigations Series Map I-2628, version 1.0, 25 p., 2 plates, scale
1:100,000.

Billingsley, G.H., and Wellmeyer, J.L., 2003, Geologic map of the Mount Trumbull 30'
X 60' quadrangle, Mohave and Coconino Counties, northwestern Arizona: U.S.
Geological Survey Geologic Investigations Series I-2766, scale 1:100,000,
https://pubs.usgs.gov/imap/i2766/

Birdseye, C. H., 1924, Plan and profile of the Colorado River from Lees Ferry, Arizona, to Black Canyon, Arizona-Nevada, and the Virgin River, Nevada: U.S. Geological Survey, 21 sheets, scale 1:36,680.

Bohannon, R.G., Grow, J.A., Miller, J.J., and Blank, R.H., Jr., 1993, Seismic stratigraphy and tectonic development of Virgin River depression and associated basins, southeastern Nevada and northwestern Arizona: Geological Society of America Bulletin, v. 105, p. 501-520.

Brumbaugh, D.S., 1987, A tectonic boundary for the southern Colorado Plateau: Tectonophysics, v. 136, p. 125– 136, doi: 10.1016/0040-1951(87)90335-0.

Bursztyn, N., Pederson, J.L., Tressler, C., Mackley, R.D., and Mitchell, K.J., 2015, Rock strength along a fluvial transect of the Colorado Plateau—Quantifying a fundamental control on geomorphology: Earth and Planetary Science Letters, v. 429, p. 90–100, doi:10.1016/j .epsl.2015.07.042.

Calvet, M., Gunnell, Y., Braucher, R., Hez, G., Bourles, D., Guillou, V., Delmas, M., 2015, Cave levels as proxies for measuring post-orogenic uplift: Evidence from cosmogenic dating of alluvium-filled caves in the French Pyrenees: Geomorphology, v. 246, p. 617-633.

Castleton, JJ, Moore, J, Aaron, J, Christl, M, and Ivy-Ochs, S., 2016, Dynamics and legacy of 4.8 ka rock avalanche that dammed Zion Canyon, Utah, USA: GSA Today, v. 26, no. 6, p. 4-9.

Chapin, C.E., 2008, Interplay of oceanographic and paleoclimate events with tectonism during middle to late Miocene sedimentation across the southwestern USA: Geosphere, v. 4, p. 976–991, doi:10.1130/GES00171.1.

Clark, M., House, M., Royden, L., Whipple, K., Burchfi el, B., Zhang, X., and Tang, W., 2005, Late Cenozoic uplift of southeastern Tibet: Geology, v. 33, p. 525–528, doi: 10.1130/G21265.1.

Cook, K.L., Whipple, K.X., Heimsath, A.M., and Hanks, T.C., 2009, Rapid incision of the Colorado River in Glen Canyon—Insights from channel profi les, local incision rates, and modeling of lithologic controls: Earth Surface Processes and Landforms, v. 34, no. 7, p. 994–1010.

Crossey, L.J., Karlstrom, K.E., Dorsey, R., Pearce, J.L., Wan, E., Beard, L.S., Asmeron, Y., Polyak, V., Crow, R., Cohen, A., and Bright, J., 2015, The importance of groundwater in propagating downward integration of the 6–5 Ma Colorado River system—Geochemistry of springs, travertines and lacustrine carbonates of the Grand Canyon region over the past 12 million years: Geosphere, doi: 10 .1130 /GES01073 .1.

Crow, R.S., 2012. Neotectonic evolution of Grand Canyon: interaction between volcanism, river incision, epeirogenic uplift, and faulting [PhD dissertation]: University of New Mexico. 217 pp.

Crow, R., Karlstrom, K., Asmerom, Y., Schmandt. B., Polyak, V., and Dufrane, A., 2011, Shrinking of the Colorado Plateau via lithospheric mantle erosion: evidence from Nd and Sr isotopes and geochronology of Neogene basalts: Geology, v. 39, no. 1, p. 27-30, doi: 10.1130/G31611.1.

Crow, R., Karlstrom, K., Darling, A., Crossey, L., Polyak, V., Granger, D., Asmerom, Y., Schmandt, B., 2014, Steady incision of Grand Canyon at the million year timeframe: a case for mantle-driven differential uplift: Earth Planetary Science Letters, v. 397,

p. 159–173.

Crow, R.S., Karlstrom, K.E., Howard, K.A., Beard, L.S., House, P.K., Sharp, W., Polyak, W., Peters, L., Asmerom, Y., McIntosh, W., Block, D., Crossey, L.C, 2016, Integrating lower Colorado River alluvial deposits and Grand Canyon incision constraints to reconstruct paleo Colorado River profiles and determine Colorado Plateau uplif, in Going Loco: Investigations along the Lower Colorado River, 16th, California State University Desert Studies Consortium, p. 87-90.

Damon, P.E., Shafiqullah, M., Harris, R.C., and Spencer, J.E., 1996, Compilation of unpublished Arizona K-Ar dates from the University of Arizona Laboratory of Isotope Geochemistry, 1971-1991: Arizona Geological Survey Open-Fire Report 96-18, 56 p.

Darling, A., 2016, The Roles of erosion rate and rock strength in the evolution of canyons along the Colorado River [Ph.D. dissertation]: Arizona State University, 239 p.

Darling, A., and Whipple. K., 2015, Geomorphic constraints on the age of the western Grand Canyon: Geosphere, v. 11, p. 958–976.

Davis, G.H., 1999, Structural geology of the Colorado Plateau region of southern Utah, with special emphasis on deformation bands: Geological Society of America Special Paper 342, 157 p.

Dickinson, W.R., and Gehrels, G.E., 2008, Sediment delivery to the Cordilleran foreland basin: Insights from U-Pb ages of detrital zircons in upper Jurassic and Cretaceous strata of the Colorado Plateau: American Journal of Science, v. 308, p. 1041-1082.

Dickinson, W.R., Karlstrom, K.E., Hanson, A.D., Gehrels, G.E., Pecha, M., Cather, S.M., and Kimbrough, D.L., 2014, Detrital zircon U-Pb evidence precludes paleo–

Colorado River sediment in the exposed Muddy Creek Formation of the Virgin
River depression: Geosphere, v. 10, no. 6, p. 1123–1138, doi: 10 .1130 /GES01097
.1

Donahue, M.S., Karlstrom, K.E., Aslan, A., Darling, A., Granger, D., Wan, E.,
Dickinson, R.G., and Kirby, E., 2013, Quaternary bedrock incision of the ~1 Ma
Black Canyon of the Gunnison, Colorado, associated with knickpoint transience and
mantle-driven uplift: Geosphere, v. 9, p. 815–826, doi: 10 .1130 /GES00847 .1.

Downing, R.F., 2000, Imaging the mantle in southwestern Utah using geochemistry and
geographic information systems [M.S. thesis]: Las Vegas, University of Nevada, 128
p.

Faulds, J.E., Smith, E.I., and Gans, P., 1999, Spatial and temporal patterns of magmatism
and extension in the Northern Colorado River Extensional Corridor, Nevada and
Arizona: A preliminary report: in Faulds, J.E., ed., Cenozoic Geology of the
Northern Colorado River Extensional Corridor, Southern Nevada and Northwestern
Arizona: Economic implications of regional segmentation structures: Nevada
Petroleum Society 1999 Field Trip Guidebook, Reno, Nevada, p. 171-183.

Faulds, J.E., Wallace, M.A., Gonzales, L.A., and Heizler, M.T., 2001, Depositional
environment and paleogeographic implications of the late Miocene Hualapai
Limestone, northwestern Arizona and southern Nevada, in Young, R.A., and
Spamer, E.E., eds., Colorado River origin and evolution—proceedings of the
symposium held at Grand Canyon National Park in June 2000: Grand Canyon
Association Monograph 12, p. 81-88.

Faulds, J.E., Schreiber, B.C., Langenheim, V.E., Hinz, N.H., Shaw, T.H., Heizler, M.T.,

Perkins, M.E., El Tabkh, Mohammed, and Kunk, M.J., 2016, Paleogeographic implications of late Miocene lacustrine and nonmarine evaporate deposits in the Lake Mead region—Immediate precursors to the Colorado River: Geosphere, v. 12, p. 721–767, doi:10.1130/GES01143.1.

Fenton, C.R., Webb, R.H., Pearthree, P.A., Cerling, T.E., and Poreda, R.J., 2001, Displacement rates on the Toroweap and Hurricane faults: Implications for Quaternary downcutting in the Grand Canyon, Arizona: Geology, v. 29, p. 1035–1038, doi: 10.1130/0091-7613(2001)029<1035:DROTTA>2.0.CO;2.

Feuerbach, D.L., Smith, E.I., Shafiqullah, M., and Damon, P.E., 1991, New K-Ar dates for Late Miocene to Early Pliocene mafic volcanic rocks in the Lake Mead area, Nevada and Arizona: Isochron West, no. 57, p. 17-20.

Fitzgerald, P.G., Fryxell, J.E., and Wernicke, B.P., 1991, Miocene crustal extension and uplift in southeastern Nevada: Constraints from fission track analysis: Geology, v. 19, p. 1013–1016, doi: 10.1130/0091-7613 (1991)0192.3.

Fitzgerald, P.G., Duebendorfer, E.M., Faulds, J.E., and O'Sullivan, P., 2009, South Virgin–White Hills detachment fault system of SE Nevada and NW Arizona: Applying apatite track thermochronology to constrain the tectonic evolution of a major continental detachment fault: Tectonics, v. 28, p. TC2001, doi: 10.1029/2007TC002194.

Forrester, S.W., 2009, Provenance of the Miocene–Pliocene Muddy Creek Formation near Mesquite, Nevada [M.S. thesis]: University of Nevada–Las Vegas, 148 p.

Goldstrand, P.M., 1992, Evolution of Late Cretaceous and early Tertiary basins of southwest Utah based on clastic petrology: Journal of Sedimentary Petrology, v. 62,

p. 495–507, doi: 10 .1306 /D4267933 -2B26 -11D7 -8648000102C1865D.

Goldstrand, P.M., 1994, Tectonic development of Upper Cretaceous to Eocene strata of southwest Utah: Geological Society of America Bulletin, v. 106, p. 145–154, doi: 10 .1130 /0016 -7606 (1994)106 2 .3 .CO; 2.

Gordon, R. G., and D. M. Jurdy, 1986, Cenozoic global plate motions: Journal of Geophysics Research, v. 91, p. 12389–12406, doi:10.1029/JB091iB12p12389.

Grater, R.K., 1945, Landslide in Zion Canyon, Zion National Park, Utah: The Journal of Geology, v. 53, p. 116–124, doi: 10.1086/625254.

Hacker, D.B., 1998, Catastrophic gravity sliding and volcanism associated with the growth of laccoliths—examples from early Miocene hypabyssal intrusions of the Iron Axis magmatic province, Pine Valley Mountains, southwestern Utah [Ph.D. dissertation]: Kent State University, 5 plates, 258 p.

Hacker, D.B., Holm, D.K., Rowley, P.D., and Blank, H.R., 2002, Associated Miocene laccoliths, gravity slides, and volcanic rocks, Pine Valley Mountains and Iron Axis region, southwestern Utah, in Lund, W.R., ed., Field guide to geologic excursions in southwestern Utah and adjacent areas of Arizona and Nevada: U.S. Geological Survey Open-File Report OF 02-0172, p. 235-283.

Hacker, D.B., Petronis, M.S., Holm, D.K., and Geissman, J.W., 2007, Shallow emplacement mechanisms of the Miocene Iron Axis laccolith group, southwest Utah, in Lund, W.R., ed., Field guide to geologic excursions in southern Utah: Utah Geological Association Publication 35, 49 p.

Hamblin, W.K., Damon, P.E., and Bull, W.B., 1981, Estimates of vertical crustal strain rates along the western margins of the Colorado Plateau: Geology, v. 9, p. 293-298.

Harlan, S.S., Duebendorfer, E.M., and Deibert, J.E., 1998, New 40Ar/39Ar isotopic dates from the Miocene volcanic rocks in the Lake Mead area and southern Las Vegas Range, Nevada: Canadian Journal of Earth Science, v. 35, p. 495-503.

Hayden, J.M., 2004, Geologic map of The Divide quadrangle, Washington County, Utah: Utah Geological Survey Map 197, 32 p., 2 plates, scale 1:24,000.

Hayden, J. M., and Sable, E. G., 2008, Geologic Map of the Virgin quadrangle, Washington County, Utah: Utah Geological Survey, scale 1:24,000.

Higgins, J.M., 2003, Geology of Snow Canyon State Park, Utah, in Sprinkel, D.A., Chidsey, T.C., and Anderson, P.B., eds., Geology of Utah's parks and monuments: Utah Geological Association and Bryce Canyon Natural History Association, Utah Geological Association Publication 28, second edition, p. 479-494.

Howard, K.A., and Bohannan, R.G., 2001, Lower Colorado River: Upper Cenozoic deposits, incision, and evolution, in Young, R.A., and Spamer, E.E., eds., Colorado River origin and evolution: Grand Canyon National Park, Grand Canyon Association, p. 101–106.

Howard, K.A., Beard, L.S., Kuntz, M.A., Kunk, M.J., Sarna-Wojcicki, A.M., Perkins, M.E., and Lucchitta, I., 2010, Erosion of tilted fault blocks and deposition of coarse sediments in half-graben basins during late stages of extension: Gold Butte area, Basin and Range Province, in Umhoefer, P.J., Beard, L.S., and Lamb, M.A., eds., Miocene Tectonics of the Lake Mead Region, Central Basin and Range: Geological Society of America Special Paper 463, p. 147–170, doi: 10 .1130 /2010 .2463 (07) .

Howard, K.A., House, P.K., Dorsey, R.J., and Pearthree, P.A., 2015, River-evolution and tectonic implications of a major Pliocene aggradation on the lower Colorado River,

the Bullhead Alluvium: Geosphere, v. 11, p. 1–30, doi: 10 .1130 /GES01059 .1 .

Jackson, G.W., 1990, Tectonic geomorphology of the Toroweap Fault, western Grand Canyon, Arizona; Implications for transgression of faulting on the Colorado Plateau: Arizona Geological Survey Open-File Report 90-4, 67 p.

Karlstrom, K.E., Crow, R.S., Peters, L., McIntosh, W., Raucci, J., Crossey, L.J. Umhoefer, P., and Dunbar, N., 2007, 40Ar/39Ar and field studies of Quaternary basalts in Grand Canyon and model for carving Grand Canyon: Quantifying the interaction of river incision and normal faulting across the western edge of the Colorado Plateau: Geological Society of America Bulletin, v. 119, no. 11-12, p. 1283–1312.

Karlstrom, K.E., Crow, R., Crossey, L.J., Coblentz, D., and Van Wijk, J.W., 2008, Model for tectonically driven incision of the younger than 6 Ma Grand Canyon: Geology, v. 36, no. 11, p. 835–838, doi: 10 .1130 /G25032A.1.

Karlstrom, K.E. et al., 2012, Mantle-driven dynamic uplift of the Rocky Mountains and Colorado Plateau and its surface response: Toward a unified hypothesis: Lithosphere, v. 4, no. 1, p. 3–22, doi:10.1130 /L150 .1 .

Karlstrom, K.E., Darling, A., Crow, R., Lazear, G., Aslan, A., Granger, D., Kirby, E., Crossey, L., and Whipple, K., 2013, Colorado River chronostratigraphy at Lee's Ferry, Arizona, and the Colorado Plateau bull's eye of incision; Forum Comment: Geology, v. 41, no. 12, p. E303, doi: 10 .1130 /G34550C .1

Kirby, E., and Whipple, K., 2001, Quantifying differential rock-uplift rates via stream profile analysis: Geology, v. 29, p. 415–418, doi: 10.1130/00917613(2001)029<0415:qdrurv> 2.0.co;2.

Kirby, E., and Whipple, K.X., 2012, Expression of active tectonics in erosional landscapes: Journal of Structural Geology, v. 44, p. 54–75, doi: 10.1016/j.jsg.2012.07.009.

Kirby, E., Whipple, K.X., Tang, W., and Chen, Z., 2003, Distribution of active rock uplift along the eastern margin of the Tibetan Plateau: Inferences from bedrock channel longitudinal profiles: Journal of Geophysical Research: Solid Earth, v. 108, no. B4, doi: 10 .1029 /2001JB000861 .

Kuiper, K.F., Deino, A., Hilgen, F.J., Krijgsman, W., Renne, P.R., and Wijbrans, J.R., 2008, Synchronizing rock clocks of Earth history: Science, v. 320, p. 500–504, doi:10.1126/science.1154339.

Lazear, G., Karlstrom, K., Aslan, A., Kelley, S., 2013, Denudation and flexural isostatic response of the Colorado Plateau and southern Rocky Mountain region since 10 Ma: Geosphere, v. 9, p. 781–791, http://dx.doi.org/10.1130/GES00784.1.

Levander, A., Schmandt, B., Miller, M.S., Liu, K., Karlstrom, K.E., Crow, R.S., Lee, C.-T.A., Humphreys, E.D., 2011, Continuing Colorado plateau uplift by delamination-style convective lithospheric downwelling: Nature, v. 472, p. 461–466.

Longwell, C.R., 1928, Geology of the Muddy Mountains, Nevada: U.S. Geological Survey Bulletin 798, p. 91–97.

Lucchitta, I., 1979, Late Cenozoic uplift of the southwestern Colorado Plateau and adjacent lower Colorado River region: Tectonophysics, v. 61, p. 63-95.

Ludington, S., Moring, B.C., Miller, R.J., Stone, P.A., Bookstrom, A.A., Bedford, D.R., Evans, J.G., Haxel, G.A., Nutt, C.J., Flyn, K.S., Hopkins, M.J., 2007, Preliminary integrated geologic map databases for the United States Western States: California,

Nevada, Arizona, Washington, Oregon, Idaho, and Utah, Version 1.3: United States

Geological Survey Open-File Report 2005-1305,

http://pubs.usgs.gov/of/2005/1305/index.htm.

Lund, W.R., and Everitt, B.J., 1998, Reconnaissance paleoseismic investigation of the

Hurricane fault in southwestern Utah, in Pearthree, P.A., Lund, W.R., Stenner, H.D.,

and Everitt, B.L., eds., Paleoseismologic investigations of the Hurricane fault in

southwestern Utah and northwestern Arizona—final project report: National

Earthquake Hazards Reduction Program, unpublished report for U.S. Geological

Survey, p. 8-48.

Lund, W.R., Pearthree, P.A., Amoroso, L., Hozik, M.J., and Hatfield, S.C., 2001,

Paleoseismic investigation of earthquake hazard and long-term movement history of

the Hurricane fault, southwestern Utah and northwestern Arizona—final technical

report: National Earthquake Hazards Reduction Program, unpublished report for

U.S. Geological Survey, award no. 99HQGR0026, 120 p.

Lund, W.R., Knudsen, T.R., and Vice, G.S., 2008, Paleoseismic reconnaissance of the

Sevier fault, Kane and Garfield Counties, Utah: Utah Geological Survey Special

Study 122, Paleoseismology of Utah, v. 16, 31 p.

Meek, N., and Douglass, J., 2001, Lake overflow: An alternative hypothesis for Grand

Canyon incision and development of the Colorado River, in Young, R.A., and

Spamer, E.E., eds., Colorado River—Origin and evolution: Grand Canyon, Arizona,

Grand Canyon Association, p. 199–206.

Min, K., Mundil, R., Renne, P., and Ludwig, K.R., 2000, A test for systematic errors in

40Ar/39Ar geochronology through comparison with U/Pb analysis of a 1.1-Ga

rhyolite: Geochimica et Cosmochimica Acta, v. 64, p. 73–98, doi: 10.1016/S0016-7037(99)00204-5.

Minster, J. B., and T. H. Jordan, 1978, Present-day plate motions, Journal of Geophysics Research, v. 83, p. 5331–5354, doi:10.1029/JB083iB11p05331.

Molnar, P., 2004, Late Cenozoic increase in accumulation rates of terrestrial sediment: How might climate change have affected erosion rates?: Annual Review of Earth and Planetary Science, v. 32, p. 67–89, doi:10.1146 /annurev.earth.32.091003.143456.

Moucha, R., Forte, A.M., Rowley, D.B., Mitrovica, J.X., Simmons, N.A., Grand, S.P., 2009, Deep mantle forces and the uplift of the Colorado Plateau: Geophysics Research Letters, v. 36, p. 1-6.

Moore, R. T., 1972, Geology of the Virgin and Beaverdam Mountains, Arizona: Arizona Bureau of Mines Bulletin 186, 65 p.

Muntean, T. W., 2012, Muddy Creek Formation: A Record of Late Neogene Tectonics and Sedimentation in Southern Nevada [Ph.D. dissertation]: University of Nevada-Las Vegas, 270 p.

National Atlas of the United States, 2010, United States Annual Average Precipitation, 1990-2009: National Atlas of the United States (http://nationalatlas.gov/atlasftp.html)

Nelson, S.T., and Tingey, D.G., 1997, Time-transgressive and extension-related basaltic volcanism in southwest Utah and vicinity: Geological Society of America Bulletin, v. 109, p. 1249–1265, doi: 10.1130/0016-7606(1997) 1092.3.CO;2.

Novak, S.W., 1984, Eruptive history of the rhyolitic Kane Springs Wash volcanic center,

Nevada: Journal of Geophysical Research, v. 89, p. 8603–8615, doi: 10 .1029/JB089iB10p08603 .

Ouimet, W.B., Whipple, K.X., and Granger, D.E., 2009, Beyond threshold hillslopes: Channel adjustment to base-level fall in tectonically active mountain ranges: Geology, v. 37, no. 7, p. 579–582, doi:10.1130/G30013A.1.

Ouimet, W., Whipple, K.X., Royden, L., Reiners, P., Hodges, K., and Pringle, M., 2010, Regional incision of the eastern margin of the Tibetan Plateau: Lithosphere, v. 2, no. 1, p. 50–63, doi: 10.1130/L57.1.

Pazzaglia, F.J., Gardner, T.W., and Merritts, D.J., 1998, Bedrock fluvial incision and longitudinal profile development over geologic time scales determined by fluvial terraces, in Tinkler, K.J., and Wohl, E.E., eds., Rivers over rock: Fluvial processes in bedrock channels: American Geophysical Union Geophysical Monograph 107, p. 207–236.

Pearthree, P.A., 1998, Quaternary fault data and map for Arizona: Arizona Geological Survey Open-File Report 98-24, 122 p.

Pederson, J.L., 2008, The mystery of the pre-Grand Canyon Colorado River – Results from the Muddy Creek Formation: GSA Today, v. 18, no. 3, p. 4-10.

Pederson, J., Karlstrom, K., Sharp, W., and McIntosh, W., 2002, Differential incision of the Grand Canyon related to Quaternary faulting – Constraints from U-series and Ar/Ar dating: Geology, v.30, p. 739-742.

Pederson, J.L., and Tressler, C., 2012, Colorado River long-profile metrics: The hunt for knickzones and their meaning: Earth and Planetary Science Letters, v. 345–348, p. 171–179, doi:10.1016/j.epsl.2012.06.047.

Pederson, J.L., Cragun, W.S., Hidy, A.J., Rittenour, T.M., and Gosse, J.C., 2013, Colorado River chronostratigraphy at Lee's Ferry, Arizona, and the Colorado Plateau bull's eye of incision: Geology, v. 41, p. 427–430, doi: 10 .1130 /G34051 .1.

Pelletier, J.D., 2010, Numerical modeling of the late Cenozoic geomorphic evolution of the Grand Canyon: Geological Society of America Bulletin, v. 122, p. 595–608.

Quigley, M.C., Karlstrom, K.E., Kelley, S., and Heizler, M., 2010, Timing and mechanisms of basement uplift and exhumation in the Colorado Plateau–Basin and Range transition zone, Virgin Mountain anticline, Nevada-Arizona, in Umhoefer, P.J., Beard, L.S., and Lamb, M.A., eds., Miocene Tectonics of the Lake Mead Region, Central Basin and Range: Geological Society of America Special Paper 463, doi: 10.1130/2010.2463(14).

Reiners, P.W., Brady, R., Farley, K.A., Fryxell, J.E., Wernicke, B., and Lux, D., 2000, Helium and argon thermochronometry of the Gold Butte block, South Virgin Mountains, Nevada: Earth and Planetary Science Letters, v. 178, p. 315–326, doi: 10.1016/S0012-821X(00)00080-7.

Reynolds, S.J., Florence, F.P., Welty, J.W., Roddy, M.S., Currier, D.A., Anderson, A.V., and Keith, S.B., 1986, Compilation of radiometric age determinations in Arizona: Arizona Bureau of Geology and Mineral Technology, Geological Survey Branch, Bulletin 197, 258 p.

Rosenberg, R., Kirby, E., Aslan, A., Karlstrom, K., Heizler, M., and Ouimet, W., 2014, Late Miocene erosion and evolution of topography along the western slope of the Colorado Rockies: Geosphere, v. 10, p. 641–663, doi: 10 .1130 /GES00989 .1

Rowley, P.D., Mehnert, H.H., Naeser, C.W., Snee, L.W., Cunningham, C.G., Steven,

T.A., Anderson, J.J., Sable, E.G., and Anderson, R.E., 1994, Isotopic Ages and Stratigraphy of Cenozoic Rocks of the Marysvale Volcanic Field and Adjacent Areas, West-Central Utah: U.S. Geological Survey Bulletin 2071, 35 p.

Rowley, P.D., Williams, V.S., Vice, G.s., Maxwell, D.J., Hacker, D.B., Snee, L.W., and Mackin, J.H., 2006, Interim geologic map of the Cedar City 30'x60' quadrangle, Iron and Washing Counties, Utah: Utah Geological Survey Open-File Report 476DM, scale 1:100,000.

Roy, M., Jordan, T.H., and Pederson, J., 2009, Colorado Plateau magmatism and uplift by warming of heterogeneous lithosphere: Nature, v. 459, p. 978-982, doi: 10.1038/nature08052.

Sable, E. G., and Hereford, R., 2004, Geologic map of the Kanab 30′ × 60′ quadrangle, Utah and Arizona: U.S. Geological Survey Geologic Investigation Series Map I-2655, scale 1:100,000.

Sanchez, A., 1995, Mafic volcanism in the Colorado Plateau/Basin-and-Range transition zone, Hurricane, Utah [M.S. thesis]: Las Vegas, University of Nevada, 92 p., scale 1:52,000.

Schiefelbein, I.M., 2002, Fault segmentation, fault linkage, and hazards along the Sevier fault, southwestern Utah [M.S. thesis]: Las Vegas, University of Nevada, 134 p., 5 plates in pocket.

Schildgen, T.F., Hodges, K.V., Whipple, K.X, Reiners, P.W., and Pringle, M.S., 2007, Uplift of the western margin of the Andean plateau revealed from canyon incision history, southern Peru: Geology, v. 35, p. 523–526, doi: 10.1130/G23532A.1.

Schmandt, B. and Humphreys, E. D., 2010, Complex subduction and small-scale

convection revealed by body wave tomography of the western U.S. upper mantle:
Earth and Planetary Science Letters, v. 297, p.435-445,
doi:10.1016/j.epsl.2010.06.047

Schmidt, J.L., Zeitler, P.K., Pazzaglia, K.J., Tremblay, M.M., Shuster, D.L., and Fox, M.,
2015, Knickpoint evolution on the Yarlung River: Evidence for late Cenozoic uplift
of the southeastern Tibetan Plateau margin: Earth and Planetary Science Letters,
v. 430, p. 448–457, doi:10 .1016/j.epsl.2015.08.041

Schoenbohm, L.M., Burchfiel, B.C., and Liangzhong, C., 2006, Propagation of surface
uplift, lower crustal flow, and Cenozoic tectonics of the southeast margin of the
Tibetan Plateau: Geology, v. 34, p. 813–816, doi: 10.1130/G22679.1.

Seong, Y.B., Owen, L.A., Bishop, M.P., Bush, A., Clendon, P., Copland, L., Finkel,
R.C., Kamp, U., and Shroder , J.F., Jr., 2008, Rates of fluvial bedrock incision
within an actively uplifting orogen: Central Karakoram Mountains, northern
Pakistan: Geomorphology, v. 97, p. 274–286, doi:10.1016/j.geomorph.2007.08.011.

Sine, C.R., Wilson, D., Gao, W., Grand, S.P., Aster, R., Ni, J., and Baldridge, W.S.,
2008, Mantle structure beneath the western edge of the Colorado Plateau:
Geophysical Research Letters, v. 35, L10303, doi: 10.1029/2008GL033391.

Small, E., Anderson, R.S., 1998, Pleistocene relief production in Laramide mountain
ranges, western United States: Geology, v. 26, no. 2, p. 123-126.

Smith, R.B., and Arabasz, W.J., 1991, Seismicity of the Intermountain seismic belt, in
Slemmons, D.B., Engdahl, E.R., Zoback, M.D., and Blackwell, D.D., eds.,
Neotectonics of North America: Boulder, Colorado: Geological Society of America,
Decade Map Volume, p. 185-228

Spencer, J.E., Peters, L., McIntosh, W.C., and Patchett, P.J., 2001, 40Ar/39Ar geochronology of the Hualapai Limestone and Bouse Formation and implications for the age of the lower Colorado River, in Young, R.A., and Spamer, E.E., eds., The Colorado River—Origin and Evolution: Grand Canyon, Arizona, Grand Canyon Association Monograph 12, p. 89–91.

Swenberg, Carl Taylor, 2012, The fluvial Muddy Creek Formation near Overton, Nevada [M.S. thesis]: Las Vegas, University of Nevada, 70 p. http://digitalscholarship.unlv.edu/thesesdissertations/1524.

Thompson, K.G., 1985, Stratigraphy and petrology of the Hamblin-Cleopatra Volcano, Clark County, Nevada [M.S. thesis]: University of Texas, Austin, 306 p.

Utah Geological Survey and New Mexico Geochronology Research Laboratory, 2007a, 40Ar/39Ar geochronology results from the Antelope Peak, Central East, Goldstrike, Page Ranch, and Saddle Mountain quadrangles, Utah: Utah Geological Survey Open-File Report 508, variously paginated, http://geology.utah.gov/online/analytical_data.htm

Utah Geological Survey and New Mexico Geochronology Research Laboratory, 2007b, 40Ar/39Ar geochronology results for the Chriss Canyon, Hells Kitchen Canyon SW, Jordan Narrows, Lehi, Mussentuchit Flat, Springdale West, and Veyo quadrangles, Utah: Utah Geological Survey Open-File Report 495, variously paginated, http://geology.utah.gov/online/analytical_data.htm.

Utah Geological Survey and New Mexico Geochronology Research Laboratory, 2008, 40Ar/39Ar geochronology results from the Veyo, Gunlock, Billies Mountain, The Flat Tops, Maple Ridge, Hebron, Enterprise, and Central West quadrangles, Utah:

Utah Geological Survey Open-File Report 513 parts I and II, variously paginated, http://geology.utah.gov/online/analytical_data.htm.

van Wijk, J.W., Baldridge, W.S., van Hunen, J., Goes, S., Aster, R., Coblentz, D.D., Grand, S.P., Ni, J., 2010, Small-scale convection at the edge of the Colorado Plateau: Implications for topography, magmatism, and evolution of Proterozoic lithosphere: Geology, v. 38, p. 611–614.

Wannamaker, P. E., Bartley, J. M., Sheehan, A. F., Jones, C. H., Lowry, A. R., Dumitru, T. A., Ehlers, T. A., Holbrook, W. S., Farmer, G. L., Unsworth, M. J., Hall, D. B., Chapman, D. S., Okaya, D. A., John, B. E. and Wolfe, J. A., 2001, Great Basin–Colorado Plateau Transition in Central Utah: An Interface between Active Extension and Stable Interior, in Erskine, M.C., Faulds, J.E., Bartley, J.M., and Rowley, P., eds., The Geological Transition: Colorado Plateau to Basin and Range, Proc. J. Hoover Mackin Symposium, UGA/AAPG Guidebook 30/GB78, Cedar City, Utah, September 20–23, p. 1–38.

Wenrich, K. J., Billingsley, G. H., and Blackerby, B. A, 1995, Spatial migration and compositional changes of Miocene-Quaternary magmatism in the Western Grand Canyon: Journal of Geophysical Research, v. 100, no. B7, p. 10,417-10,440.

West, M., Ni, J., Baldridge, W.S., Wilson, D., Aster, R., Gao, W., and Grand, S., 2004, Crust and upper mantle shear wave structure of the southwest United States: Implications for rifting and support for high elevation: Journal of Geophysical Research, v. 109, B03309, doi: 10.1029/2003JB002575.

Williams, V.S., 1996, Preliminary geologic map of the Mesquite quadrangle, Clark and Lincoln Counties, Nevada and Mohave County, Arizona: U.S. Geological Survey

Open-File Report 96-676.

Willis, G. C., and Biek, R. F., 2001, Quaternary incision rates of the Colorado River and major tributaries in the Colorado Plateau, Utah, in Young, R. A., and Spamer, E. E., eds., Colorado River—Origin and Evolution: Grand Canyon, Arizona, Grand Canyon Association, p. 119-123.

Willis, G.C., and Hylland, M.D., 2002, Interim geologic map of The Guardian Angels quadrangle, Washington County, Utah: Utah Geological Survey Open-File Report 395, 27 p., scale 1:24,000.

Willis, G.C., Biek, R.F., and Hayden, J.M., 2006, New age of the Santa Clara (Snow Canyon State Park) basalt flow: Utah Geological Survey, Survey Notes, v. 38, no. 3, p. 4-5.

Winn, C., Karlstrom, K.E., Shuster, D.L., Kelley, S., Fox, M., 2017, 6 Ma Age of carving westernmost Grand Canyon: Reconciling geologic data with combined AFT, (U–Th)/He, and 4He/3He thermochronologic data: Earth Planetary Science Letters, http://dx.doi.org/10.1016/j.epsl.2017.06.051.

Wobus, C., Whipple, K.X., Kirby, E., Snyder, N., Johnson, J., Spyropolou, K., Crosby, B.T., and Sheehan, D., 2006, Tectonics from topography: Procedures, promise, and pitfalls, in Willett, S.D., Hovius, N., Brandon, M.T., and Fisher, D., eds., Tectonics, climate, and landscape evolution: Geological Society of America Special Paper 398, p. 55–74, doi: 10 .1130 /2006 .2398 (04).